iScience

Article

# Fate plasticity of interneuron specification

## Graphical abstract

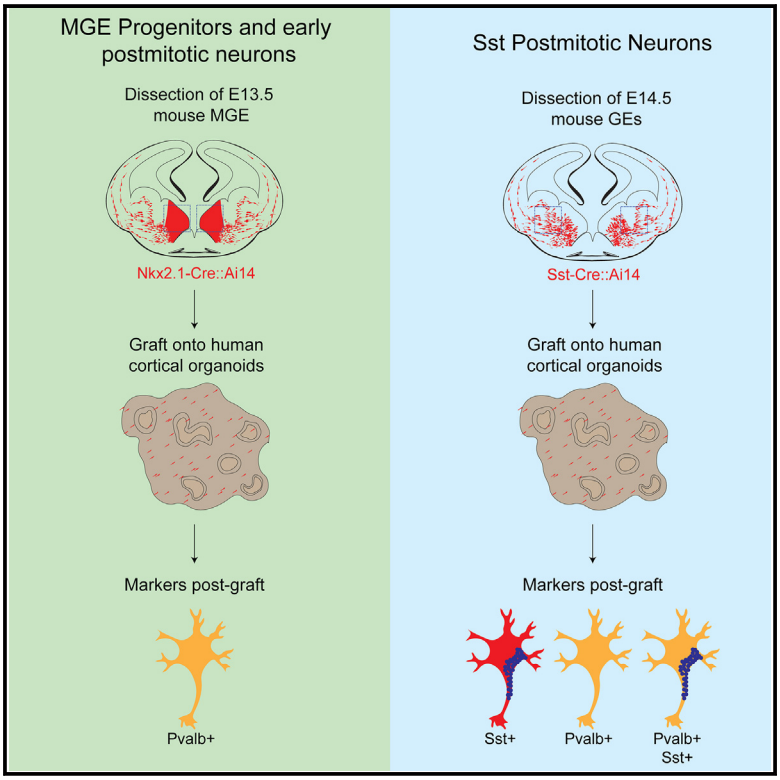


## Highlights

- Human 3D models drive efficient Pvalb+ interneuron differentiation from mouse MGEs
- Induced Pvalb+ interneurons exhibit identity-specific markers and proper soma size
- Projection neurons drive Pvalb fate in a non-autonomous manner
- Sst+ interneurons can upregulate Pvalb when grafted in a new environment

## Authors

Mohammed A. Mostajo-Radji, Walter R. Mancia Leon, Arnar Breevoort, ..., Arnold R. Kriegstein, Arturo Alvarez-Buylla, Alex A. Pollen

## Correspondence

mmostajo@ucsc.edu (M.A.M.-R.), alex.pollen@ucsf.edu (A.A.P.)

## In brief

Natural sciences; Biological sciences; Neuroscience; Systems neuroscience; Cellular neuroscience

Mostajo-Radji et al., 2025, iScience *28*, 112295
April 18, 2025 
https://doi.org/10.1016/j.isci.2025.112295

CellPress

iScience

CellPress
OPEN ACCESS

Article

# Fate plasticity of interneuron specification

Mohammed A. Mostajo-Radji,[1,2,3,10,*] Walter R. Mancia Leon,[1,4] Arnar Breevoort,[1,2] Jesus Gonzalez-Ferrer,[3,5] Hunter E. Schweiger,[3,6] Julian Lehrer,[3] Li Zhou,[1,2] Matthew T. Schmitz,[1,2] Yonatan Perez,[1,2] Tanzila Mukhtar,[1,2] Ash Robbins,[3,7] Julia Chu,[2] Madeline G. Andrews,[1,2,9] Frederika N. Sullivan,[3] Dario Tejera,[1] Eric C. Choy,[3,6] Mercedes F. Paredes,[2] Mircea Teodorescu,[3,7] Arnold R. Kriegstein,[1,2] Arturo Alvarez-Buylla,[1,4,8] and Alex A. Pollen[1,2,*]

[1]The Eli and Edythe Broad Center of Regeneration Medicine and Stem Cell Research, University of California, San Francisco, San Francisco, CA 94143, USA
[2]Department of Neurology, University of California, San Francisco, San Francisco, CA 94143, USA
[3]Genomics Institute, University of California, Santa Cruz, Santa Cruz, CA 95064, USA
[4]Department of Neurological Surgery, University of California, San Francisco, San Francisco, CA 94143, USA
[5]Department of Biomolecular Engineering, University of California, Santa Cruz, Santa Cruz, CA 95064, USA
[6]Department of Molecular, Cell and Developmental Biology, University of California, Santa Cruz, Santa Cruz, CA 95064, USA
[7]Department of Electrical and Computer Engineering, University of California, Santa Cruz, Santa Cruz, CA 95064, USA
[8]Kavli Institute for Fundamental Neuroscience, University of California, San Francisco, San Francisco, CA 94143, USA
[9]Present address: School of Biological and Health Systems Engineering, Arizona State University, Tempe, AZ 85281, USA
[10]Lead contact
*Correspondence: mmostajo@ucsc.edu (M.A.M.-R.), alex.pollen@ucsf.edu (A.A.P.)
https://doi.org/10.1016/j.isci.2025.112295

## SUMMARY

Neuronal subtype generation in the mammalian central nervous system is governed by competing genetic programs. The medial ganglionic eminence (MGE) produces two major cortical interneuron (IN) populations, somatostatin (Sst) and parvalbumin (Pvalb), which develop on different timelines. The extent to which external signals influence these identities remains unclear. Pvalb-positive INs are crucial for cortical circuit regulation but challenging to model *in vitro*. We grafted mouse MGE progenitors into diverse 2D and 3D co-culture systems, including mouse and human cortical, MGE, and thalamic models. Strikingly, only 3D human corticogenesis models promoted efficient, non-autonomous Pvalb differentiation, characterized by upregulation of Pvalb maturation markers, downregulation of Sst-specific markers, and the formation of perineuronal nets. Additionally, lineage-traced postmitotic Sst-positive INs upregulated Pvalb when grafted onto human cortical models. These findings reveal unexpected fate plasticity in MGE-derived INs, suggesting that their identities can be dynamically shaped by the environment.

## INTRODUCTION

The cerebral cortex contains both excitatory projection neurons (PNs) and inhibitory interneurons (INs). While the mechanisms underlying the generation and maintenance of this neuronal diversity remain incompletely understood, recent cell atlas studies reveal a significantly greater diversity of neurons in the adult cortex compared to the prenatal stage.[1,2] This suggests that external cues during migration and maturation may play a key role in shaping neuronal identity.[1–7] During embryonic development, PNs and INs originate from distinct progenitor pools: PNs are generated locally in the ventricular zone of the developing telencephalon, while INs migrate long distances from the medial and caudal ganglionic eminences (MGE and CGE) and the preoptic area (POA) to reach their final cortical destinations.[8–11] Upon reaching the cortex, INs integrate into local circuits by forming connections with PNs.

Several studies underscore the critical role of extrinsic cues in shaping IN development,[12] influencing migration and lamination,[13,14] synaptic wiring,[15,16] morphological and electrophysiological maturation,[13,17] and survival.[18–20] However, the extent to which external signals specify IN subtypes remains an open question.[20–24] For example, findings in a *Fezf2*-knockout mouse model, where subcerebral PNs are replaced by callosal PNs,[25] reveal a fate switch between two subclasses of Pvalb-positive INs.[20] Remarkably, even after migration and initial synaptic wiring with PNs, Pvalb/Fzd6-positive INs lose their molecular subclass identity and instead acquire the identity of Pvalb/Slc39a8-positive INs.[20] This suggests that extrinsic signals can influence IN fate well beyond early developmental stages.

Previous studies on MGE-derived IN progenitors have identified distinct spatial and temporal origins for different IN subtypes.[26–28] For instance, Sst-positive INs are primarily generated early from dorsal MGE progenitors, whereas Pvalb-positive INs are mainly produced later from ventral MGE progenitors.[26,27,29] The transcription factor *Mef2c* has been implicated in early postmitotic MGE-derived INs destined to become Pvalb INs, indicating that early molecular programs guide subtype specification.[30,31] However, single-cell RNA sequencing of the developing mouse brain shows that IN progenitors from different ganglionic eminences share similar transcriptional profiles, which diverge later during differentiation.[2,30–33] Furthermore, in contrast to PN subtypes,

which follow similar maturation timelines,[34] MGE-derived IN subtypes exhibit distinct maturation trajectories: Sst-positive INs are specified and incorporated into circuits early in development,[21,35] whereas Pvalb-positive INs mature later during postnatal life.[36–38] Notably, sensory input plays a critical role in postnatal Pvalb IN maturation,[36] raising the possibility that early environmental cues may trigger distinct genetic programs that further diversify MGE-derived IN subtypes.

Grafting studies have been pivotal in uncovering the role of developmental cues in various biological processes.[39] For instance, heterochronic transplantation experiments have shown that MGE-derived INs play an intrinsic role in the maturation of cortical circuits.[40,41] Interspecies chimeric models provide additional insights into how intrinsic and extrinsic factors regulate neuronal maturation rates.[42–45] These models are especially valuable because they modify both developmental timing (heterochrony) and gene expression patterns. Human brain development, for example, occurs over a much longer time frame than that of rodents,[46] and many genes have evolved to exhibit different expression patterns across species, even though the underlying cell types are conserved.[47,48] Differences in timing and gene expression in these interspecies models may help identify novel environmental factors that influence cell fate specification and maturation.[49,50]

Using mouse and human 2D co-culture and 3D organotypic and organoid models, we demonstrate that the cortical environment influences not only the timing of MGE IN specification but also the final molecular identity of developing INs. Remarkably, when mouse MGE cells are grafted onto 3D human cortical tissue—both primary organotypic cultures and cortical organoids—they rapidly differentiate a population mainly comprised of Pvalb-positive INs weeks earlier than in typical development. Additionally, we show that a subset of lineage-traced, postmitotic Sst-positive INs can be induced to upregulate Pvalb in the 3D human cortical environment. These findings reveal the plasticity of MGE-derived IN fate, demonstrate the critical influence of environmental factors in refining neuronal identity, and highlight *in vitro* conditions that promote efficient differentiation of mouse Pvalb INs.

## RESULTS

### Absence of pre-specification in unsupervised clustering of IN lineage

To assess the degree of neuronal subtype specification within MGE-derived populations during embryonic development, we analyzed single-cell gene expression data from the developing mouse telencephalon (E13 to P10, see method details).[6,31,51–54] Our analysis revealed six postmitotic clusters of INs originating from *Nkx2.1*-expressing regions in the MGE and ventromedial forebrain (VMF), including three clusters giving rise to striatal INs and *Npy*-expressing cortical INs, which indicate early diversification within some MGE-derived populations (Figures 1A and 1B). However, only a single cluster was identified for the majority of cortical Pvalb and Sst INs. Cells within this cluster expressed key markers like *Lhx6*, *Maf*, and *Sst*, but did not express *Pvalb* and could not be divided into distinct Pvalb or Sst subtypes at this developmental stage. In addition, the genes *ErbB4*, essential for tangential migration to the cortex, and *Mef2c,* involved in maturation, were expressed by the entire cluster at this stage (Figure 1C), though these genes later exhibit selective reduction in Sst and enrichment in Pvalb INs.[30,31,55] Although subtle signatures of pre-specification may already be visible in supervised analyses of embryonic cells anchored to adult datasets,[2,3,31,33] these findings highlight that distinct transcriptomic Pvalb subtypes are not apparent by unsupervised clustering.

### Human cortical environment induces rapid upregulation of Pvalb in mouse MGE-derived INs

Previous studies have demonstrated the successful grafting of mouse neuronal progenitors into organotypic brain slices of rats, showing that xenografted mouse neurons can integrate into a host from a different species.[56–58] These models have helped clarify cell-cell interactions and the extrinsic regulation of neuronal migration.[56] However, because of the relatively similar developmental timelines between these species, the question of whether a heterochronic environment can influence cell fate remains unexplored.

To investigate whether the host environment can influence the identity of neuronal progenitors, we grafted mouse E13.5 MGE-derived IN progenitors onto organotypic cultures of human and mouse embryonic cortex (Figures 2A–2C and S2). The donor MGE cells were from the *Nkx2.1*-Cre mouse line, which specifically targets MGE/POA neuronal progenitors and their descendants.[59] We crossed these with the Ai14 mouse line, which contains a floxed td-Tomato reporter gene in the ROSA26 locus.[60] The identity of the differentiated mouse INs was determined via immunohistochemistry. Remarkably, the grafted mouse MGE progenitors exhibited distinct fates depending on the host species. Specifically, when grafted onto E14.5 wild-type (WT) mouse brain organotypic slices, 27.00 ± 3.94% of cells differentiated into Sst-positive INs at 7 days post-graft (DPG), while 72.99 ± 3.94% of the cells were immunonegative for both Sst and Pvalb (Figure 2D). Across three grafting batches, none of the cells were Pvalb-positive (Figure 2D), consistent with the fact that Pvalb is not typically upregulated in mice until the third postnatal week. In contrast, when mouse MGE progenitors were grafted onto human gestational week (GW) 22 primary cortical slices (from three different donors), 82.94 ± 11.60% of the INs were Pvalb-positive, with 16.81 ± 13.29% remaining double-negative at 7 DPG (Figure 2D). Notably, none of the grafted INs were Sst-positive alone, and only 0.98 ± 1.69% co-expressed both Pvalb and Sst (Figure 2D).

Importantly, while human MGE-derived INs migrate into the cortex before GW22, resident human INs do not express Pvalb until postnatal stages.[61–63] Consistent with this, we did not detect Pvalb expression in human cells within our organotypic cultures, although Sst-positive INs in the host tissue were readily observed (Figures 2B and 2C). To verify the functionality of the Pvalb antibody, we performed immunostaining on postmortem samples ranging from GW39 to 57 years old. Pvalb was detected in the GW39 striatum and in older cortical samples, but not in the GW39 cortex, consistent with its developmental absence (Figure S1). This confirms that the lack of Pvalb in GW22 organotypic cultures is due to the developmental stage, not an issue with antibody specificity.

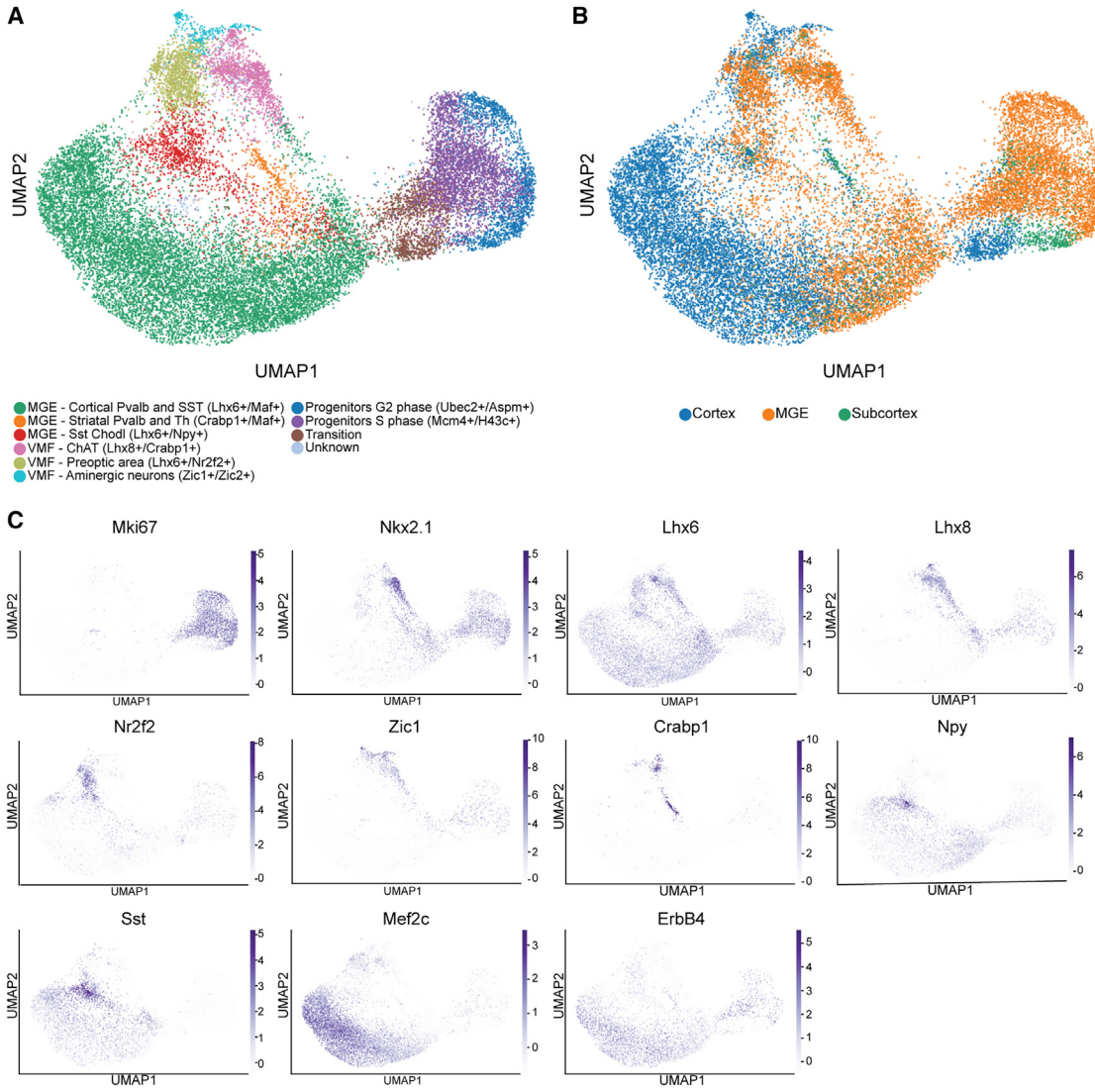


**Figure 1. Early diversity of MGE and VMF-derived interneurons**

(A) Single-cell transcriptomic analysis identifies six distinct classes of postmitotic interneurons derived from the MGE and VMF, characterized by the expression of *Gad1*, *Gad2*, *Dlx* genes, *Lhx6*, and *Nkx2.1*. Cells are color-coded by cluster in a UMAP representation of the single-cell transcriptomes.

(B) Classification of INs based on their region of origin.

(C) Expression of key marker genes defining each cluster, plotted on the UMAP. Notably, *Pvalb* expression was absent across all analyzed cells.

To further investigate the observed species-dependent differences in Pvalb induction and minimize potential imaging biases, we conducted an additional experiment in which unlabeled WT IN progenitors were grafted onto GW21.6–23 cortical slices from three individuals (Figures 2E and S3). We distinguished mouse and human cells post hoc by immunostaining for human nuclear antigen (HNA), which specifically recognizes human, but not mouse, nuclei. At 7 DPG, we detected Pvalb-positive INs, all of which were HNA-negative. Notably, Pvalb upregulation occurred at 7 DPG, equivalent to mouse postnatal day 0, demonstrating that the human cortical environment not only induces Pvalb expression in mouse cells but does so at an accelerated rate, three weeks earlier than it would occur *in vivo*.

## Long-term chimeric models reveal integration of mouse INs in human cortical organoids

We next investigated whether grafting mouse INs onto human cortical organoids could recapitulate the Pvalb induction observed after grafting into human organotypic slice cultures. Since organotypic cultures are typically limited to about one week,[64,65] we hypothesized that chimeric induced pluripotent stem cell (iPSC)-derived cortical organoids would allow for long-term analysis of the host environment's influence.[66,67] To create a long-term chimeric model, we grafted mouse E13.5 MGE progenitors and early postmitotic INs onto human cortical organoids (Figure 3A). Previous studies have demonstrated that deep-layer PNs are crucial for the proper migration of

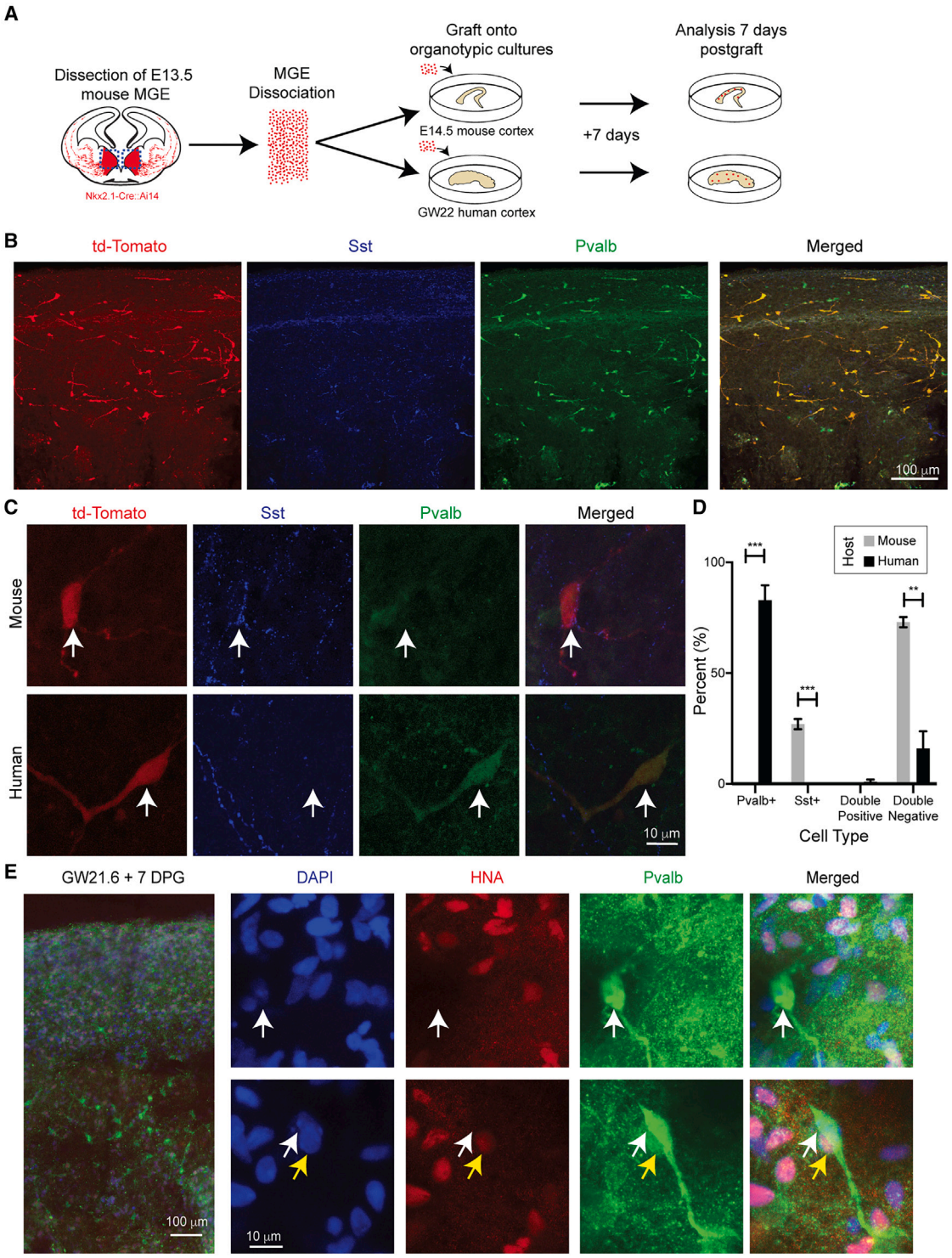


**Figure 2. Host-dependent differentiation of mouse MGE progenitors**

Grafting of mouse MGE progenitors onto mouse and human cortical organotypic cultures generate different IN populations at 7 DPG.

(A) Schematic of the experimental design. E13.5 mouse MGE cells were dissociated and grafted onto either GW22 human or E14.5 mouse cortical organotypic cultures to examine IN differentiation at 7 days DPG.

(B) Representative image of a GW22 human cortical slice grafted with E13.5 td-Tomato-labeled mouse INs, 7 DPG. Scale bar, 100 μm.

(C) Grafting onto E14.5 mouse organotypic cultures predominantly generates Sst-positive INs, while grafting onto GW22 human organotypic cultures primarily induces the differentiation of Pvalb-positive INs. Scale bar, 10 μm.

*(legend continued on next page)*

MGE-derived INs into the cortex during embryonic development.[14] Thus, we used 6-8 week-old human cortical organoids as hosts, corresponding to the peak period of deep-layer PN neurogenesis (roughly equivalent to the end of first trimester and early second trimester in human fetal development).[68]

To evaluate whether mouse INs can migrate within the human organoid hosts, we conducted live imaging of chimeric organoids at 1 DPG, capturing hourly observations for 24 h. Consistent with prior *in vivo* and *in vitro* studies,[69,70] we observed that mouse cells exhibited high migratory activity within the human cortical organoids. The grafted mouse cells displayed exploratory behavior, neurite branching, and nucleokinesis typical of migrating INs from the MGE (Figure 3B). This indicates that mouse INs can identify the appropriate substrate and signals within the human cortical environment to support their migration.

To assess the final positioning of the grafted INs, we employed light-sheet microscopy to visualize whole organoids at 5 WPG (weeks post-graft) (equivalent to P42 in mouse *in vivo* development), after IN migration and development were complete. We cleared the tissue before imaging to ensure comprehensive visualization of the entire organoid. Our analysis showed that the grafted mouse INs migrated throughout much of the organoid (Figure 3C); however, most were localized at the periphery (Figure 3C). In organoids, newborn PNs tend to localize at the periphery, while the center often forms a necrotic core.[71] Several hypotheses could explain the peripheral localization of the grafted INs: (1) the INs may be attracted to the periphery, where the majority of excitatory PNs reside, similar to MGE cell migration *in vivo*[14]; (2) INs might be unable to penetrate the organoid core; or (3) INs that migrate to the core may not survive. To differentiate between these possibilities, we used rare organoids in which PNs differentiate internally within the core. After grafting mouse INs onto these organoids and performing immunostaining for the pan-neuronal marker Map2 at 5 WPG, we consistently found INs near Map2-positive clusters, irrespective of their location (Figures 3D and S4A). Notably, Map2-negative regions were largely devoid of mouse INs, even in peripheral areas (Figures 3D and S4A). Together, these observations suggest that grafted mouse INs preferentially localize in areas containing PNs.

Previous studies using monosynaptic tracing of human stem cell-derived PNs grafted into mouse hosts have shown that mouse INs can form functional synapses with human cortical PNs.[72] This suggests that in our grafting paradigm, mouse INs might integrate into human organoids. To test this, we examined the integration of grafted INs into human cortical organoids using genetic, molecular, and physiological approaches. First, we used the Ai34 reporter line, which contains a floxed synaptophysin (Syp)-td-Tomato fusion gene inserted into the ROSA26 locus.[73] Since Syp is a presynaptic vesicle membrane protein, expression of the fusion gene correlates with synapse formation.[73] At 5 WPG, we detected strong fusion gene expression throughout the grafted INs, indicating active synapse formation (Figure 3E). In complementary experiments, we immunostained grafted *Nkx2.1*-Cre::Ai14 cells for the excitatory postsynaptic marker Psd95 at 5 WPG (Figures 3F and S4B). Since human PNs are the sole source of excitatory synapses in the organoids, the presence of PSD95 in grafted INs indicates that the mouse INs were receiving synaptic input from human PNs.

We next asked whether the grafted INs exhibited spontaneous activity, a characteristic observed across the central nervous system even in early circuit development.[74] Using calcium imaging, we explored the activity of grafted INs, leveraging the Ai96 mouse line, which carries the genetically encoded calcium indicator GCaMP6s floxed in the ROSA26 locus.[75] We crossed these mice with *Nkx2.1*-Cre mice and allowed the INs to develop for 4 months post-graft (MPG). Calcium imaging in MGE-derived INs, especially Pvalb-positive INs, is challenging due to Pvalb's role as a slow calcium buffer, which dampens calcium transients and complicates imaging.[76] Therefore, we concentrated our analysis on axodendritic processes, which serve as effective readouts of synaptic integration.[77] At baseline, without external stimuli, we observed strong calcium transients in the axodendritic processes (Figures 3G and S4C), suggesting spontaneous activity in grafted INs.

Finally, to evaluate the impact of mouse IN integration into human PN networks, we conducted calcium imaging in organoids grafted with *Nkx2.1*-Cre::Ai14 cells at 5 WPG. Control organoids, generated from the same batches, were not grafted with mouse INs. To label PNs, we utilized the Fluo-8 AM dye, which can be incorporated into both human and mouse neurons. In grafted organoids, we focused specifically on tdTomato-negative cells to target human PNs. Compared to non-grafted controls, which displayed minimal activity, the grafted organoids exhibited robust synchronous neuronal activity (Figures 3H, S4D, and S4E; Videos S1 and S2), as expected in networks containing active Pvalb-positive INs.[78,79] Altogether, these results show that grafted mouse INs successfully integrate into human PN networks within chimeric organoid models.

## Human cortical organoids recapitulate the accelerated Pvalb expression observed in organotypic cultures

To investigate whether human cortical organoids could recapitulate the accelerated Pvalb expression seen in organotypic cultures, we first analyzed the identity of INs at 2 DPG (equivalent to E15.5 in mouse *in vivo* development), a stage when the cells were still migratory (Figure 3B). Strikingly, approximately 50% of grafted INs were already positive for Pvalb at this early time point (Figures 4A and S5) (49.51 ± 6.11% Pvalb-positive, 0% Sst-positive, 0.40 ± 0.70% Pvalb and Sst double-positive, and 50.07 ± 6.67% double-negative).

We next examined the identity of grafted INs at later stages. Immunostaining for Pvalb and Sst at 7 DPG (equivalent to P0 in mouse *in vivo* development) revealed that 66.56 ± 4.38% of grafted INs expressed Pvalb (Figures 4B and S6), similar to

(D) Quantification of IN populations across mouse and human host environments. Unpaired parametric Student's t test without Welch's correction: ** = $p < 0.01$ and *** = $p < 0.001$. Error bars represent the standard error of the mean (SEM). $n = 535$ for cells grafted onto human organotypic slices and 264 for cells grafted onto mouse organotypic slices.

(E) Grafting of unlabeled MGE progenitors allows unbiased identification of Pvalb-positive INs. White arrows denote mouse nuclei, and yellow arrows point to adjacent human cells. Scale bars, 100 μm for the low magnification image and 10 μm for the high magnification images. See also Figures S1–S3.

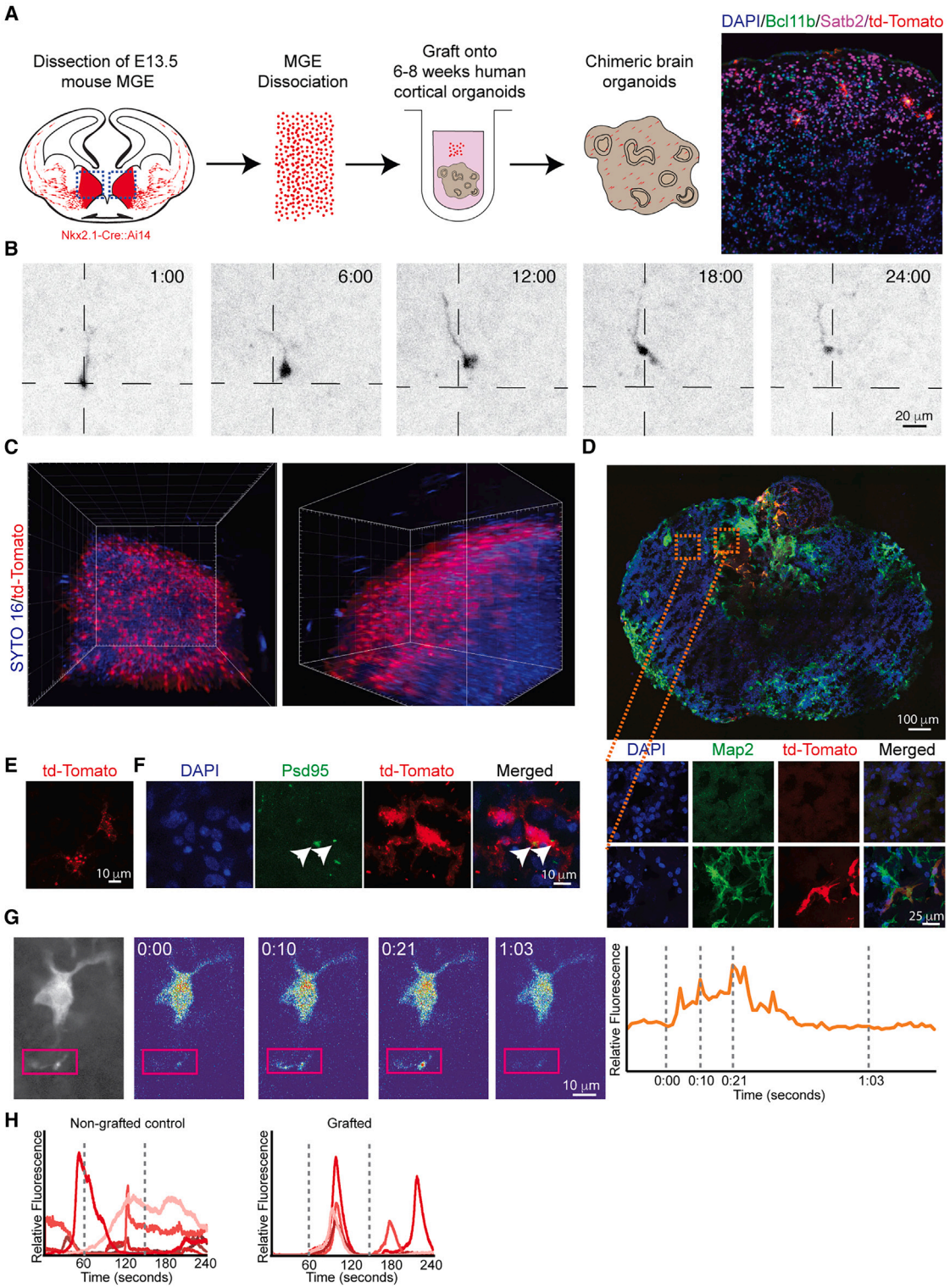


**Figure 3. Development of long-term chimeric organoid models**

(A) Experimental design: The MGE from mouse embryos at E13.5 is microdissected and grafted onto human organoids that are 6–8 weeks old.

(B) IN migration at 1 DPG: Longitudinal live imaging captures a representative migratory IN over a 24-h period. The cell soma's position 1 h after the experiment starts is marked for reference.

(C) Lightsheet imaging of a grafted organoid. SYTO 16 dye labels all nuclei within the organoid.

*(legend continued on next page)*

what we observed in mouse INs grafted onto human GW22 organotypic cultures (Figure 4C, $p > 0.05$). Notably, no cells expressed Sst alone; however, there was a modest but statistically significant increase in double-positive (Pvalb and Sst) cells compared to those grafted onto primary human organotypic cultures (Figure 4C, primary human = 0.98 ± 1.69%, organoid = 9.57 ± 4.29%; $p < 0.05$). The remaining 23.86 ± 8.67% of INs were negative for both markers, a proportion comparable to that seen in grafts onto organotypic slices (Figure 4C, $p > 0.05$). By 28 DPG (equivalent to P35 in mouse *in vivo* development), the percentage of Pvalb-positive INs had increased to 95.83 ± 7.22%, with no Sst-positive or double-positive cells (4.16 ± 7.21% double-negative) (Figure 4D). These findings indicate a progressive acquisition of the Pvalb expression in INs at a faster rate and higher proportion than expected during normal mouse development (Figure 4E), suggesting that the 3D human cortical tissue provides extrinsic cues that drive the fate of MGE progenitors.

To independently validate these results, we grafted INs from *Pvalb*-Cre mice[80] crossed with Ai14 reporter mice. Normally, Pvalb expression in these mice is not detectable until at least three weeks postnatally.[37] However, when these *Pvalb*-Cre::Ai14 INs were grafted onto human cortical organoids, we observed robust td-Tomato expression at 7 DPG, confirmed by immunostaining (Figure S7A). This independent approach further supports the accelerated Pvalb expression induced by the human cortical environment.

To assess whether this rapid Pvalb induction is specific to the human cortical environment or can be triggered by any 3D organoid context, we grafted genetically labeled mouse MGE cells onto mouse 3D organoid cultures. We generated mouse primary organoids by dissociating E14.5 mouse cortices and culturing them in neuronal differentiation media,[81] which produces cortical neurons of both upper and deep layer identities (Figures S7B and S7C). In these cultures, only 1.01 ± 0.43% of grafted INs were Pvalb-positive at 7 DPG. In contrast, 20.91 ± 1.61% of the grafted INs expressed Sst, while 78.07 ± 1.93% remained negative for both markers (Figures 4F and 4G). These results closely resembled those obtained from grafts onto primary mouse organotypic cultures (Figures 2D and S7D), suggesting that the mouse cortical environment does not induce accelerated Pvalb expression in mouse MGE cells.

At 28 DPG, a time equivalent to the peak of Pvalb expression *in vivo* (∼P35), we found that only 0.95 ± 1.65% of grafted INs in mouse organoids expressed Pvalb ($p > 0.05$ compared to 7 DPG). However, 28.97 ± 4.18% of the cells were Sst-positive, and 67.30 ± 1.09% remained double-negative ($p < 0.01$ compared to 7 DPG; Figures S7E and S7F) (Figure 4H).

Importantly, the Pvalb identity is retained in grafted INs at 2 MPG, a time point equivalent to adulthood in mice (Figure S7G). These results, combined with the differences in IN identities between mouse and human organoids and the progressive acquisition of Pvalb in human hosts (Figures 4E and S7F), suggest that environmental cues play a critical role in shaping IN identity.

## 3D human environment promotes additional features of Pvalb identity in mouse INs

Pvalb and Sst are terminal markers of distinct IN subtypes. Due to the differences in their developmental timelines, additional markers distinguishing these fates have been identified. Notably, the transcription factors *Mef2c* and *Nr2f2* (also known as *Coup-TF2*) play crucial roles. *Mef2c*, a marker of neuronal maturation[68] (Figure S8), is thought to identify early Pvalb-fated INs.[30,31] In contrast, *Nr2f2* promotes Sst identity and suppresses Pvalb fate within the MGE.[82] To investigate these markers, we quantified the percentages of Mef2c-positive and Nr2f2-positive INs at 7 DPG.

Before analyzing the organoids, we validated the Mef2c antibody, which had not been tested in neuronal tissue. We performed immunostaining in the developing cortex at embryonic day 15.5 (E15.5), focusing on the excitatory cortical lineage as an independent and well characterized system. In this lineage, Mef2c labels maturing neurons and is absent in progenitors and newborn neurons[2,5,68] (Figure S8A). In our validation, we find that Mef2c was excluded from Mki67-positive progenitors in the ventricular and subventricular zones but colocalized with Bcl11b (also known as Ctip2)-positive, maturing deep-layer PNs in the cortical plate (Figures S8B–S8D). These observations confirmed the specificity of the Mef2c antibody.

We then examined the grafted organoids and found that 90.38 ± 8.99% of mouse MGE-derived INs grafted onto human organoids upregulated Mef2c at 7 DPG (Figures 5A and S8E). This result aligns with the observed upregulation of Pvalb in INs within human 3D cultures. Conversely, no Mef2c-positive INs were found in grafts onto mouse organoids ($p < 0.0001$) (Figure 5A). In contrast, 25.26 ± 2.19% of INs grafted onto human organoids were Nr2f2-positive, whereas 90.09 ± 1.50% of INs in mouse organoids expressed Nr2f2 ($p < 0.0001$) (Figure 5B).

MGE-derived cells express *ErbB4* as they migrate to the cortex, but in mature cortical circuits, *ErbB4* is retained exclusively in Pvalb INs, not Sst INs.[55] Immunostaining for ErbB4 at 7 DPG

(D) INs localize to neuronal regions: grafted INs migrate toward neuronal regions of the organoid, marked by Map2 expression. Top: A whole section of the organoid. Scale bar, 100 μm. Bottom: comparison of Map2-poor and Map2-rich regions. Scale bar, 25 μm.

(E) Synaptic marker expression at 5 WPG: The *Nkx2.1*-Cre::Ai34 mouse line reveals strong Syp presence in grafted INs at 5 WPG, indicating the formation of presynaptic vesicles. Scale bar, 10 μm.

(F) Postsynaptic excitatory marker Psd95 puncta are detected in grafted INs (labeled with *Nkx2.1*-Cre::Ai14) at 5 WPG, suggesting afferent excitatory synapses. Scale bar, 10 μm.

(G) Calcium imaging at 4 MPG: using the *Nkx2.1*-Cre::Ai96 mouse line, axodendritic calcium transients are observed in grafted INs (highlighted by magenta rectangles). Scale bar, 10 μm.

(H) Calcium imaging at 5 WPG: using the Fluo-8 AM dye, we labeled both mouse and human neurons. Left: calcium transients observed in non-grafted control organoids. Right: calcium transients in tdTomato-negative cells within grafted organoids. Each colored line represents a distinct region of interest. See also Figure S4 and Videos S1 and S2.

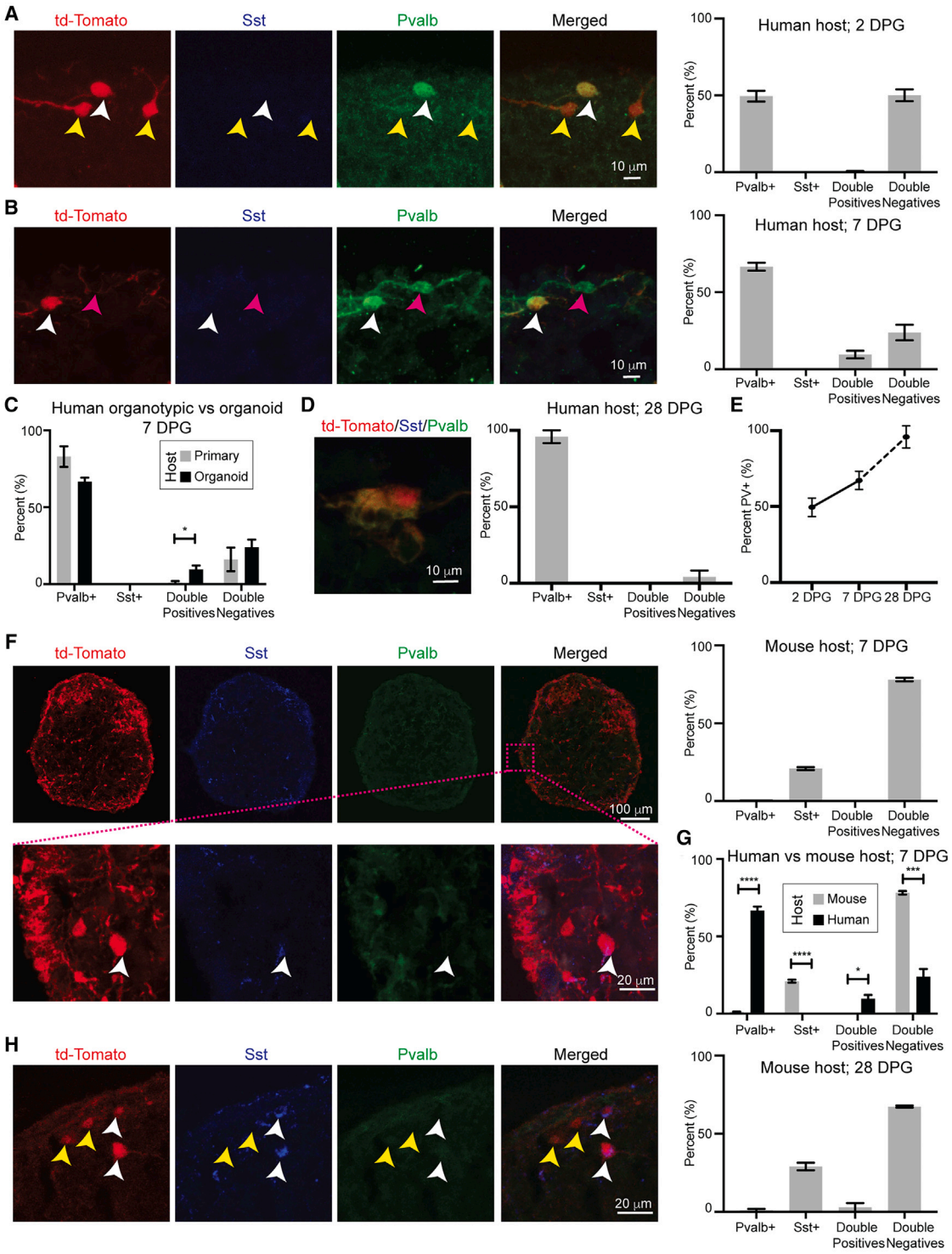


**Figure 4. Organoid models recapitulate species-specific biases in Pvalb and Sst expression in grafted INs**

(A–E) Grafting of mouse INs onto human organoids: (A) Representative image and quantification of grafted INs onto human organoids at 2 DPG. White arrow indicates a Pvalb-positive mouse IN. Scale bar, 10 μm. $n$ = 250 cells. Yellow arrows indicate Pvalb-negative mouse INs. (B) Representative image and quantification of grafted INs at 7 DPG. Scale bar, 10 μm. $n$ = 277 cells. The white arrow indicates a Pvalb-positive mouse IN, and the magenta arrow indicates an IN that did not express td-Tomato, likely representing a neuron that failed to recombine the td-Tomato gene. (C) Comparison of cell types generated at 7 DPG between primary human host cultures (gray) and human organoids (black). Data from Figures 2B and 4B are included. $n$ = 535 for cells grafted onto human organotypic

*(legend continued on next page)*

again revealed species-specific differences: 55.45 ± 7.49% of INs grafted onto human organoids expressed ErbB4, while only 4.95 ± 1.76% of INs grafted onto mouse organoids were positive for this marker ($p < 0.001$) (Figure 5C).

Previous studies showed that a subset of Pvalb-positive INs also express *Bdnf*,[83,84] while no other IN subtype is known to produce Bdnf. Bdnf regulates the maturation of Pvalb INs.[85] Cortical organoids rarely express this gene,[67,68,86] and our organoid protocol does not add exogenous Bdnf (see method details). We therefore performed immunostaining for Bdnf and HNA in human cortical organoid containing mouse IN at 8 WPG to distinguish the species of the Bdnf expressing cells. We found extensive Bdnf expression in grafted organoids, but only in HNA-negative (mouse) cells, confirming that the Bdnf-expressing cells were of mouse origin (Figure 5D).

Next, we analyzed perineuronal nets (PNNs), extracellular matrix structures that preferentially ensheath Pvalb INs, facilitating their maturation and regulating circuit plasticity.[87] PNNs are influenced by surrounding neurons, including PNs and Pvalb-negative INs.[88] Col19A1, a gene involved in PNN regulation, is highly expressed in mature neurons of cortical organoids[68] and in developing deep-layer PNs in the human prefrontal cortex.[5] The earliest detectable PNNs in the mouse cortex typically emerge around postnatal days 7–10 and continue developing until 4–5 weeks of age.[89] To assess PNN formation around grafted INs, we used biotin-conjugated Wisteria floribunda agglutinin (WFA), a specific marker that binds N-acetylgalactosamines in PNNs. Remarkably, we observed the initial appearance of PNNs as early as 2 DPG, which corresponds to E15.5 in mouse development (Figure S9A). Over time, PNN formation around the grafted INs progressively increased, culminating in robust WFA labeling by 5 WPG (Figures 5E and S9). These findings suggest that the human organoid environment effectively supports the maturation and integration of PNNs around grafted INs.

Finally, we measured the soma size of grafted INs in both mouse and human hosts, as neuronal size is often correlated with identity.[16] Pvalb-positive INs are among the largest IN subtypes in the cortex.[90,91] We observed that INs grafted onto mouse organoids had an average soma area of 128.33 ± 65.90 $\mu m^2$, whereas those grafted onto human organoids were significantly larger, with an average soma size of 207.33 ± 39.03 $\mu m^2$ (Figure 5F). This is consistent with previous measurements of mouse IN populations.[91]

In conclusion, alongside the upregulation of Pvalb, Mef2c, ErbB4, and Bdnf, the downregulation of Nr2f2 and Sst, the assembly of PNNs, and the increase in cell size, our data indicate that the 3D human cortical environment induces multiple features of Pvalb identity in mouse-derived INs.

## Human 3D cortical environment is necessary for Pvalb induction in mouse INs

To determine whether the 3D cortical environment is not only sufficient but also necessary for instructing Pvalb fate in MGE progenitor short-term graft models, we co-cultured mouse MGE progenitors with dissociated cortical cells from E14.5 mice and GW22 human hosts in a 2D setting. After 7 days in culture (DIC), we analyzed the identity of the grafted cells using immunostaining. Unlike the 3D human environment in organotypic or organoid cultures, no Pvalb-positive INs were observed in these 2D co-cultures. Furthermore, Sst expression varied depending on the condition: co-culturing with mouse cortical cells resulted in 25.85 ± 4.93% Sst-positive INs, while co-culturing with human cortical cells led to a 1.7-fold increase, with 40.61 ± 4.94% Sst-positive INs ($p < 0.01$) (Figure 6A).

Given that the 2D co-culture with human cortical cells produced a higher proportion of Sst-positive INs, we questioned whether this increase was driven by direct cell-to-cell interactions or diffusible signals. To explore this, we cultured mouse MGE progenitors in media conditioned by primary human cortical cells grown in 2D. After 7 DIC, the percentage of Sst-positive INs was similar between cells grown in conditioned media and those co-cultured directly with primary human cells (37.49 ± 5.08% Sst-positive INs, $p > 0.05$) (Figures 6B and S10). This suggests that the Sst induction observed in 2D co-cultures was mediated by diffusible factors in the media.

We then examined whether the specification of Pvalb-positive INs in our chimeric grafts required a cortical environment, or if Pvalb could be upregulated in other 3D human brain contexts. To address this, we grafted mouse MGE INs onto human MGE and thalamic organoids. MGE organoids served as a control for matching the regional identity of the INs' birthplace, while thalamic organoids represented a nearby region where MGE-derived INs typically do not migrate[92] (Figures S11A and S11B). The outcomes were markedly different: at 7 DPG, grafting mouse MGE INs onto human MGE organoids resulted in 51.78 ± 3.03% Sst-positive INs, with no cells expressing Pvalb alone. However, 1.07 ± 1.87% of the cells co-expressed both Pvalb and Sst (Figures 6C, 6D, S11C, and S11D). In contrast, most INs grafted onto thalamic organoids died shortly after grafting (Figure 6C). Together, these findings indicate that the 3D human cortical environment is essential for the early induction of Pvalb markers in grafted mouse INs.

## Human INs do not upregulate Pvalb shortly after being grafted onto human cortical organoids

Given the rapid upregulation of Pvalb observed in mouse INs grafted onto human cortical organoids, we next investigated whether grafting human INs would produce a similar effect. Previous studies involving the fusion of cortical and ventral

slices and $n = 277$ for cells grafted onto human organoids. (D) Representative image and quantification of grafted INs onto human organoids at 28 DPG. Scale bar, 10 μm. $n = 166$ cells. (E) Progressive acquisition of Pvalb expression in INs over time in human organoid hosts.
(F–H) Grafting of mouse INs onto mouse organoids: (F) Representative image and quantification of grafted INs onto mouse organoids at 7 DPG. Scale bars, 100 μm for the low magnification images and 20 μm for the high magnification images. $n = 189$ cells. (G) Comparison of IN populations generated in mouse (gray) versus human (black) organoid hosts at 7 DPG. Data from Figures 4B and 4F. $n = 277$ cells for grafts onto human organoids and $n = 189$ cells for grafts onto mouse organoids. (H) Representative image and quantification of grafted INs onto mouse organoids at 28 DPG. Scale bar, 20 μm. $n = 248$ cells. Unpaired parametric Student's t test without Welch's correction: * = $p < 0.05$; *** = $p < 0.001$; **** = $p < 0.0001$. Error bars represent SEM. See also Figures S5–S7.

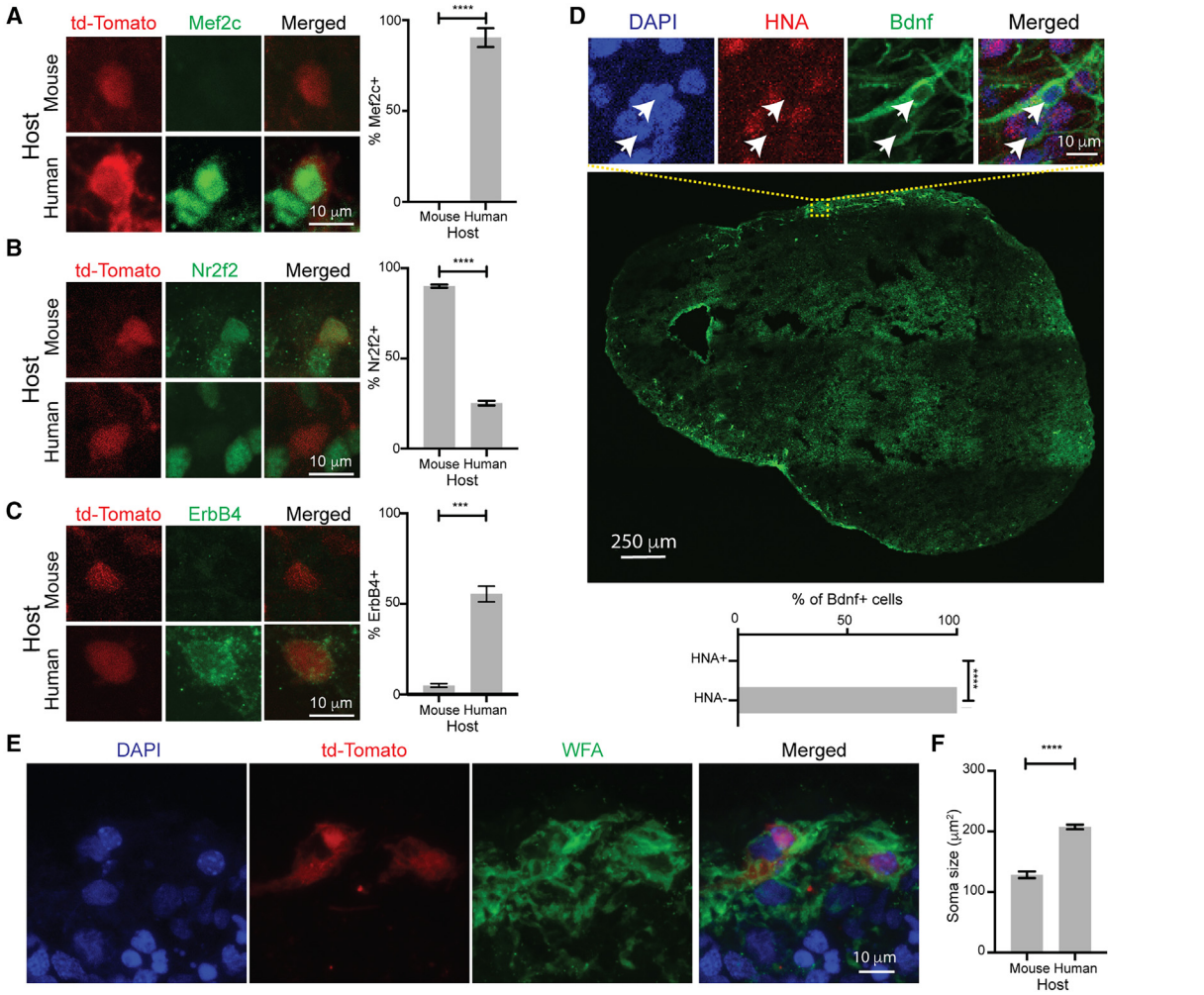


**Figure 5. Human cortical organoids influence multiple aspects of Pvalb IN identity**

(A) Representative images and quantification of Mef2c expression in INs grafted into mouse and human organoids at 7 DPG. Scale bar, 10 μm. *n* = 282 cells for grafts onto mouse organoids and *n* = 252 cells for grafts onto human organoids.

(B) Representative images and quantification of Nr2f2 expression in INs grafted into mouse and human organoids at 7 DPG. Scale bar, 10 μm. *n* = 189 cells for grafts onto mouse organoids and *n* = 327 cells for grafts onto human organoids.

(C) Representative images and quantification of ErbB4 expression in INs grafted onto mouse and human organoids at 7 DPG. Scale bar, 10 μm. *n* = 254 cells for grafts onto mouse organoids and *n* = 208 cells for grafts onto human organoids.

(D) Representative image showing Bdnf and HNA staining in human organoids at 8 WPG. Scale bars, 250 μm for the low magnification image and 10 μm for the high magnification images. All Bdnf-positive cells were HNA-negative, indicating they were not of human origin. *n* = 323 cells.

(E) Labeling of PNNs with biotinylated WFA in human organoids at 5 WPG. Scale bar, 10 μm.

(F) Comparison of the soma size of INs grafted into mouse versus human organoid hosts. *n* = 107 cells for grafts onto mouse organoids and *n* = 118 for grafts onto human organoids. Unpaired parametric Student's t test without Welch's correction: *** = $p < 0.001$; **** = $p < 0.0001$. Error bars represent SEM. See also Figures S8 and S9.

organoids reported Pvalb upregulation only after several months in co-culture and at low efficiency.[93,94] This delayed response may be attributed to the slower developmental timeline of human INs or to missing conditions during iPSC-derived IN induction that could bias differentiation away from a Pvalb identity.

To minimize potential biases in iPSC induction, we grafted primary IN progenitors microdissected from the MGE of three different GW18-19 donors onto human cortical organoids (Figure S12A). GW18-19 represents the peak of IN neurogenesis in the human MGE.[95] The grafted cells were labeled using an adenovirus expressing eGFP under the CMV promoter. Immunolabeling of grafted cells 7 DPG revealed that 99.87 ± 0.34% of eGFP+ cells were negative for both Sst and Pvalb (Figures S12B and S12C). Instead, the cells were positive for the neuronal progenitor marker Nestin[32] (Figure S12D), indicating that the grafted human cells remained undifferentiated. Although we cannot rule out Pvalb upregulation at later time points, we conclude that the early (< 7 DPG) upregulation of Pvalb is specific to mouse INs. This aligns with recent findings indicating that human MGE-derived INs require at least 3–4 months in

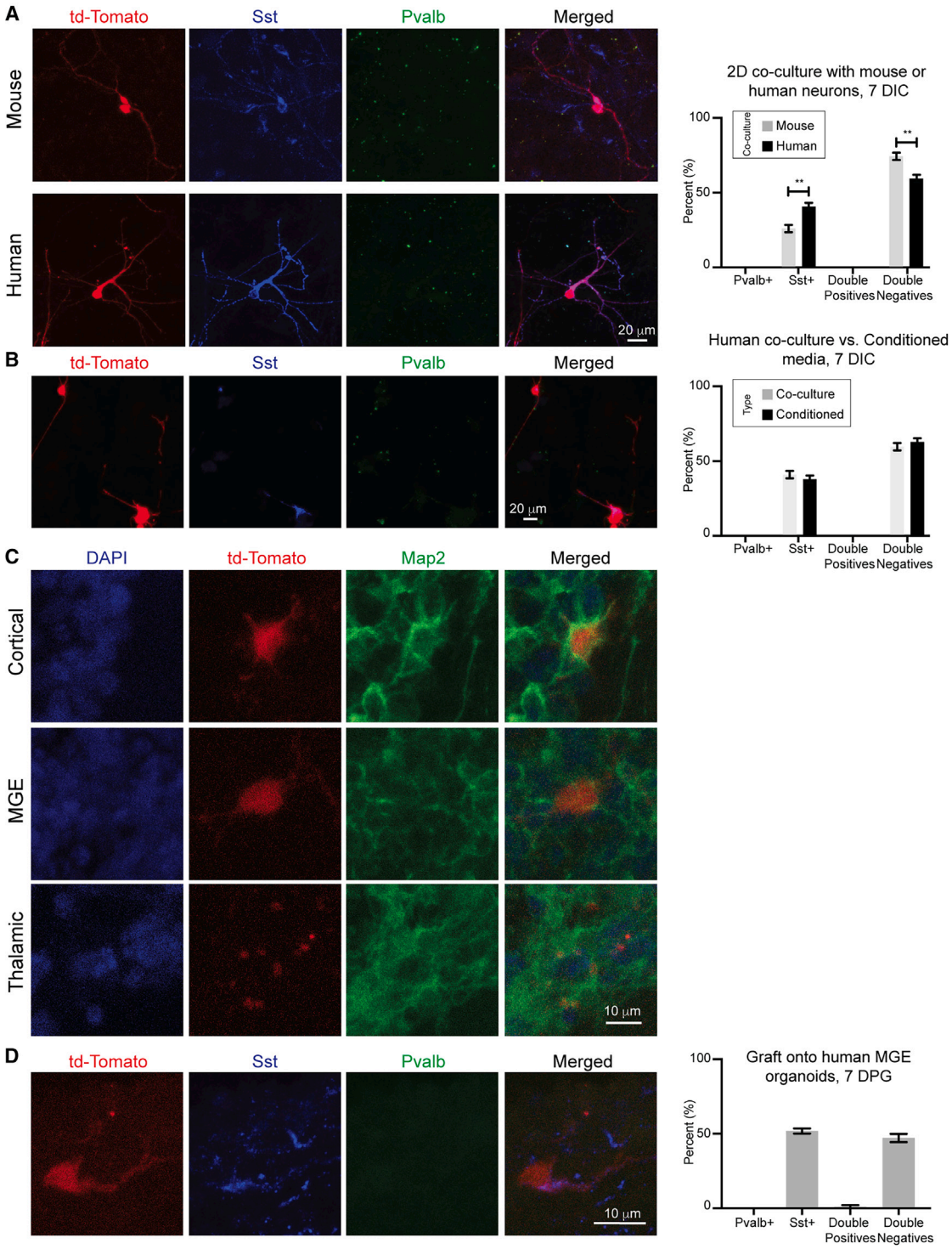


**Figure 6. Non-3D human cortical models do not instruct Pvalb fate**

(A) Representative images and quantification of INs co-cultured with primary mouse and human cortical cells. Scale bar, 20 μm. $n = 364$ cells for co-cultures with mouse cells and $n = 437$ cells for co-cultures with human cells. No Pvalb-positive INs were observed at 7 DIC.

(B) Representative images and quantification of INs cultured in media conditioned by primary human cortical cells at 7 DIC. Scale bar, 20 μm. Human co-culture results are the same as in 6A. $n = 437$ cells for co-cultures with human cells and $n = 212$ cells for conditioned media.

*(legend continued on next page)*

co-culture with PNs to upregulate Pvalb,[94,96] a timeline still more rapid than that of human development (Figure S1).

### Non-cell-autonomous regulation of Pvalb fate

We next investigated whether non-cell-autonomous factors could influence Pvalb fate acquisition. We first focused on modifying the media composition, specifically the removal of fetal bovine serum (FBS), which is known to contain a complex mixture of nutrients that activate various signaling pathways, including those essential for neuronal maturation.[97–99] We hypothesized that removing FBS from the differentiation protocol might affect maturation, including the induction of Pvalb in grafted mouse INs. To explore this, we generated human cortical organoids under FBS-free conditions and grafted them with mouse INs (see method details). At 45 DIC, we confirmed the presence of corticofugal and early-born callosal PNs in these organoids (Figure S13). We analyzed the identity of the INs at 14 DPG (Figures S14 and 15). Notably, while these INs expressed several markers associated with Pvalb identity, including *Mef2c*, *ErbB4*, and the recently identified *Cox6A2*,[100] they maintained an immature phenotype and did not express *Pvalb* itself (Figures S14B–S14F).

FBS regulates numerous pathways, including the mammalian target of rapamycin (mTOR) pathway,[101] which has been implicated in the specification of Pvalb-positive INs.[19,91,102–106] Specifically, activation of the mTOR pathway, such as through the knockout of its upstream inhibitor *Tsc1* in MGE-derived INs, has been shown to modestly but significantly increase the number of Pvalb-positive INs in the mouse brain.[91] In addition, mTOR has been shown to mediate PN-Pvalb IN connectivity.[103] Therefore, we next assessed the mTOR pathway's role in Pvalb fate acquisition. We hypothesized that inhibiting mTOR activity with high concentrations (250 nM) of rapamycin would reduce the number of Pvalb-expressing INs in human cortical organoids. To test this, organoids cultured under the original conditions (with FBS) were treated with rapamycin for 14 days starting on the day of grafting, while control organoids received vehicle treatment (Figure 7A). mTOR activity was assessed by immunostaining for phosphorylated ribosomal protein S6 (pS6), a downstream marker of mTOR signaling and a well-established indicator of Pvalb fate in MGE-derived INs.[91] In the control group, 90.00 ± 8.82% of grafted INs were pS6-positive at 14 days post-grafting (DPG) (Figure 7B), consistent with earlier results (Figures 4 and 5). Surprisingly, 85.78 ± 12.84% of rapamycin-treated grafted INs also showed pS6 positivity ($p > 0.01$) (Figure 7B), indicating that phosphorylation of S6 in grafted MGE-derived INs was resistant to rapamycin inhibition.

Typically, ERK/Mapk activity is low in INs compared to PNs.[107] The rapamycin-resistant pS6 expression observed in the grafted INs could potentially result from upregulation of the ERK/Mapk pathway.[108,109] Prior studies have shown that hyperactivation of ERK/Mapk in the MGE selectively reduces Pvalb-positive INs while leaving Sst-positive INs unaffected.[107] To explore this possibility, we quantified phosphorylated ERK1/2 (pERK) levels in both control and rapamycin-treated organoids at 14 DPG. The overall percentage of INs expressing pERK was low and did not differ significantly between control and rapamycin-treated groups (11.69 ± 4.36% in controls vs. 14.04 ± 4.35% in rapamycin-treated organoids, $p > 0.05$) (Figure S16A). These findings suggest that the observed pS6 expression is not due to aberrant ERK/Mapk activation following rapamycin treatment.

The developing human cortex is known to have high mTOR activity in the PN lineage,[5,110] a pattern also observed in organoid models.[68,110] Consistent with our previous work,[68,110] we found that rapamycin treatment nearly eliminated pS6 expression in the host cells, with only 1.82 ± 1.34% of rapamycin-treated cells showing pS6 positivity, compared to 31.39 ± 9.39% in controls ($p < 0.01$) (Figure S16B). It is well established that mTOR inhibition in the PN lineage affects the morphology and connectivity of postmitotic PNs.[111–113] This differential response—grafted INs being resistant to rapamycin while host PNs were sensitive—allowed us to examine the impact of PN lineage manipulation on the acquisition of Pvalb fate in grafted INs. At 14 DPG (equivalent to P21 in mouse *in vivo* development), 71.66 ± 2.91% of grafted INs in control organoids were Pvalb-positive, consistent with our earlier observation of progressive Pvalb fate acquisition (Figure 4E). However, in rapamycin-treated organoids, only 7.69 ± 6.67% of grafted INs expressed Pvalb ($p < 0.001$), with 84.62 ± 13.34% of INs negative for both Pvalb and Sst (Figure 7C). These results suggest that mTOR inhibition in PNs significantly influences Pvalb specification in INs.

Lastly, while pS6 is the most common readout of mTOR activation, rapamycin may also target alternative mTOR-dependent pathways. For example, mTOR regulates 4E-BP2 independently of pS6 activation.[114] Although 4E-BP2 is essential for proper Pvalb IN function,[104] its role in Pvalb IN fate specification remains unclear. Notably, deleting 4E-BP2 in MGE progenitors or INs does not alter neuronal subtype distribution in the brain.[104] To investigate mTOR's role in Pvalb induction via non-cell-autonomous mechanisms, we treated human cortical organoids with 250 nM rapamycin for 7 days before grafting and discontinued treatment upon IN grafting (Figures S17A and S17B). This treatment abolished pS6 expression in nearly all cells (Figure S17B). Consistent with prior studies,[115] pS6 expression began to recover within 2 days of rapamycin withdrawal (Figure S17B), prompting us to focus on 2 DPG as a critical timeline for assessing mTOR's influence on fate specification. Under these conditions, 94.99 ± 6.88% of grafted INs were negative for both Pvalb and Sst, while 4.22 ± 5.76% upregulated Sst, and only 0.79 ± 1.25% upregulated Pvalb (Figures S17C–S17E). These findings suggest that Pvalb fate specification observed in our model is predominantly governed by non-cell-autonomous mechanisms dependent on mTOR activity in host cells.

(C) Representative images of INs grafted onto cortical, MGE, and thalamic organoids. MAP2, a pan-neuronal marker, is used for reference. Scale bar, 10 μm.
(D) Representative images and quantification of INs grafted into human MGE organoids at 7 DPG. Notably, additional Sst-positive cells from the host organoid were observed. Scale bar, 10 μm. $n = 202$ cells. Unpaired parametric Student's t test without Welch's correction: ** = $p < 0.01$. Error bars represent SEM. See also Figures S10–S12.

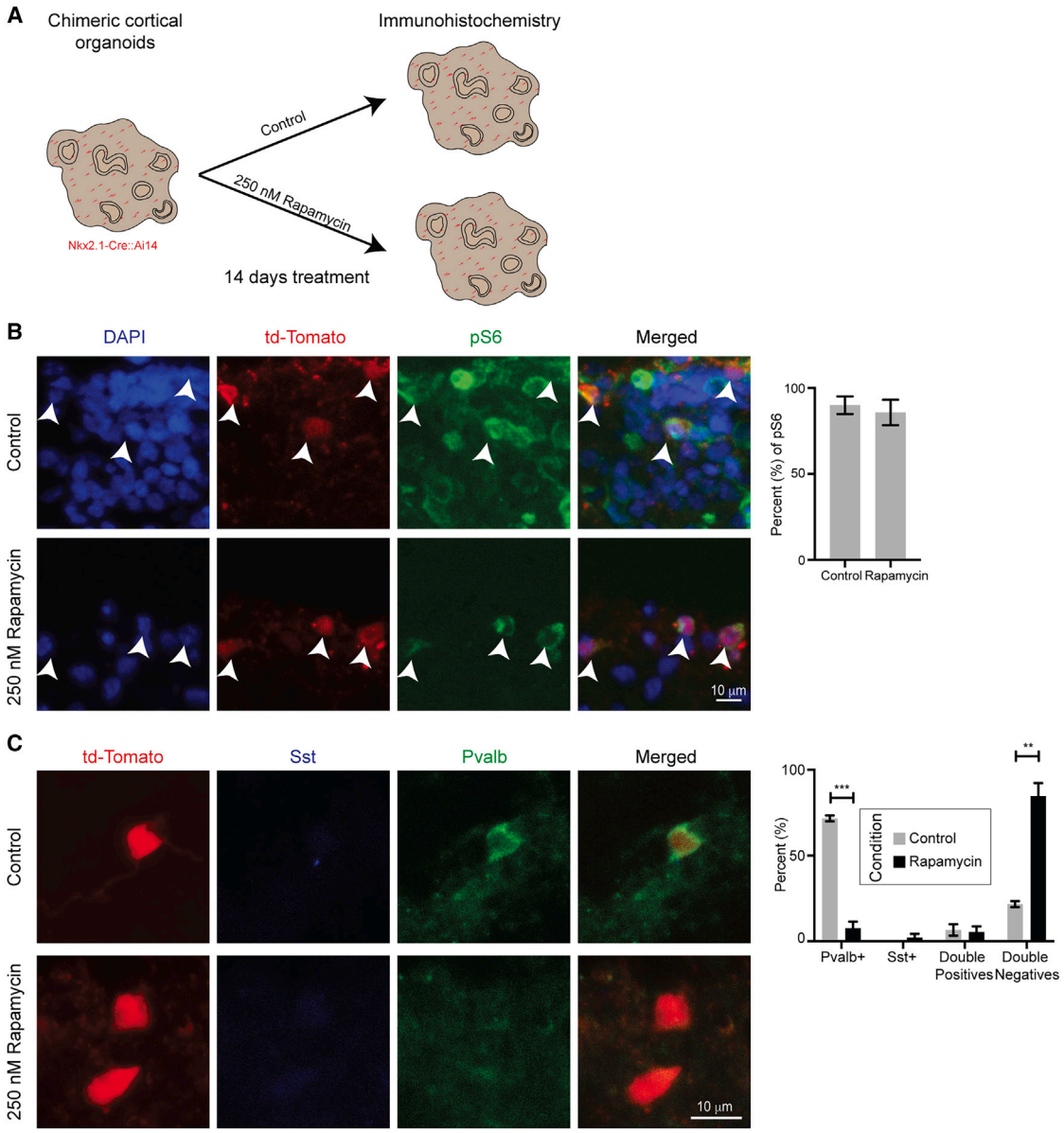


**Figure 7. Inhibition of the mTOR pathway in PNs reduces Pvalb specification**

(A) Experimental design: Chimeric cortical organoids were treated with either 250 nM Rapamycin or a vehicle (control) starting at the time of grafting and continuing for 14 days.

(B) Representative images and quantification of phosphorylated ribosomal protein S6 (pS6) in both control and rapamycin-treated organoids at 14 DPG. White arrows indicate INs positive for both td-Tomato and pS6. Scale bar, 10 μm. $n = 245$ cells for control organoids and $n = 342$ cells for rapamycin-treated organoids.

(C) Comparison of IN subtypes in control versus Rapamycin-treated organoids. Scale bar, 10 μm. $n = 182$ for control organoids and $n = 210$ for rapamycin-treated organoids. Unpaired parametric Student's t test without Welch's correction: ** = $p < 0.01$; *** = $p < 0.001$. Error bars represent SEM. See also Figures S13–S17.

## Early postmitotic Sst-positive INs can be induced to upregulate Pvalb

*In vivo* lineage reprogramming experiments in mouse cortical PNs have shown a progressive loss of fate plasticity as neurons develop and mature, with a sharp decline shortly after neurons become postmitotic.[16,116–118] However, whether similar mechanisms to preserve cell fate occur in INs and whether these mechanisms are intrinsic and universal throughout the central nervous system remains unclear.[119] To address this, we asked whether postmitotic, lineage-traced Sst-positive INs could be induced to upregulate Pvalb after grafting into a human cortical organoid.

We utilized the well-characterized *Sst-Cre* mouse, which expresses Cre recombinase specifically in postmitotic Sst INs with minimal leakage into other IN subtypes.[91,120] By crossing this mouse with the *Ai14* reporter mouse, we were able to label postmitotic Sst INs during embryonic development.[91,120] We

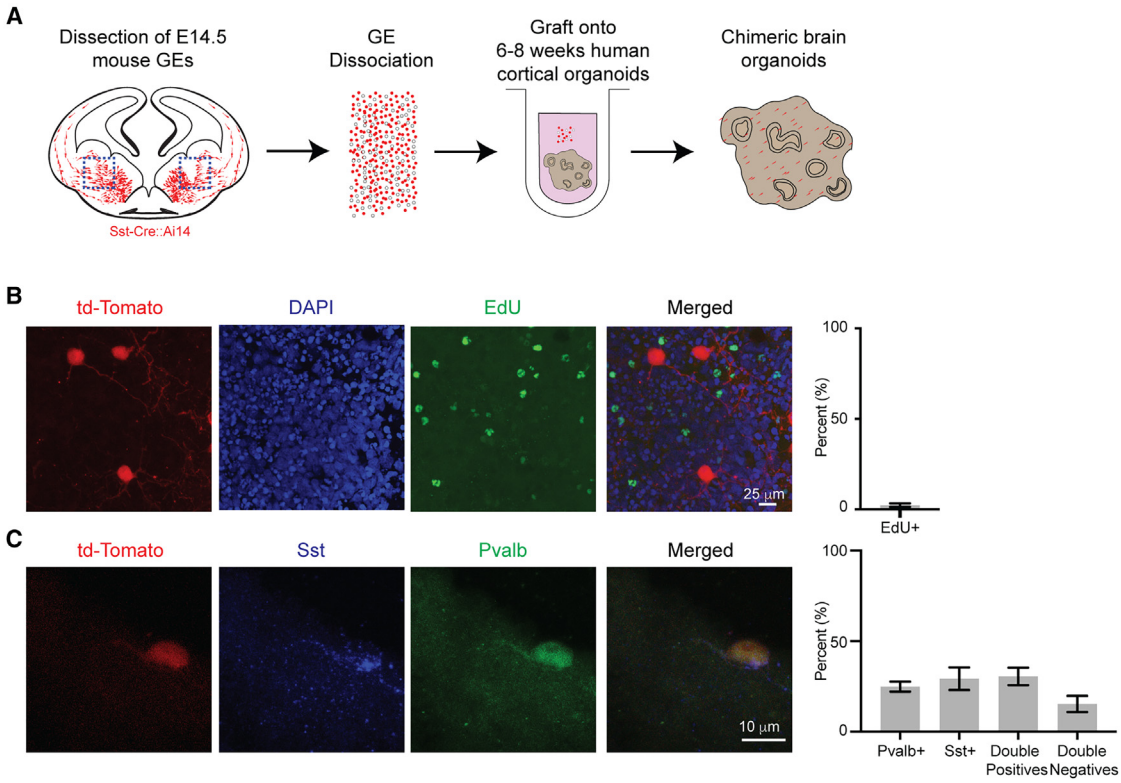


**Figure 8. Induction of Pvalb in early postmitotic Sst-positive INs**

(A) Experimental design: The entire ventral telencephalon was dissected, dissociated into single cells, and grafted onto human brain organoids.

(B) Representative image and quantification from an EdU incorporation assay, showing the postmitotic state of grafted INs. Scale bar, 25 μm. *n* = 332 cells.

(C) Representative image and quantification of the identity of grafted INs at 14 DPG in human organoids. Scale bar, 10 μm. *n* = 199 cells. See also Figure S18.

modified our protocol to enrich this population (Figure 8A): (1) Dissections were performed at E14.5, when Sst-positive INs have acquired their identity[26]; and (2) as postmitotic INs are highly migratory, we dissected the entire ventral telencephalon to account for migrating INs en route to the cortex.

To confirm the postmitotic state of the grafted cells, we treated them with 5-ethynyl-2′-deoxyuridine (EdU) immediately after grafting and for 2 days. EdU, a thymidine analog, is incorporated into the DNA of dividing cells. Analysis of EdU incorporation at 14 DPG confirmed that only 2.31 ± 3.05% of grafted cells were EdU-positive, indicating that the vast majority of *Sst*-Cre::Ai14 cells were postmitotic at the time of grafting (Figure 8B).

Next, we performed immunostaining for Pvalb and Sst at 14 DPG (Figures 8C, 8D, and S18A). We observed that only about one-third (29.28 ± 13.99%) of the grafted *Sst*-Cre::Ai14 INs were positive for Sst alone (Figure 8C). Conversely, half of the grafted INs were immunopositive for Pvalb, with 24.89 ± 6.18% positive for Pvalb alone, and 30.51 ± 10.79% double-positive for both Pvalb and Sst (Figure 8C). In contrast, when grafted into mouse organoids, most INs (66.13 ± 3.17%; $p < 0.001$) preserved their Sst-positive identity, indicating maintenance of cell fate. Pvalb expression was infrequent, with only 0.92 ± 0.82% of cells being Pvalb-positive and 0.38 ± 0.66% exhibiting both Pvalb and Sst expression. The remaining cells (28.90 ± 3.10%) were double-negative (Figures S18B and S18C). These results contrast sharply with those obtained using *Nkx2.1*-Cre::Ai14 progenitors, which predominantly gave rise to Pvalb+ INs, with minimal overlap between the two markers (Figures 9A and 9B). Considering the distinct populations of Sst-positive and Pvalb-positive INs generated when *Nkx2.1*-Cre::Ai14 or *Sst*-Cre::Ai14 donor lines are grafted into human organoid hosts (Figures 9A and 9B), we conclude that INs exhibit a progressive restriction in their cell fate plasticity. Remarkably, however, over half of the grafted postmitotic Sst-positive INs were still capable of up-regulating Pvalb, despite having already expressed Sst. Given that leakage of the *Sst-Cre* mouse into Pvalb INs is less than 10%[91] and that the co-localization of Pvalb and Sst is rare in the cerebral cortex,[91,121,122] these results reveal an unexpected level of plasticity in the fate of cortical INs.

## DISCUSSION

*In vitro* studies have offered valuable insights into the genetic mechanisms regulating neuronal differentiation. For example, both primary and ES-derived cortical progenitors cultured *in vitro* have been shown to generate PNs in a sequential manner, with deep-layer neurons emerging before upper-layer neurons, closely mimicking *in vivo* development.[123,124] Moreover, ES-derived PNs retain their areal identity, and when grafted, they selectively integrate into cortical regions that match their

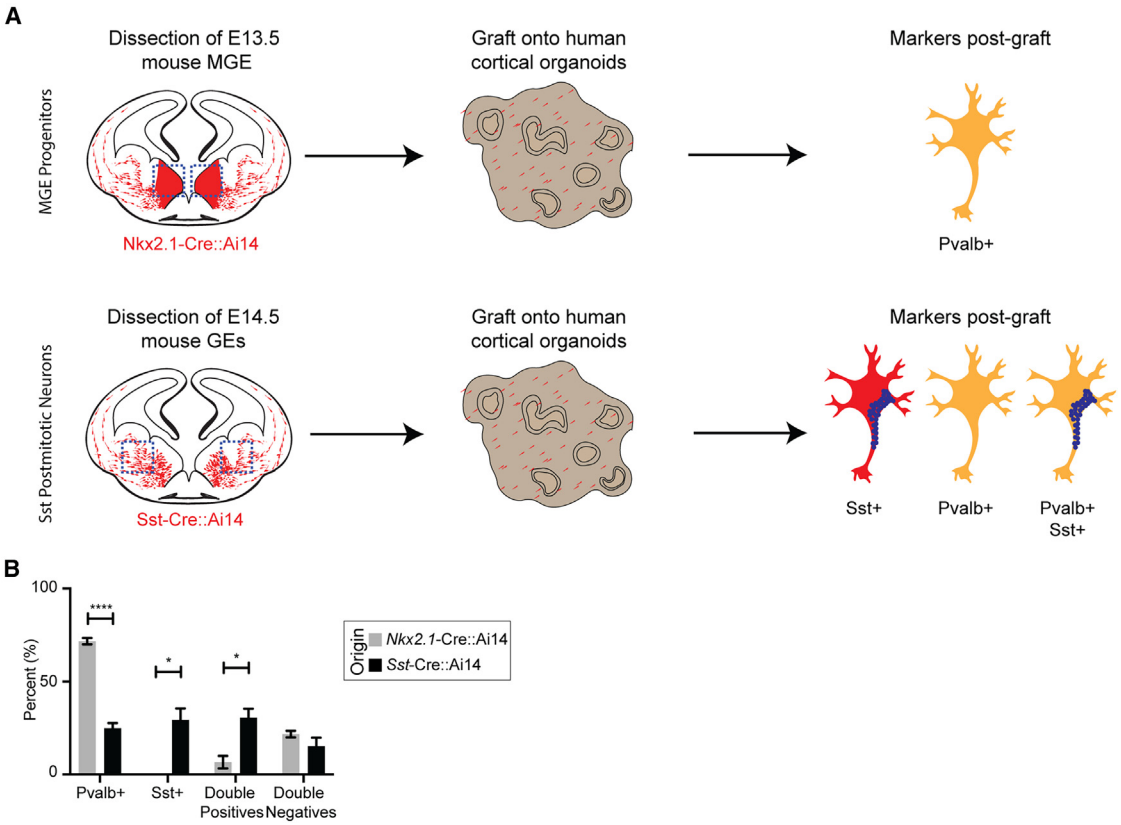


**Figure 9. Comparison of Pvalb and Sst upregulation in progenitor vs. postmitotic IN grafts at 14 DPG**

(A) Schematic representation of the experimental results. Top: grafting mouse E13.5 IN progenitors and early postmitotic INs onto human cortical organoids results in the upregulation of Pvalb in the majority of grafted cells. Bottom: grafting mouse E14.5 lineage-traced Sst INs results in INs expressing either Sst, Pvalb, or co-expressing both markers (Sst/Pvalb double-positive). Note: In both experiments, a minority of INs were double-negative for Sst and Pvalb.

(B) Comparison of cell types generated at 14 DPG in organoids grafted with either E13.5 *Nkx2.1*-Cre::Ai14 (progenitor origin; same as control in Figure 7C) or E14.5 *Sst*-Cre::Ai14 (postmitotic origin; same as Figure 8C) grafts. $n = 182$ cells for E13.5 *Nkx2.1*-Cre::Ai14 and $n = 332$ cells for E14.5 *Sst*-Cre::Ai14. Unpaired parametric Student's t test without Welch's correction: * = $p < 0.05$; **** = $p < 0.0001$. Error bars represent SEM.

origin.[125] These observations suggest that intrinsic factors predominantly control the specification of PN subtypes. MGE progenitors and Sst-positive INs have also been successfully differentiated from pluripotent stem cells in both 2D and 3D cultures. However, Pvalb-positive INs are observed at much lower frequencies *in vitro*.[3,93,94,126–134] The percentage of Pvalb-positive INs can be increased by co-culturing with PNs over extended periods,[3,93,94,126,128,129] suggesting that interactions with PNs may contribute to Pvalb identity specification. Consistent with this, we observed that grafting mouse MGE progenitors onto human MGE organoids did not induce Pvalb expression (Figure 6), whereas grafting them into human cortical hosts led to a significant upregulation of Pvalb (Figures 2 and 4). These results suggest that the local environment enhances maturation of INs and acquisition of the full phenotypic characteristics.[96]

Modulation of Pvalb identity has been previously observed in heterochronic transplantation studies. However, the appearance of Pvalb-positive cells was delayed, and the proportion of Pvalb-positive INs was lower than expected. For example, when MGE progenitors were grafted into the visual cortex of juvenile mice, the majority differentiated into Sst-positive INs, with only ~30% adopting a Pvalb fate after one month.[40] Grafting the same progenitors into the adult mouse visual cortex slightly increased the proportion of Pvalb-positive INs to ~40%, while ~20% became Sst-positive.[135] Notably, grafting MGE progenitors into the adult hippocampus reduced Pvalb expression to ~10%, with most cells adopting an Sst fate.[136] These findings suggest two possible explanations: either a previously underappreciated degree of fate plasticity in MGE progenitors influenced by the surrounding environment, or a cell-type-specific pattern of apoptosis. Supporting the notion of environmental induction of IN fate, previous work has shown that heterotopic transplantation of early postnatal cortical INs into the hippocampus results in approximately 37% of transplanted INs maturing into nNOS-positive INs, a subtype rarely observed in the cerebral cortex.[24]

In this study, we identified environmental conditions that promote rapid and extensive differentiation of MGE progenitors into Pvalb-positive INs. These INs developed further characteristics of Pvalb identity, including the expression of additional molecular markers, the loss of Sst markers, an increase in soma size, and the formation of PNNs surrounding their soma. Furthermore, we showed that approximately 50% of lineage-traced, early

postmitotic Sst-positive INs can upregulate Pvalb when grafted into a human cortical environment (Figures 8 and 9). This finding is reminiscent of the PN lineage, where overexpression of *Fezf2* in early postmitotic callosal PNs induced corticofugal molecular programs in ~50% of the overexpressing cells.[16,117] However, in contrast to PNs, where *Fezf2* fails to alter fate in adult neurons,[117] MGE-derived postmitotic INs may retain plasticity in their differentiation potential into adulthood.[137] Fate plasticity has also been suggested in other interneuron populations. For example, sensory input has been shown to induce a neurotransmitter switch between Sst-positive and dopaminergic interneurons in the adult hypothalamus,[138,139] and a similar transition has been speculated to occur in primate INs.[140–142] Additionally, increased colocalization of the CGE-associated protein calbindin and Pvalb in humans has been proposed as a cortical specialization.[143] Recent scRNA-seq data have revealed extensive colocalization of neurotransmitters in INs across species and transcriptional similarities between cortical Pvalb and Sst INs.[144–146] However, the fast and direct transition between these IN cell types has not been previously shown.

It is generally believed that neurons of the central nervous system possess an intrinsic maturation clock that resists acceleration by external factors, such as developmental cues or the electrophysiological properties of cortical PNs.[43,44,147] However, it has been shown that Pvalb-positive IN differentiation and maturation can be influenced by sensory input, neuronal activity, or molecular signals.[37,85,137,148] Our findings align with this concept: Pvalb and other markers of this IN subtype were rapidly upregulated in mouse MGE cells after grafting onto human organoids, occurring weeks earlier than expected based on *in vivo* timelines (Figures 4 and 5). These results suggest that neuronal differentiation and maturation may be accelerated in certain contexts,[50,149] at least for this particular IN subtype. Chimeric models, such as the ones we described here, offer powerful tools for studying the non-cell-autonomous regulation of neuronal development and maturation, with implications for understanding neurodevelopmental processes, evolution, and disease.[49]

The *in vitro* generation of several neuronal subtypes, besides Pvalb INs, has proven challenging. While cortical organoids contain radial glia, which theoretically should generate all excitatory neurons subtypes, specific neurons like layer 4 granular neurons and layer 5 Von Economo and Betz cells have yet to be observed in these models.[67,68,86] The differentiation of layer 4 granular neurons seems to rely on thalamic input,[22,150,151] and similarly, mature excitatory input from PNs is believed to regulate Pvalb expression in INs.[18,19,152] Interestingly, in our chimeric cultures, we observed a significant upregulation of Pvalb in grafted mouse INs despite the immaturity of the host human PNs, with this upregulation occurring well before mature electrophysiological activity was detected in either human[132,133,153] or mouse[81,154–157] 3D *in vitro* cortical models. This suggests that mature PN electrophysiological activity likely did not drive Pvalb induction in these experiments. Moreover, it seems improbable that diffusible factors alone triggered Pvalb fate induction, as neither 2D co-culture with human PNs nor conditioned media exposure resulted in significant Pvalb upregulation (Figure 6). Interestingly, we noted a reduced proportion of Sst-positive INs in co-culture with mouse PNs, compared to those cultured with human PNs or exposed to conditioned media, indicating that diffusible factors may influence Sst identity (Figure 6). However, for Pvalb upregulation, it is more plausible that direct cell-to-cell contact within the 3D structure of human cortical cultures was key to the rapid induction of mouse Pvalb cells. Supporting this idea, research in 3D cerebellar development models, including organoids[158] and grafting IPSC-derived neurons into human fetal cerebellar slices[159] has demonstrated that a human 3D architecture is crucial for the proper development and maturation of Purkinje cells, which have long presented a challenge for *in vitro* modeling.

We further showed that manipulating human PNs during grafting, either through FBS depletion or rapamycin treatment, significantly altered the fate of grafted mouse INs (Figure 7). The mTOR pathway is pivotal in PN differentiation and maturation and is tightly regulated during PN development, a process preserved in PSC-derived models, including 2D neurons and organoids.[160] *In vivo*, mTOR activation in PNs via Pten deletion during development[111] or adulthood[112] drastically increased soma size, dendritic length, and arborization but reduced spine density in distal dendritic regions, suggesting impaired synaptic plasticity. Under mTOR-inhibited conditions, we observed a striking reduction in Pvalb induction in grafted INs, indicating that mTOR activity in PNs is crucial for their interactions with maturing INs. These results suggest that coordinated cell-to-cell contacts between PNs and maturing INs can drive the differentiation of Pvalb-positive INs.

In summary, we present a chimeric cortical organoid model that accelerates mouse IN differentiation and significantly increases the proportion of Pvalb-positive cells under *in vitro* conditions. While the factors driving the rapid differentiation of mouse MGE cells into Pvalb INs within human cortical tissue remain unclear, our findings, alongside those of others,[20,94,96] suggest that interactions with PNs are critical for inducing this identity. The optimal co-culture conditions for efficiently differentiating human Pvalb INs, however, remain to be determined. Nevertheless, the chimeric culture system described here offers a platform for exploring the mechanisms of IN differentiation and maturation. It also highlights the potential of 3D organoid models for generating neuronal subtypes that have been challenging to study *in vitro*.

## Limitations of the study

The chimeric models used in this study, including primary organotypic cultures and brain organoids, provide valuable insights into IN differentiation. However, these *in vitro* systems are inherently artificial and do not fully replicate the complexity of the *in vivo* brain. Furthermore, we previously demonstrated that cellular stress within brain organoids can impair neuronal differentiation.[161] Recent machine learning analyses have also shown that such impairment predominantly affects the transition from radial glia to early PNs, while ventral precursors and INs in organoids exhibit relatively higher fidelity.[162] Notably, label transfer from primary fetal tissue to organoids has accurately assigned IN fate across multiple organoid lines.[162]

An alternative hypothesis for the enrichment of Pvalb-positive INs in our chimeric models is that it may result from selective apoptosis of Sst-positive INs. In a separate study, *Fezf2*

knockout mice demonstrated that Sst-positive INs undergo selective cell death in response to the absence of subcerebral PNs.[20] However, several lines of evidence suggest that selective cell death is unlikely to account for the Pvalb-positive enrichment observed in our models. First, host human organotypic cultures and organoids still contain Sst-positive INs that coexist with grafted mouse INs (Figure 2B). Second, in our experiments involving the grafting of lineage-traced mouse Sst INs, approximately 50% of the cells grafted onto human organoids retained the Sst marker by 14 DPG. (Figure 8C). Finally, in our grafted IN progenitors, we observed Pvalb upregulation as early as 2 DPG (Figure 4A), indicating that the enrichment of Pvalb-positive cells is more likely driven by the selective induction of this identity rather than the loss of Sst-positive cells.

This study focused on the extrinsic control of IN identity but does not exclude the role of species-specific intrinsic mechanisms in IN responses to signals inducing Pvalb-positive identity. While PNs exhibit distinct area- and species-specific features, MGE-derived INs are considered evolutionarily conserved.[163] Transcriptomic profiling of the adult human, monkey, and mouse cortex highlights Pvalb-positive INs as one of the most conserved neuronal subtypes.[47] Conserved transcriptional programs governing MGE-derived IN diversity have also been observed across mammals during embryonic and early postnatal stages.[6,31,33,53,164] Differential timing in gene expression networks may explain, at least in part, the varying graft responses of mouse and human INs. Species differences in mitochondrial metabolism, associated with neuronal maturation and differentiation timing, are an interesting area of further focus.[165–167] Accelerating mitochondrial metabolism in human PNs has been shown to enhance genetic networks tied to maturation,[166] but whether this applies across neuronal subtypes remains unknown. Pvalb-positive INs, with their high excitatory drive and rapid action potential generation, have higher metabolic demands.[168] The mitochondrial biogenesis protein PGC-1$\alpha$ is crucial for Pvalb induction in INs[169] and its deficiency affects synchronous GABAergic release and the expression of several Pvalb-enriched markers.[79] PGC-1$\alpha$ is known to be activity-dependent, yet grafting in human organoids occurs before the onset of strong activity.[132,133,153] Despite this, human organoids experience significant metabolic stress,[161] which could alter mitochondrial biogenesis.[170] Since external cues and intrinsic responses are not mutually exclusive, future studies using chimeric models to manipulate PNs and INs separately could clarify species-specific signal responses and IN specification. Additionally, allotransplantation into mouse organoids, which exhibit faster activity than human hosts, could provide insights into activity-dependent Pvalb upregulation.[154–157]

## RESOURCE AVAILABILITY

### Lead contact

Further information or requests for reagents, resources, and data should be addressed to the lead contact, Mohammed A. Mostajo-Radji (mmostajo@ucsc.edu).

### Materials availability

This study did not generate new unique reagents.

### Data and code availability

Single cell RNA sequencing data have been deposited in GEO, under accession number GSE278531. Additional data reported in this paper will be shared by the lead contact upon request. This study did not generate new code. Any additional information required to reanalyze the data reported in this paper is available from the lead contact upon request.

## ACKNOWLEDGMENTS

We are grateful to the families who generously donated tissue samples. We thank Tomasz Nowakowski and David Haussler for their feedback and discussions throughout the development of this manuscript, Daniel Lim for providing laboratory space to carry out part of this research, David Shin for supplying the thalamic organoids, Sainath Mamde and Sara Medor for their expertise in bioinformatics, Steven Cincotta for contributing mouse tissue, and Arpana Arjun, Kevin Barber, Luigi Enriquez, Gaia Skibinski, and Saul Kato for their assistance with calcium imaging. We also acknowledge Kyle Marchuk and the UCSF Biological Imaging Development Center for their support in light-sheet imaging. We thank Alain Chedotal and his team for generously sharing protocols for thick tissue immunostaining and clearing, which we accessed through the Tissue Clearing and 3D Imaging Course at the Institut de la Vision (Paris, France). Additionally, we are grateful to Andrew Elefanty for sharing the hES-3 NKX2.1-GFP reporter line.

This research was supported by Schmidt Futures (SF857) awarded to M.T. and A.A.P.; the Chan Zuckerberg Biohub to A.A.P.; the UCSF Program for Breakthrough Biomedical Research (PBBR) to A.A.P.; the National Human Genome Research Institute (1RM1HG011543) to M.T.; the National Science Foundation (NSF grants NSF2134955 and NSF2034037) to M.T.; the National Institute of Mental Health (1U24MH132628) to M.A.M.-R.; and the California Institute for Regenerative Medicine (grant DISC4-16285) to M.A.M.-R., M.T., and A.A.P., as well as grant DISC4-16337 to M.A.M.-R. Additional support was provided by the University of California Office of the President (M25PR9045) to M.A.M.-R. and M.T. M.A.M.-R. also received partial support from the TL1 TR001871 fellowship through the NIH National Center for Advancing Translational Sciences. H.E.S. is supported by the National Science Foundation Graduate Research Fellowship.

## AUTHOR CONTRIBUTIONS

M.A.M.-R., A.A.-B., and A.A.P. conceived the project. M.A.M.-R., W.R.M.L., A.B., J.G.-F., H.E.S., J.L., L.Z., M.T.S., Y.P., T.M., A.R., J.C., M.G.A., F.N.S., D.T., and E.C.C. performed the experiments and analyzed the data. M.A.M.-R., M.F.P., M.T., A.R.K., A.A.-B., and A.A.P. supervised the work. M.A.M.-R. and A.A.P. wrote this manuscript with contributions from all authors.

## DECLARATION OF INTERESTS

M.A.M.-R. and A.A.P. are listed as inventors on a patent application concerning the *in vitro* generation of Pvalb-positive INs. Additionally, M.A.M.-R. and J.L. are inventors on a separate patent application related to machine learning models for neuron classification. L.Z. is an employee of Milecell Biotechnology. D.T. is an employee of Aperture Therapeutics. A.A.-B. and A.R.K. are co-founders and members of the scientific advisory board of Neurona Therapeutics. W.R.M.L. is an employee of Neurona Therapeutics. A.R. is a co-founder and the chief technology officer of Immergo Labs. M.T. is a member of the scientific advisory board of Immergo Labs. M.T. serves as an advisory board member of Open Culture Science, Inc. M.A.M.-R. is an advisor for Atoll Financial Group.

## STAR★METHODS

Detailed methods are provided in the online version of this paper and include the following:

- KEY RESOURCES TABLE
- EXPERIMENTAL MODEL AND STUDY PARTICIPANT DETAILS

## SUPPLEMENTAL INFORMATION

Supplemental information can be found online at https://doi.org/10.1016/j.isci.2025.112295.

Received: October 15, 2024
Revised: January 21, 2025
Accepted: March 24, 2025
Published: March 27, 2025

## REFERENCES

1. Cadwell, C.R., Bhaduri, A., Mostajo-Radji, M.A., Keefe, M.G., and Nowakowski, T.J. (2019). Development and Arealization of the Cerebral Cortex. Neuron *103*, 980–1004. https://doi.org/10.1016/j.neuron.2019.07.009.
2. Di Bella, D.J., Habibi, E., Stickels, R.R., Scalia, G., Brown, J., Yadollahpour, P., Yang, S.M., Abbate, C., Biancalani, T., Macosko, E.Z., et al. (2021). Molecular logic of cellular diversification in the mouse cerebral cortex. Nature *595*, 554–559. https://doi.org/10.1038/s41586-021-03670-5.
3. Allison, T., Langerman, J., Sabri, S., Otero-Garcia, M., Lund, A., Huang, J., Wei, X., Samarasinghe, R.A., Polioudakis, D., Mody, I., et al. (2021). Defining the nature of human pluripotent stem cell-derived interneurons via single-cell analysis. Stem Cell Rep. *16*, 2548–2564. https://doi.org/10.1016/j.stemcr.2021.08.006.
4. Harb, K., Richter, M., Neelagandan, N., Magrinelli, E., Harfoush, H., Kuechler, K., Henis, M., Hermanns-Borgmeyer, I., Calderon de Anda, F., and Duncan, K. (2022). Pum2 and TDP-43 refine area-specific cytoarchitecture post-mitotically and modulate translation of Sox5, Bcl11b, and Rorb mRNAs in developing mouse neocortex. Elife *11*, e55199. https://doi.org/10.7554/eLife.55199.
5. Nowakowski, T.J., Bhaduri, A., Pollen, A.A., Alvarado, B., Mostajo-Radji, M.A., Di Lullo, E., Haeussler, M., Sandoval-Espinosa, C., Liu, S.J., Velmeshev, D., et al. (2017). Spatiotemporal gene expression trajectories reveal developmental hierarchies of the human cortex. Science *358*, 1318–1323. https://doi.org/10.1126/science.aap8809.
6. Schmitz, M.T., Sandoval, K., Chen, C.P., Mostajo-Radji, M.A., Seeley, W.W., Nowakowski, T.J., Ye, C.J., Paredes, M.F., and Pollen, A.A. (2022). The Development and Evolution of Inhibitory Neurons in the Primate Cerebrum. Nature *603*, 871–877. https://doi.org/10.1038/s41586-022-04510-w.
7. Ozair, M.Z., Kirst, C., van den Berg, B.L., Ruzo, A., Rito, T., and Brivanlou, A.H. (2018). hPSC Modeling Reveals that Fate Selection of Cortical Deep Projection Neurons Occurs in the Subplate. Cell Stem Cell *23*, 60–73.e6. https://doi.org/10.1016/j.stem.2018.05.024.
8. Anderson, S., Mione, M., Yun, K., and Rubenstein, J.L. (1999). Differential Origins of Neocortical Projection and Local Circuit Neurons: Role of Dlx Genes in Neocortical Interneuronogenesis. Cereb. Cortex *9*, 646–654. https://doi.org/10.1093/cercor/9.6.646.
9. Nery, S., Fishell, G., and Corbin, J.G. (2002). The caudal ganglionic eminence is a source of distinct cortical and subcortical cell populations. Nat. Neurosci. *5*, 1279–1287. https://doi.org/10.1038/nn971.
10. Wichterle, H., Alvarez-Dolado, M., Erskine, L., and Alvarez-Buylla, A. (2003). Permissive corridor and diffusible gradients direct medial ganglionic eminence cell migration to the neocortex. Proc. Natl. Acad. Sci. *100*, 727–732. https://doi.org/10.1073/pnas.242721899.
11. Xu, Q., Cobos, I., De la Cruz, E., Rubenstein, J.L., and Anderson, S.A. (2004). Origins of cortical interneuron subtypes. J. Neurosci. *24*, 2612–2622. https://doi.org/10.1523/JNEUROSCI.5667-03.2004.
12. Wamsley, B., and Fishell, G. (2017). Genetic and activity-dependent mechanisms underlying interneuron diversity. Nat. Rev. Neurosci. *18*, 299–309. https://doi.org/10.1038/nrn.2017.30.
13. De Marco García, N.V., Karayannis, T., and Fishell, G. (2011). Neuronal activity is required for the development of specific cortical interneuron subtypes. Nature *472*, 351–355. https://doi.org/10.1038/nature09865.
14. Lodato, S., Rouaux, C., Quast, K.B., Jantrachotechatchawan, C., Studer, M., Hensch, T.K., and Arlotta, P. (2011). Excitatory projection neuron subtypes control the distribution of local inhibitory interneurons in the cerebral cortex. Neuron *69*, 763–779. https://doi.org/10.1016/j.neuron.2011.01.015.
15. Wester, J.C., Mahadevan, V., Rhodes, C.T., Calvigioni, D., Venkatesh, S., Maric, D., Hunt, S., Yuan, X., Zhang, Y., Petros, T.J., and McBain, C.J. (2019). Neocortical projection neurons instruct inhibitory interneuron circuit development in a lineage-dependent manner. Neuron *102*, 960–975.e6. https://doi.org/10.1016/j.neuron.2019.03.036.
16. Ye, Z., Mostajo-Radji, M.A., Brown, J.R., Rouaux, C., Tomassy, G.S., Hensch, T.K., and Arlotta, P. (2015). Instructing perisomatic inhibition by direct lineage reprogramming of neocortical projection neurons. Neuron *88*, 475–483. https://doi.org/10.1016/j.neuron.2015.10.006.
17. Pan, N.C., Fang, A., Shen, C., Sun, L., Wu, Q., and Wang, X. (2019). Early excitatory activity-dependent maturation of somatostatin interneurons in cortical layer 2/3 of mice. Cereb. Cortex *29*, 4107–4118. https://doi.org/10.1093/cercor/bhy293.
18. Southwell, D.G., Paredes, M.F., Galvao, R.P., Jones, D.L., Froemke, R.C., Sebe, J.Y., Alfaro-Cervello, C., Tang, Y., Garcia-Verdugo, J.M., Rubenstein, J.L., et al. (2012). Intrinsically determined cell death of developing cortical interneurons. Nature *491*, 109–113. https://doi.org/10.1038/nature11523.
19. Wong, F.K., Bercsenyi, K., Sreenivasan, V., Portalés, A., Fernández-Otero, M., and Marín, O. (2018). Pyramidal cell regulation of interneuron survival sculpts cortical networks. Nature *557*, 668–673. https://doi.org/10.1038/s41586-018-0139-6.
20. Wu, S.J., Dai, M., Yang, S.P., McCann, C., Qiu, Y., Marrero, G.J., Stogsdill, J.A., Di Bella, D.J., Xu, Q., Farhi, S.L., et al. (2024). Pyramidal neurons proportionately alter the identity and survival of specific cortical interneuron subtypes. Preprint at bioRxiv. https://doi.org/10.1101/2024.07.20.604399.
21. Bragg-Gonzalo, L., De León Reyes, N.S., and Nieto, M. (2021). Genetic and activity dependent-mechanisms wiring the cortex: Two sides of

the same coin. Semin. Cell Dev. Biol. *118*, 24–34. https://doi.org/10.1016/j.semcdb.2021.05.011.

22. Jabaudon, D. (2017). Fate and freedom in developing neocortical circuits. Nat. Commun. *8*, 16042. https://doi.org/10.1038/ncomms16042.
23. Pipicelli, F., Baumann, N., Di Giaimo, R., Forero-Echeverry, A., Kyrousi, C., Bonrath, R., Maccarrone, G., Jabaudon, D., and Cappello, S. (2023). Non–cell-autonomous regulation of interneuron specification mediated by extracellular vesicles. Sci. Adv. *9*, eadd8164. https://doi.org/10.1126/sciadv.add8164.
24. Quattrocolo, G., Fishell, G., and Petros, T.J. (2017). Heterotopic transplantations reveal environmental influences on interneuron diversity and maturation. Cell Rep. *21*, 721–731. https://doi.org/10.1016/j.celrep.2017.09.075.
25. Molyneaux, B.J., Arlotta, P., Hirata, T., Hibi, M., and Macklis, J.D. (2005). Fezl is required for the birth and specification of corticospinal motor neurons. Neuron *47*, 817–831. https://doi.org/10.1016/j.neuron.2005.08.030.
26. Inan, M., Welagen, J., and Anderson, S.A. (2012). Spatial and Temporal Bias in the Mitotic Origins of Somatostatin- and Parvalbumin-Expressing Interneuron Subgroups and the Chandelier Subtype in the Medial Ganglionic Eminence. Cereb. Cortex *22*, 820–827. https://doi.org/10.1093/cercor/bhr148.
27. Wonders, C.P., Taylor, L., Welagen, J., Mbata, I.C., Xiang, J.Z., and Anderson, S.A. (2008). A spatial bias for the origins of interneuron subgroups within the medial ganglionic eminence. Dev. Biol. *314*, 127–136. https://doi.org/10.1016/j.ydbio.2007.11.018.
28. Hu, J.S., Vogt, D., Sandberg, M., and Rubenstein, J.L. (2017). Cortical interneuron development: a tale of time and space. Devenir *144*, 3867–3878. https://doi.org/10.1242/dev.132852.
29. McKenzie, M.G., Cobbs, L.V., Dummer, P.D., Petros, T.J., Halford, M.M., Stacker, S.A., Zou, Y., Fishell, G.J., and Au, E. (2019). Non-canonical Wnt Signaling through Ryk Regulates the Generation of Somatostatin- and Parvalbumin-Expressing Cortical Interneurons. Neuron *103*, 853–864.e4. https://doi.org/10.1016/j.neuron.2019.06.003.
30. Allaway, K.C., Gabitto, M.I., Wapinski, O., Saldi, G., Wang, C.Y., Bandler, R.C., Wu, S.J., Bonneau, R., and Fishell, G. (2021). Genetic and epigenetic coordination of cortical interneuron development. Nature *597*, 693–697. https://doi.org/10.1038/s41586-021-03933-1.
31. Mayer, C., Hafemeister, C., Bandler, R.C., Machold, R., Batista Brito, R., Jaglin, X., Allaway, K., Butler, A., Fishell, G., and Satija, R. (2018). Developmental diversification of cortical inhibitory interneurons. Nature *555*, 457–462. https://doi.org/10.1038/nature25999.
32. Lee, D.R., Rhodes, C., Mitra, A., Zhang, Y., Maric, D., Dale, R.K., and Petros, T.J. (2022). Transcriptional heterogeneity of ventricular zone cells in the ganglionic eminences of the mouse forebrain. Elife *11*, e71864. https://doi.org/10.7554/eLife.71864.
33. Mi, D., Li, Z., Lim, L., Li, M., Moissidis, M., Yang, Y., Gao, T., Hu, T.X., Pratt, T., Price, D.J., et al. (2018). Early emergence of cortical interneuron diversity in the mouse embryo. Science *360*, 81–85. https://doi.org/10.1126/science.aar6821.
34. Kroon, T., van Hugte, E., van Linge, L., Mansvelder, H.D., and Meredith, R.M. (2019). Early postnatal development of pyramidal neurons across layers of the mouse medial prefrontal cortex. Sci. Rep. *9*, 5037. https://doi.org/10.1038/s41598-019-41661-9.
35. Tuncdemir, S.N., Wamsley, B., Stam, F.J., Osakada, F., Goulding, M., Callaway, E.M., Rudy, B., and Fishell, G. (2016). Early Somatostatin Interneuron Connectivity Mediates the Maturation of Deep Layer Cortical Circuits. Neuron *89*, 521–535. https://doi.org/10.1016/j.neuron.2015.11.020.
36. Chattopadhyaya, B., Di Cristo, G., Higashiyama, H., Knott, G.W., Kuhlman, S.J., Welker, E., and Huang, Z.J. (2004). Experience and Activity-Dependent Maturation of Perisomatic GABAergic Innervation in Primary Visual Cortex during a Postnatal Critical Period. J. Neurosci. *24*, 9598–9611. https://doi.org/10.1523/JNEUROSCI.1851-04.2004.
37. Hensch, T.K. (2005). Critical period plasticity in local cortical circuits. Nat. Rev. Neurosci. *6*, 877–888. https://doi.org/10.1038/nrn1787.
38. Ma, T., Wang, C., Wang, L., Zhou, X., Tian, M., Zhang, Q., Zhang, Y., Li, J., Liu, Z., Cai, Y., et al. (2013). Subcortical origins of human and monkey neocortical interneurons. Nat. Neurosci. *16*, 1588–1597. https://doi.org/10.1038/nn.3536.
39. Alvarado-Mallart, R.M. (2000). The chick/quail transplantation model to study central nervous system development. Prog. Brain Res. *127*, 67–98. https://doi.org/10.1016/S0079-6123(00)27006-4.
40. Southwell, D.G., Froemke, R.C., Alvarez-Buylla, A., Stryker, M.P., and Gandhi, S.P. (2010). Cortical Plasticity Induced by Inhibitory Neuron Transplantation. Science *327*, 1145–1148. https://doi.org/10.1126/science.1183962.
41. Tang, Y., Stryker, M.P., Alvarez-Buylla, A., and Espinosa, J.S. (2014). Cortical plasticity induced by transplantation of embryonic somatostatin or parvalbumin interneurons. Proc. Natl. Acad. Sci. *111*, 18339–18344. https://doi.org/10.1073/pnas.1421844112.
42. Brown, J., Barry, C., Schmitz, M.T., Argus, C., Bolin, J.M., Schwartz, M.P., Van Aartsen, A., Steill, J., Swanson, S., Stewart, R., et al. (2021). Interspecies Chimeric Conditions Affect the Developmental Rate of Human Pluripotent Stem Cells. PLoS Comput. Biol. *17*, e1008778. https://doi.org/10.1371/journal.pcbi.1008778.
43. Linaro, D., Vermaercke, B., Iwata, R., Ramaswamy, A., Libé-Philippot, B., Boubakar, L., Davis, B.A., Wierda, K., Davie, K., Poovathingal, S., et al. (2019). Xenotransplanted Human Cortical Neurons Reveal Species-Specific Development and Functional Integration into Mouse Visual Circuits. Neuron *104*, 972–986.e6. https://doi.org/10.1016/j.neuron.2019.10.002.
44. Marchetto, M.C., Hrvoj-Mihic, B., Kerman, B.E., Yu, D.X., Vadodaria, K.C., Linker, S.B., Narvaiza, I., Santos, R., Denli, A.M., Mendes, A.P., et al. (2019). Species-specific maturation profiles of human, chimpanzee and bonobo neural cells. Elife *8*, e37527. https://doi.org/10.7554/eLife.37527.
45. Zheng, C., Hu, Y., Sakurai, M., Pinzon-Arteaga, C.A., Li, J., Wei, Y., Okamura, D., Ravaux, B., Barlow, H.R., Yu, L., et al. (2021). Cell competition constitutes a barrier for interspecies chimerism. Nature *592*, 272–276. https://doi.org/10.1038/s41586-021-03273-0.
46. Semple, B.D., Blomgren, K., Gimlin, K., Ferriero, D.M., and Noble-Haeusslein, L.J. (2013). Brain development in rodents and humans: Identifying benchmarks of maturation and vulnerability to injury across species. Prog. Neurobiol. *106–107*, 1–16. https://doi.org/10.1016/j.pneurobio.2013.04.001.
47. Bakken, T.E., Jorstad, N.L., Hu, Q., Lake, B.B., Tian, W., Kalmbach, B.E., Crow, M., Hodge, R.D., Krienen, F.M., Sorensen, S.A., et al. (2021). Comparative cellular analysis of motor cortex in human, marmoset and mouse. Nature *598*, 111–119. https://doi.org/10.1038/s41586-021-03465-8.
48. Hodge, R.D., Bakken, T.E., Miller, J.A., Smith, K.A., Barkan, E.R., Graybuck, L.T., Close, J.L., Long, B., Johansen, N., Penn, O., et al. (2019). Conserved cell types with divergent features in human versus mouse cortex. Nature *573*, 61–68. https://doi.org/10.1038/s41586-019-1506-7.
49. Mostajo-Radji, M.A., Schmitz, M.T., Montoya, S.T., and Pollen, A.A. (2020). Reverse engineering human brain evolution using organoid models. Brain Res. *1729*, 146582. https://doi.org/10.1016/j.brainres.2019.146582.
50. Wallace, J.L., and Pollen, A.A. (2024). Human neuronal maturation comes of age: cellular mechanisms and species differences. Nat. Rev. Neurosci. *25*, 7–29. https://doi.org/10.1038/s41583-023-00760-3.
51. Bhaduri, A., Nowakowski, T.J., Pollen, A.A., and Kriegstein, A.R. (2018). Identification of cell types in a mouse brain single-cell atlas using low

sampling coverage. BMC Biol. *16*, 113. https://doi.org/10.1186/s12915-018-0580-x.

52. Loo, L., Simon, J.M., Xing, L., McCoy, E.S., Niehaus, J.K., Guo, J., Anton, E.S., and Zylka, M.J. (2019). Single-cell transcriptomic analysis of mouse neocortical development. Nat. Commun. *10*, 134. https://doi.org/10.1038/s41467-018-08079-9.
53. La Manno, G., Siletti, K., Furlan, A., Gyllborg, D., Vinsland, E., Mossi Albiach, A., Mattsson Langseth, C., Khven, I., Lederer, A.R., Dratva, L.M., et al. (2021). Molecular architecture of the developing mouse brain. Nature *596*, 92–96. https://doi.org/10.1038/s41586-021-03775-x.
54. Zeisel, A., Hochgerner, H., Lönnerberg, P., Johnsson, A., Memic, F., Van Der Zwan, J., Häring, M., Braun, E., Borm, L.E., La Manno, G., et al. (2018). Molecular architecture of the mouse nervous system. Cell *174*, 999–1014.e22. https://doi.org/10.1016/j.cell.2018.06.021.
55. Sun, Y., Ikrar, T., Davis, M.F., Gong, N., Zheng, X., Luo, Z.D., Lai, C., Mei, L., Holmes, T.C., Gandhi, S.P., and Xu, X. (2016). Neuregulin-1/ErbB4 Signaling Regulates Visual Cortical Plasticity. Neuron *92*, 160–173. https://doi.org/10.1016/j.neuron.2016.08.033.
56. Daviaud, N., Garbayo, E., Schiller, P.C., Perez-Pinzon, M., and Montero-Menei, C.N. (2013). Organotypic cultures as tools for optimizing central nervous system cell therapies. Exp. Neurol. *248*, 429–440. https://doi.org/10.1016/j.expneurol.2013.07.012.
57. Jäderstad, L.M., Jäderstad, J., and Herlenius, E. (2010). Graft and host interactions following transplantation of neural stem cells to organotypic striatal cultures. Regen. Med. *5*, 901–917. https://doi.org/10.2217/rme.10.80.
58. Tønnesen, J., Parish, C.L., Sørensen, A.T., Andersson, A., Lundberg, C., Deisseroth, K., Arenas, E., Lindvall, O., and Kokaia, M. (2011). Functional Integration of Grafted Neural Stem Cell-Derived Dopaminergic Neurons Monitored by Optogenetics in an In Vitro Parkinson Model. PLoS One *6*, e17560. https://doi.org/10.1371/journal.pone.0017560.
59. Xu, Q., Tam, M., and Anderson, S.A. (2008). Fate mapping Nkx2.1-lineage cells in the mouse telencephalon. J. Comp. Neurol. *506*, 16–29. https://doi.org/10.1002/cne.21529.
60. Madisen, L., Zwingman, T.A., Sunkin, S.M., Oh, S.W., Zariwala, H.A., Gu, H., Ng, L.L., Palmiter, R.D., Hawrylycz, M.J., Jones, A.R., et al. (2010). A robust and high-throughput Cre reporting and characterization system for the whole mouse brain. Nat. Neurosci. *13*, 133–140. https://doi.org/10.1038/nn.2467.
61. Letinic, K., and Kostovic, I. (1998). Postnatal development of calcium-binding proteins calbindin and parvalbumin in human visual cortex. Cereb. Cortex *8*, 660–669. https://doi.org/10.1093/cercor/8.7.660.
62. Uylings, H.B.M., Delalle, I., Petanjek, Z., and Koenderink, M.j.t. (2002). Structural and immunocytochemical differentiation of neurons in prenatal and postnatal human prefrontal cortex. Neuroembryol. Aging *1*, 176–186. https://doi.org/10.1159/000066268.
63. Zecevic, N., Hu, F., and Jakovcevski, I. (2011). Cortical interneurons in the developing human neocortex. Dev. Neurobiol. *71*, 18–33. https://doi.org/10.1002/dneu.20812.
64. Croft, C.L., Futch, H.S., Moore, B.D., and Golde, T.E. (2019). Organotypic brain slice cultures to model neurodegenerative proteinopathies. Mol. Neurodegener. *14*, 45. https://doi.org/10.1186/s13024-019-0346-0.
65. Humpel, C. (2015). Organotypic brain slice cultures: A review. Neuroscience (San Diego, CA, U. S.) *305*, 86–98. https://doi.org/10.1016/j.neuroscience.2015.07.086.
66. Kadoshima, T., Sakaguchi, H., Nakano, T., Soen, M., Ando, S., Eiraku, M., and Sasai, Y. (2013). Self-organization of axial polarity, inside-out layer pattern, and species-specific progenitor dynamics in human ES cell–derived neocortex. Proc. Natl. Acad. Sci. *110*, 20284–20289. https://doi.org/10.1073/pnas.1315710110.
67. Quadrato, G., Nguyen, T., Macosko, E.Z., Sherwood, J.L., Min Yang, S., Berger, D.R., Maria, N., Scholvin, J., Goldman, M., Kinney, J.P., et al. (2017). Cell diversity and network dynamics in photosensitive human brain organoids. Nature *545*, 48–53. https://doi.org/10.1038/nature22047.
68. Pollen, A.A., Bhaduri, A., Andrews, M.G., Nowakowski, T.J., Meyerson, O.S., Mostajo-Radji, M.A., Di Lullo, E., Alvarado, B., Bedolli, M., Dougherty, M.L., et al. (2019). Establishing Cerebral Organoids as Models of Human-Specific Brain Evolution. Cell *176*, 743–756.e17. https://doi.org/10.1016/j.cell.2019.01.017.
69. Faux, C., Rakic, S., Andrews, W., and Britto, J.M. (2012). Neurons on the Move: Migration and Lamination of Cortical Interneurons. Neurosignals *20*, 168–189. https://doi.org/10.1159/000334489.
70. Lepiemme, F., Silva, C.G., and Nguyen, L. (2021). Time lapse recording of cortical interneuron migration in mouse organotypic brain slices and explants. STAR Protoc. *2*, 100467. https://doi.org/10.1016/j.xpro.2021.100467.
71. Giandomenico, S.L., Sutcliffe, M., and Lancaster, M.A. (2021). Generation and long-term culture of advanced cerebral organoids for studying later stages of neural development. Nat. Protoc. *16*, 579–602. https://doi.org/10.1038/s41596-020-00433-w.
72. Real, R., Peter, M., Trabalza, A., Khan, S., Smith, M.A., Dopp, J., Barnes, S.J., Momoh, A., Strano, A., Volpi, E., et al. (2018). In vivo modeling of human neuron dynamics and Down syndrome. Science *362*, eaau1810. https://doi.org/10.1126/science.aau1810.
73. Daigle, T.L., Madisen, L., Hage, T.A., Valley, M.T., Knoblich, U., Larsen, R.S., Takeno, M.M., Huang, L., Gu, H., Larsen, R., et al. (2018). A Suite of Transgenic Driver and Reporter Mouse Lines with Enhanced Brain-Cell-Type Targeting and Functionality. Cell *174*, 465–480.e22. https://doi.org/10.1016/j.cell.2018.06.035.
74. Allene, C., Cattani, A., Ackman, J.B., Bonifazi, P., Aniksztejn, L., Ben-Ari, Y., and Cossart, R. (2008). Sequential generation of two distinct synapse-driven network patterns in developing neocortex. J. Neurosci. *28*, 12851–12863. https://doi.org/10.1523/JNEUROSCI.3733-08.2008.
75. Madisen, L., Garner, A.R., Shimaoka, D., Chuong, A.S., Klapoetke, N.C., Li, L., van der Bourg, A., Niino, Y., Egolf, L., Monetti, C., et al. (2015). Transgenic mice for intersectional targeting of neural sensors and effectors with high specificity and performance. Neuron *85*, 942–958. https://doi.org/10.1016/j.neuron.2015.02.022.
76. Caillard, O., Moreno, H., Schwaller, B., Llano, I., Celio, M.R., and Marty, A. (2000). Role of the calcium-binding protein parvalbumin in short-term synaptic plasticity. Proc. Natl. Acad. Sci. *97*, 13372–13377. https://doi.org/10.1073/pnas.230362997.
77. Ali, F., and Kwan, A.C. (2020). Interpreting in vivo calcium signals from neuronal cell bodies, axons, and dendrites: a review. Neurophotonics *7*, 011402. https://doi.org/10.1117/1.NPh.7.1.011402.
78. Agetsuma, M., Hamm, J.P., Tao, K., Fujisawa, S., and Yuste, R. (2018). Parvalbumin-positive interneurons regulate neuronal ensembles in visual cortex. Cereb. Cortex *28*, 1831–1845. https://doi.org/10.1093/cercor/bhx169.
79. Lucas, E.K., Dougherty, S.E., McMeekin, L.J., Reid, C.S., Dobrunz, L.E., West, A.B., Hablitz, J.J., and Cowell, R.M. (2014). PGC-1$\alpha$ provides a transcriptional framework for synchronous neurotransmitter release from parvalbumin-positive interneurons. J. Neurosci. *34*, 14375–14387. https://doi.org/10.1523/JNEUROSCI.1222-14.2014.
80. Hippenmeyer, S., Vrieseling, E., Sigrist, M., Portmann, T., Laengle, C., Ladle, D.R., and Arber, S. (2005). A Developmental Switch in the Response of DRG Neurons to ETS Transcription Factor Signaling. PLoS Biol. *3*, e159. https://doi.org/10.1371/journal.pbio.0030159.
81. Ciarpella, F., Zamfir, R.G., Campanelli, A., Ren, E., Pedrotti, G., Bottani, E., Borioli, A., Caron, D., Di Chio, M., Dolci, S., et al. (2021). Murine cerebral organoids develop network of functional neurons and hippocampal brain region identity. iScience *24*, 103438. https://doi.org/10.1016/j.isci.2021.103438.
82. Hu, J.S., Vogt, D., Lindtner, S., Sandberg, M., Silberberg, S.N., and Rubenstein, J.L.R. (2017). Coup-TF1 and Coup-TF2 control subtype and

laminar identity of MGE-derived neocortical interneurons. Devenir *144*, 2837–2851. https://doi.org/10.1242/dev.150664.

83. Cellerino, A., Maffei, L., and Domenici, L. (1996). The distribution of brain-derived neurotrophic factor and its receptor trkB in parvlbumin-containing neurons of the rat visual cortex. Eur. J. Neurosci. *8*, 1190–1197. https://doi.org/10.1111/j.1460-9568.1996.tb01287.x.
84. Tomas, F.J.B., Turko, P., Heilmann, H., Trimbuch, T., Yanagawa, Y., Vida, I., and Münster-Wandowski, A. (2020). BDNF Expression in Cortical GABAergic Interneurons. Int. J. Mol. Sci. *21*, 1567. https://doi.org/10.3390/ijms21051567.
85. Huang, Z.J., Kirkwood, A., Pizzorusso, T., Porciatti, V., Morales, B., Bear, M.F., Maffei, L., and Tonegawa, S. (1999). BDNF Regulates the Maturation of Inhibition and the Critical Period of Plasticity in Mouse Visual Cortex. Cell *98*, 739–755. https://doi.org/10.1016/S0092-8674(00)81509-3.
86. Velasco, S., Kedaigle, A.J., Simmons, S.K., Nash, A., Rocha, M., Quadrato, G., Paulsen, B., Nguyen, L., Adiconis, X., Regev, A., et al. (2019). Individual brain organoids reproducibly form cell diversity of the human cerebral cortex. Nature *570*, 523–527. https://doi.org/10.1038/s41586-019-1289-x.
87. Wen, T.H., Binder, D.K., Ethell, I.M., and Razak, K.A. (2018). The perineuronal 'safety' net? Perineuronal net abnormalities in neurological disorders. Front. Mol. Neurosci. *11*, 270. https://doi.org/10.3389/fnmol.2018.00270.
88. Su, J., Cole, J., and Fox, M.A. (2017). Loss of Interneuron-Derived Collagen XIX Leads to a Reduction in Perineuronal Nets in the Mammalian Telencephalon. ASN Neuro *9*, 1759091416689020. https://doi.org/10.1177/1759091416689020.
89. Horii-Hayashi, N., Sasagawa, T., Matsunaga, W., and Nishi, M. (2015). Development and structural variety of the chondroitin sulfate proteoglycans-contained extracellular matrix in the mouse brain. Neural Plast. *2015*, 256389. https://doi.org/10.1155/2015/256389.
90. Kooijmans, R.N., Sierhuis, W., Self, M.W., and Roelfsema, P.R. (2020). A Quantitative Comparison of Inhibitory Interneuron Size and Distribution between Mouse and Macaque V1, Using Calcium-Binding Proteins. Cereb. Cortex Commun. *1*, tgaa068. https://doi.org/10.1093/texcom/tgaa068.
91. Malik, R., Pai, E.L.L., Rubin, A.N., Stafford, A.M., Angara, K., Minasi, P., Rubenstein, J.L., Sohal, V.S., and Vogt, D. (2019). Tsc1 represses parvalbumin expression and fast-spiking properties in somatostatin lineage cortical interneurons. Nat. Commun. *10*, 4994. https://doi.org/10.1038/s41467-019-12962-4.
92. Jager, P., Moore, G., Calpin, P., Durmishi, X., Salgarella, I., Menage, L., Kita, Y., Wang, Y., Kim, D.W., Blackshaw, S., et al. (2021). Dual midbrain and forebrain origins of thalamic inhibitory interneurons. Elife *10*, e59272. https://doi.org/10.7554/eLife.59272.
93. Birey, F., Andersen, J., Makinson, C.D., Islam, S., Wei, W., Huber, N., Fan, H.C., Metzler, K.R.C., Panagiotakos, G., Thom, N., et al. (2017). Assembly of functionally integrated human forebrain spheroids. Nature (London, U. K.) *545*, 54–59. https://doi.org/10.1038/nature22330.
94. Walsh, R.M., Crabtree, G.W., Kalpana, K., Jubierre, L., Koo, S.Y., Ciceri, G., Gogos, J.A., Kruglikov, I., and Studer, L. (2024). Cortical assembloids support the development of fast-spiking human PVALB+ cortical interneurons and uncover schizophrenia-associated defects. Preprint at bioRxiv. https://doi.org/10.1101/2024.11.26.624368.
95. Paredes, M.F., Mora, C., Flores-Ramirez, Q., Cebrian-Silla, A., Del Dosso, A., Larimer, P., Chen, J., Kang, G., Gonzalez Granero, S., Garcia, E., et al. (2022). Nests of dividing neuroblasts sustain interneuron production for the developing human brain. Science *375*, eabk2346. https://doi.org/10.1126/science.abk2346.
96. Bershteyn, M., Zhou, H., Fuentealba, L., Chen, C., Subramanyam, G., Cherkowsky, D., Salvatierra, J., Sezan, M., Maury, Y., Havlicek, S., et al. (2024). Human stem cell-derived GABAergic interneuron development reveals early emergence of subtype diversity followed by gradual electrochemical maturation. Preprint at BioRxiv. https://doi.org/10.1101/2024.12.03.626662.
97. Bardy, C., Van Den Hurk, M., Eames, T., Marchand, C., Hernandez, R.V., Kellogg, M., Gorris, M., Galet, B., Palomares, V., Brown, J., et al. (2015). Neuronal medium that supports basic synaptic functions and activity of human neurons in vitro. Proc. Natl. Acad. Sci. *112*, E2725–E2734. https://doi.org/10.1073/pnas.1504393112.
98. Edwards, D., Das, M., Molnar, P., and Hickman, J.J. (2010). Addition of glutamate to serum-free culture promotes recovery of electrical activity in adult hippocampal neurons in vitro. J. Neurosci. Methods *190*, 155–163. https://doi.org/10.1016/j.jneumeth.2010.04.030.
99. Liu, S., Yang, W., Li, Y., and Sun, C. (2023). Fetal bovine serum, an important factor affecting the reproducibility of cell experiments. Sci. Rep. *13*, 1942. https://doi.org/10.1038/s41598-023-29060-7.
100. Sanz-Morello, B., Pfisterer, U., Winther Hansen, N., Demharter, S., Thakur, A., Fujii, K., Levitskii, S.A., Montalant, A., Korshunova, I., Mammen, P.A.P., et al. (2020). Complex IV subunit isoform COX6A2 protects fast-spiking interneurons from oxidative stress and supports their function. EMBO J. *39*, e105759. https://doi.org/10.15252/embj.2020105759.
101. Wu, X., Ma, J., Jia, S., Zhang, X., Zhang, X., An, Z., Wei, Y., Xing, X., Wen, F., Gao, Y., and Bao, S. (2022). High concentration of FBS can save mTOR down-regulation caused by *Mycoplasma bovis* infection. Vet. Sci. *9*, 630. https://doi.org/10.3390/vetsci9110630.
102. Amegandjin, C.A., Choudhury, M., Jadhav, V., Carriço, J.N., Quintal, A., Berryer, M., Snapyan, M., Chattopadhyaya, B., Saghatelyan, A., and Di Cristo, G. (2021). Sensitive period for rescuing parvalbumin interneurons connectivity and social behavior deficits caused by TSC1 loss. Nat. Commun. *12*, 3653. https://doi.org/10.1038/s41467-021-23939-7.
103. Bernard, C., Exposito-Alonso, D., Selten, M., Sanalidou, S., Hanusz-Godoy, A., Aguilera, A., Hamid, F., Oozeer, F., Maeso, P., Allison, L., et al. (2022). Cortical wiring by synapse type–specific control of local protein synthesis. Science *378*, eabm7466. https://doi.org/10.1126/science.abm7466.
104. Sharma, V., Sood, R., Lou, D., Hung, T.Y., Lévesque, M., Han, Y., Levett, J.Y., Wang, P., Murthy, S., Tansley, S., et al. (2021). 4E-BP2–dependent translation in parvalbumin neurons controls epileptic seizure threshold. Proc. Natl. Acad. Sci. USA *118*, e2025522118. https://doi.org/10.1073/pnas.2025522118.
105. Vogt, D., Cho, K.K.A., Lee, A.T., Sohal, V.S., and Rubenstein, J.L.R. (2015). The Parvalbumin/Somatostatin Ratio Is Increased in Pten Mutant Mice and by Human PTEN ASD Alleles. Cell Rep. *11*, 944–956. https://doi.org/10.1016/j.celrep.2015.04.019.
106. Wundrach, D., Martinetti, L.E., Stafford, A.M., Bilinovich, S.M., Angara, K., Prokop, J.W., Crandall, S.R., and Vogt, D. (2020). A human TSC1 variant screening platform in GABAergic cortical interneurons for genotype-to-phenotype assessments. Front. Mol. Neurosci. *13*, 573409. https://doi.org/10.3389/fnmol.2020.573409.
107. Holter, M.C., Hewitt, L.T., Nishimura, K.J., Knowles, S.J., Bjorklund, G.R., Shah, S., Fry, N.R., Rees, K.P., Gupta, T.A., Daniels, C.W., et al. (2021). Hyperactive MEK1 Signaling in Cortical GABAergic Neurons Promotes Embryonic Parvalbumin Neuron Loss and Defects in Behavioral Inhibition. Cereb. Cortex *31*, 3064–3081. https://doi.org/10.1093/cercor/bhaa413.
108. Roux, P.P., Shahbazian, D., Vu, H., Holz, M.K., Cohen, M.S., Taunton, J., Sonenberg, N., and Blenis, J. (2007). RAS/ERK signaling promotes site-specific ribosomal protein S6 phosphorylation via RSK and stimulates cap-dependent translation. J. Biol. Chem. *282*, 14056–14064. https://doi.org/10.1074/jbc.M700906200.
109. Sawicka, K., Pyronneau, A., Chao, M., Bennett, M.V.L., and Zukin, R.S. (2016). Elevated ERK/p90 ribosomal S6 kinase activity underlies audiogenic seizure susceptibility in fragile X mice. Proc. Natl. Acad. Sci. *113*, E6290–E6297. https://doi.org/10.1073/pnas.1610812113.
110. Andrews, M.G., Subramanian, L., and Kriegstein, A.R. (2020). mTOR signaling regulates the morphology and migration of outer radial glia in

developing human cortex. Elife *9*, e58737. https://doi.org/10.7554/eLife.58737.

111. Chow, D.K., Groszer, M., Pribadi, M., Machniki, M., Carmichael, S.T., Liu, X., and Trachtenberg, J.T. (2009). Laminar and compartmental regulation of dendritic growth in mature cortex. Nat. Neurosci. *12*, 116–118. https://doi.org/10.1038/nn.2255.

112. Gallent, E.A., and Steward, O. (2018). Neuronal PTEN deletion in adult cortical neurons triggers progressive growth of cell bodies, dendrites, and axons. Exp. Neurol. *303*, 12–28. https://doi.org/10.1016/j.expneurol.2018.01.005.

113. LiCausi, F., and Hartman, N.W. (2018). Role of mTOR Complexes in Neurogenesis. Int. J. Mol. Sci. *19*, 1544. https://doi.org/10.3390/ijms19051544.

114. Hartman, N.W., Lin, T.V., Zhang, L., Paquelet, G.E., Feliciano, D.M., and Bordey, A. (2013). mTORC1 targets the translational repressor 4E-BP2, but not S6 kinase 1/2, to regulate neural stem cell self-renewal in vivo. Cell Rep. *5*, 433–444. https://doi.org/10.1016/j.celrep.2013.09.017.

115. Nalbandian, A., Llewellyn, K.J., Nguyen, C., Yazdi, P.G., and Kimonis, V.E. (2015). Rapamycin and chloroquine: the in vitro and in vivo effects of autophagy-modifying drugs show promising results in valosin containing protein multisystem proteinopathy. PLoS One *10*, e0122888. https://doi.org/10.1371/journal.pone.0122888.

116. De la Rossa, A., Bellone, C., Golding, B., Vitali, I., Moss, J., Toni, N., Lüscher, C., and Jabaudon, D. (2013). In vivo reprogramming of circuit connectivity in postmitotic neocortical neurons. Nat. Neurosci. *16*, 193–200. https://doi.org/10.1038/nn.3299.

117. Rouaux, C., and Arlotta, P. (2013). Direct lineage reprogramming of post-mitotic callosal neurons into corticofugal neurons in vivo. Nat. Cell Biol. *15*, 214–221. https://doi.org/10.1038/ncb2660.

118. Rouaux, C., and Arlotta, P. (2010). Fezf2 directs the differentiation of corticofugal neurons from striatal progenitors in vivo. Nat. Neurosci. *13*, 1345–1347. https://doi.org/10.1038/nn.2658.

119. Amamoto, R., and Arlotta, P. (2014). Development-Inspired Reprogramming of the Mammalian Central Nervous System. Science *343*, 1239882. https://doi.org/10.1126/science.1239882.

120. Taniguchi, H., He, M., Wu, P., Kim, S., Paik, R., Sugino, K., Kvitsiani, D., Fu, Y., Lu, J., Lin, Y., et al. (2011). A Resource of Cre Driver Lines for Genetic Targeting of GABAergic Neurons in Cerebral Cortex. Neuron *71*, 995–1013. https://doi.org/10.1016/j.neuron.2011.07.026.

121. Gonchar, Y., Wang, Q., and Burkhalter, A. (2007). Multiple distinct subtypes of GABAergic neurons in mouse visual cortex identified by triple immunostaining. Front. Neuroanat. *1*, 3. https://doi.org/10.3389/neuro.05.003.2007.

122. Rudy, B., Fishell, G., Lee, S., and Hjerling-Leffler, J. (2011). Three groups of interneurons account for nearly 100% of neocortical GABAergic neurons. Dev. Neurobiol. *71*, 45–61. https://doi.org/10.1002/dneu.20853.

123. Gaspard, N., Bouschet, T., Herpoel, A., Naeije, G., van den Ameele, J., and Vanderhaeghen, P. (2009). Generation of cortical neurons from mouse embryonic stem cells. Nat. Protoc. *4*, 1454–1463. https://doi.org/10.1038/nprot.2009.157.

124. Shen, Q., Wang, Y., Dimos, J.T., Fasano, C.A., Phoenix, T.N., Lemischka, I.R., Ivanova, N.B., Stifani, S., Morrisey, E.E., and Temple, S. (2006). The timing of cortical neurogenesis is encoded within lineages of individual progenitor cells. Nat. Neurosci. *9*, 743–751. https://doi.org/10.1038/nn1694.

125. Espuny-Camacho, I., Michelsen, K.A., Linaro, D., Bilheu, A., Acosta-Verdugo, S., Herpoel, A., Giugliano, M., Gaillard, A., and Vanderhaeghen, P. (2018). Human Pluripotent Stem-Cell-Derived Cortical Neurons Integrate Functionally into the Lesioned Adult Murine Visual Cortex in an Area-Specific Way. Cell Rep. *23*, 2732–2743. https://doi.org/10.1016/j.celrep.2018.04.094.

126. Bagley, J.A., Reumann, D., Bian, S., Lévi-Strauss, J., and Knoblich, J.A. (2017). Fused cerebral organoids model interactions between brain regions. Nat. Methods *14*, 743–751. https://doi.org/10.1038/nmeth.4304.

127. Hu, R., Lee, L.B., Zhu, B., Cai, P., Tao, Y., Youssef, M., Girrbach, G.I., Song, Y., Wang, X., Tsankov, A., et al. (2024). Expanding GABAergic Neuronal Diversity in iPSC-Derived Disease Models. Preprint at BioRxiv. https://doi.org/10.1101/2024.12.03.626438.

128. Liu, Y., Liu, H., Sauvey, C., Yao, L., Zarnowska, E.D., and Zhang, S.C. (2013). Directed differentiation of forebrain GABA interneurons from human pluripotent stem cells. Nat. Protoc. *8*, 1670–1679. https://doi.org/10.1038/nprot.2013.106.

129. Maroof, A.M., Keros, S., Tyson, J.A., Ying, S.W., Ganat, Y.M., Merkle, F.T., Liu, B., Goulburn, A., Stanley, E.G., Elefanty, A.G., et al. (2013). Directed Differentiation and Functional Maturation of Cortical Interneurons from Human Embryonic Stem Cells. Cell Stem Cell *12*, 559–572. https://doi.org/10.1016/j.stem.2013.04.008.

130. Nicholas, C.R., Chen, J., Tang, Y., Southwell, D.G., Chalmers, N., Vogt, D., Arnold, C.M., Chen, Y.-J.J., Stanley, E.G., Elefanty, A.G., et al. (2013). Functional maturation of hPSC-derived forebrain interneurons requires an extended timeline and mimics human neural development. Cell Stem Cell *12*, 573–586. https://doi.org/10.1016/j.stem.2013.04.005.

131. Paşca, S.P. (2024). Constructing human neural circuits in living systems by transplantation. Cell *187*, 8–13. https://doi.org/10.1016/j.cell.2023.12.008.

132. Samarasinghe, R.A., Miranda, O.A., Buth, J.E., Mitchell, S., Ferando, I., Watanabe, M., Allison, T.F., Kurdian, A., Fotion, N.N., Gandal, M.J., et al. (2021). Identification of neural oscillations and epileptiform changes in human brain organoids. Nat. Neurosci. *24*, 1488–1500. https://doi.org/10.1038/s41593-021-00906-5.

133. Sharf, T., van der Molen, T., Glasauer, S.M.K., Guzman, E., Buccino, A.P., Luna, G., Cheng, Z., Audouard, M., Ranasinghe, K.G., Kudo, K., et al. (2022). Functional neuronal circuitry and oscillatory dynamics in human brain organoids. Nat. Commun. *13*, 4403. https://doi.org/10.1038/s41467-022-32115-4.

134. Xiang, Y., Tanaka, Y., Patterson, B., Kang, Y.J., Govindaiah, G., Roselaar, N., Cakir, B., Kim, K.-Y., Lombroso, A.P., Hwang, S.-M., et al. (2017). Fusion of regionally specified hPSC-derived organoids models human brain development and interneuron migration. Cell Stem Cell *21*, 383–398.e7. https://doi.org/10.1016/j.stem.2017.07.007.

135. Davis, M.F., Figueroa Velez, D.X., Guevarra, R.P., Yang, M.C., Habeeb, M., Carathedathu, M.C., and Gandhi, S.P. (2015). Inhibitory Neuron Transplantation into Adult Visual Cortex Creates a New Critical Period that Rescues Impaired Vision. Neuron *86*, 1055–1066. https://doi.org/10.1016/j.neuron.2015.03.062.

136. Hunt, R.F., Girskis, K.M., Rubenstein, J.L., Alvarez-Buylla, A., and Baraban, S.C. (2013). GABA progenitors grafted into the adult epileptic brain control seizures and abnormal behavior. Nat. Neurosci. *16*, 692–697. https://doi.org/10.1038/nn.3392.

137. Dehorter, N., Ciceri, G., Bartolini, G., Lim, L., del Pino, I., and Marín, O. (2015). Tuning of fast-spiking interneuron properties by an activity-dependent transcriptional switch. Science *349*, 1216–1220. https://doi.org/10.1126/science.aab3415.

138. Dulcis, D., Jamshidi, P., Leutgeb, S., and Spitzer, N.C. (2013). Neurotransmitter Switching in the Adult Brain Regulates Behavior. Science *340*, 449–453. https://doi.org/10.1126/science.1234152.

139. Meng, D., Li, H.Q., Deisseroth, K., Leutgeb, S., and Spitzer, N.C. (2018). Neuronal activity regulates neurotransmitter switching in the adult brain following light-induced stress. Proc. Natl. Acad. Sci. *115*, 5064–5071. https://doi.org/10.1073/pnas.1801598115.

140. Doll, H.M., Risgaard, R.D., Thurston, H., Chen, R.J., and Sousa, A.M. (2024). Evolutionary innovations in the primate dopaminergic system. Curr. Opin. Genet. Dev. *88*, 102236. https://doi.org/10.1016/j.gde.2024.102236.

141. Ma, S., Skarica, M., Li, Q., Xu, C., Risgaard, R.D., Tebbenkamp, A.T.N., Mato-Blanco, X., Kovner, R., Krsnik, Ž., De Martin, X., et al. (2022). Molecular and cellular evolution of the primate dorsolateral prefrontal cortex. Science *377*, eabo7257. https://doi.org/10.1126/science.abo7257.

142. Sousa, A.M.M., Zhu, Y., Raghanti, M.A., Kitchen, R.R., Onorati, M., Tebbenkamp, A.T.N., Stutz, B., Meyer, K.A., Li, M., Kawasawa, Y.I., et al. (2017). Molecular and Cellular Reorganization of Neural Circuits in the Human Lineage. Science *358*, 1027–1032. https://doi.org/10.1126/science.aan3456.

143. Del Rio, M.R., and De Felipe, J. (1997). Colocalization of parvalbumin and calbindin D-28k in neurons including chandelier cells of the human temporal neocortex. J. Chem. Neuroanat. *12*, 165–173. https://doi.org/10.1016/S0891-0618(96)00191-3.

144. Brunet Avalos, C., and Sprecher, S.G. (2021). Single-Cell Transcriptomic Reveals Dual and Multi-Transmitter Use in Neurons Across Metazoans. Front. Mol. Neurosci. *14*, 623148. https://doi.org/10.3389/fnmol.2021.623148.

145. Lee, B.R., Dalley, R., Miller, J.A., Chartrand, T., Close, J., Mann, R., Mukora, A., Ng, L., Alfiler, L., Baker, K., et al. (2023). Signature morphoelectric properties of diverse GABAergic interneurons in the human neocortex. Science *382*, eadf6484. https://doi.org/10.1126/science.adf6484.

146. Yao, Z., van Velthoven, C.T.J., Nguyen, T.N., Goldy, J., Sedeno-Cortes, A.E., Baftizadeh, F., Bertagnolli, D., Casper, T., Chiang, M., Crichton, K., et al. (2021). A taxonomy of transcriptomic cell types across the isocortex and hippocampal formation. Cell *184*, 3222–3241.e26. https://doi.org/10.1016/j.cell.2021.04.021.

147. Barry, C., Schmitz, M.T., Jiang, P., Schwartz, M.P., Duffin, B.M., Swanson, S., Bacher, R., Bolin, J.M., Elwell, A.L., McIntosh, B.E., et al. (2017). Species-specific developmental timing is maintained by pluripotent stem cells ex utero. Dev. Biol. *423*, 101–110. https://doi.org/10.1016/j.ydbio.2017.02.002.

148. Porter, L.L., Rizzo, E., and Hornung, J.P. (1999). Dopamine Affects Parvalbumin Expression during Cortical Development In Vitro. J. Neurosci. *19*, 8990–9003. https://doi.org/10.1523/JNEUROSCI.19-20-08990.1999.

149. Hergenreder, E., Minotti, A.P., Zorina, Y., Oberst, P., Zhao, Z., Munguba, H., Calder, E.L., Baggiolini, A., Walsh, R.M., Liston, C., et al. (2024). Combined small-molecule treatment accelerates maturation of human pluripotent stem cell-derived neurons. Nat. Biotechnol. *42*, 1515–1525. https://doi.org/10.1038/s41587-023-02031-z.

150. Monko, T., Rebertus, J., Stolley, J., Salton, S.R., and Nakagawa, Y. (2022). Thalamocortical axons regulate neurogenesis and laminar fates in the early sensory cortex. Proc. Natl. Acad. Sci. *119*, e2201355119. https://doi.org/10.1073/pnas.2201355119.

151. Pouchelon, G., Gambino, F., Bellone, C., Telley, L., Vitali, I., Lüscher, C., Holtmaat, A., and Jabaudon, D. (2014). Modality-specific thalamocortical inputs instruct the identity of postsynaptic L4 neurons. Nature *511*, 471–474. https://doi.org/10.1038/nature13390.

152. Miyamae, T., Chen, K., Lewis, D.A., and Gonzalez-Burgos, G. (2017). Distinct Physiological Maturation of Parvalbumin-Positive Neuron Subtypes in Mouse Prefrontal Cortex. J. Neurosci. *37*, 4883–4902. https://doi.org/10.1523/JNEUROSCI.3325-16.2017.

153. Trujillo, C.A., Gao, R., Negraes, P.D., Gu, J., Buchanan, J., Preissl, S., Wang, A., Wu, W., Haddad, G.G., Chaim, I.A., et al. (2019). Complex oscillatory waves emerging from cortical organoids model early human brain network development. Cell Stem Cell *25*, 558–569.e7. https://doi.org/10.1016/j.stem.2019.08.002.

154. Eiraku, M., Watanabe, K., Matsuo-Takasaki, M., Kawada, M., Yonemura, S., Matsumura, M., Wataya, T., Nishiyama, A., Muguruma, K., and Sasai, Y. (2008). Self-organized formation of polarized cortical tissues from ESCs and its active manipulation by extrinsic signals. Cell Stem Cell *3*, 519–532. https://doi.org/10.1016/j.stem.2008.09.002.

155. Elliott, M.A.T., Schweiger, H.E., Robbins, A., Vera-Choqqueccota, S., Ehrlich, D., Hernandez, S., Voitiuk, K., Geng, J., Sevetson, J.L., Core, C., et al. (2023). Internet-connected cortical organoids for project-based stem cell and neuroscience education. eNeuro *10*, ENEURO.0308-23.2023. https://doi.org/10.1523/ENEURO.0308-23.2023.

156. Park, Y., Hernandez, S., Hernandez, C.O., Schweiger, H.E., Li, H., Voitiuk, K., Dechiraju, H., Hawthorne, N., Muzzy, E.M., Selberg, J.A., et al. (2024). Modulation of neuronal activity in cortical organoids with bioelectronic delivery of ions and neurotransmitters. Cell Rep. Methods *4*, 100686. https://doi.org/10.1016/j.crmeth.2023.100686.

157. Robbins, A., Schweiger, H.E., Hernandez, S., Spaeth, A., Voitiuk, K., Parks, D.F., Van der Molen, T., Geng, J., Sharf, T., Mostajo-Radji, M.A., et al. (2024). Goal-Directed Learning in Cortical Organoids. Preprint at bioRxiv, 2024.12.07.627350. https://doi.org/10.1101/2024.12.07.627350.

158. Atamian, A., Birtele, M., Hosseini, N., Nguyen, T., Seth, A., Del Dosso, A., Paul, S., Tedeschi, N., Taylor, R., Coba, M.P., et al. (2024). Human cerebellar organoids with functional Purkinje cells. Cell Stem Cell *31*, 39–51.e6. https://doi.org/10.1016/j.stem.2023.11.013.

159. Wang, S., Wang, B., Pan, N., Fu, L., Wang, C., Song, G., An, J., Liu, Z., Zhu, W., Guan, Y., et al. (2015). Differentiation of human induced pluripotent stem cells to mature functional Purkinje neurons. Sci. Rep. *5*, 9232. https://doi.org/10.1038/srep09232.

160. Dhaliwal, N.K., Weng, O.Y., Dong, X., Bhattacharya, A., Ahmed, M., Nishimura, H., Choi, W.W.Y., Aggarwal, A., Luikart, B.W., Shu, Q., et al. (2024). Synergistic hyperactivation of both mTORC1 and mTORC2 underlies the neural abnormalities of PTEN-deficient human neurons and cortical organoids. Cell Rep. *43*, 114173. https://doi.org/10.1016/j.celrep.2024.114173.

161. Bhaduri, A., Andrews, M.G., Mancia Leon, W., Jung, D., Shin, D., Allen, D., Jung, D., Schmunk, G., Haeussler, M., Salma, J., et al. (2020). Cell stress in cortical organoids impairs molecular subtype specification. Nature *578*, 142–148. https://doi.org/10.1038/s41586-020-1962-0.

162. Gonzalez-Ferrer, J., Lehrer, J., O'Farrell, A., Paten, B., Teodorescu, M., Haussler, D., Jonsson, V.D., and Mostajo-Radji, M.A. (2024). SIMS: A deep-learning label transfer tool for single-cell RNA sequencing analysis. Cell Genom. *4*, 100581. https://doi.org/10.1016/j.xgen.2024.100581.

163. Medalla, M., Mo, B., Nasar, R., Zhou, Y., Park, J., and Luebke, J.I. (2023). Comparative features of calretinin, calbindin, and parvalbumin expressing interneurons in mouse and monkey primary visual and frontal cortices. J. Comp. Neurol. *531*, 1934–1962. https://doi.org/10.1002/cne.25514.

164. Shi, Y., Wang, M., Mi, D., Lu, T., Wang, B., Dong, H., Zhong, S., Chen, Y., Sun, L., Zhou, X., et al. (2021). Mouse and human share conserved transcriptional programs for interneuron development. Science *374*, eabj6641. https://doi.org/10.1126/science.abj6641.

165. Casimir, P., Iwata, R., and Vanderhaeghen, P. (2024). Linking mitochondria metabolism, developmental timing, and human brain evolution. Curr. Opin. Genet. Dev. *86*, 102182. https://doi.org/10.1016/j.gde.2024.102182.

166. Iwata, R., Casimir, P., Erkol, E., Boubakar, L., Planque, M., Gallego López, I.M., Ditkowska, M., Gaspariunaite, V., Beckers, S., Remans, D., et al. (2023). Mitochondria metabolism sets the species-specific tempo of neuronal development. Science *379*, eabn4705. https://doi.org/10.1126/science.abn4705.

167. Iwata, R., and Vanderhaeghen, P. (2024). Metabolic mechanisms of species-specific developmental tempo. Dev. Cell *59*, 1628–1639. https://doi.org/10.1016/j.devcel.2024.05.027.

168. Quiñones, S., Wang, J.C., Kim, E., Bottom-Tanzer, S., Armbruster, M., Macêdo, J.K., Hawkinson, T., Ribas, R., Singh, P.K., Wu, L., et al. (2024). Cortical inhibitory parvalbumin interneurons exhibit metabolic specializations coordinated by PGC-1$\alpha$ that are lost in rodents and humans after traumatic brain injury. Preprint at BioRxiv. https://doi.org/10.1101/2024.06.19.599637.

169. Cowell, R.M., Blake, K.R., and Russell, J.W. (2007). Localization of the transcriptional coactivator PGC-1$\alpha$ to GABAergic neurons during

maturation of the rat brain. J. Comp. Neurol. *502*, 1–18. https://doi.org/10.1002/cne.21211.

170. Vértesy, Á., Eichmüller, O.L., Naas, J., Novatchkova, M., Esk, C., Balmaña, M., Ladstaetter, S., Bock, C., von Haeseler, A., and Knoblich, J.A. (2022). Gruffi: an algorithm for computational removal of stressed cells from brain organoid transcriptomic datasets. EMBO J. *41*, e111118. https://doi.org/10.15252/embj.2022111118.
171. Matsumoto, Y., Hayashi, Y., Schlieve, C.R., Ikeya, M., Kim, H., Nguyen, T.D., Sami, S., Baba, S., Barruet, E., Nasu, A., et al. (2013). Induced pluripotent stem cells from patients with human fibrodysplasia ossificans progressiva show increased mineralization and cartilage formation. Orphanet J. Rare Dis. *8*, 190. https://doi.org/10.1186/1750-1172-8-190.
172. Gallego Romero, I., Pavlovic, B.J., Hernando-Herraez, I., Zhou, X., Ward, M.C., Banovich, N.E., Kagan, C.L., Burnett, J.E., Huang, C.H., Mitrano, A., et al. (2015). A panel of induced pluripotent stem cells from chimpanzees: a resource for comparative functional genomics. Elife *4*, e07103. https://doi.org/10.7554/eLife.07103.
173. Miyaoka, Y., Chan, A.H., Judge, L.M., Yoo, J., Huang, M., Nguyen, T.D., Lizarraga, P.P., So, P.-L., and Conklin, B.R. (2014). Isolation of single-base genome-edited human iPS cells without antibiotic selection. Nat. Methods *11*, 291–293. https://doi.org/10.1038/nmeth.2840.
174. Goulburn, A.L., Alden, D., Davis, R.P., Micallef, S.J., Ng, E.S., Yu, Q.C., Lim, S.M., Soh, C.-L., Elliott, D.A., Hatzistavrou, T., et al. (2011). A targeted NKX2.1 human embryonic stem cell reporter line enables identification of human basal forebrain derivatives. Stem Cell. *29*, 462–473. https://doi.org/10.1002/stem.587.
175. Xiang, Y., Cakir, B., and Park, I.H. (2020). Generation of regionally specified human brain organoids resembling thalamus development. STAR Protoc. *1*, 100001. https://doi.org/10.1016/j.xpro.2019.100001.
176. Susaki, E.A., Tainaka, K., Perrin, D., Yukinaga, H., Kuno, A., and Ueda, H.R. (2015). Advanced CUBIC protocols for whole-brain and whole-body clearing and imaging. Nat. Protoc. *10*, 1709–1727. https://doi.org/10.1038/nprot.2015.085.
177. Bray, N.L., Pimentel, H., Melsted, P., and Pachter, L. (2016). Near-optimal probabilistic RNA-seq quantification. Nat. Biotechnol. *34*, 525–527. https://doi.org/10.1038/nbt.3519.
178. Polański, K., Young, M.D., Miao, Z., Meyer, K.B., Teichmann, S.A., and Park, J.E. (2020). BBKNN: fast batch alignment of single cell transcriptomes. Bioinformatics (Edam) *36*, 964–965. https://doi.org/10.1093/bioinformatics/btz625.
179. Wolf, F.A., Angerer, P., and Theis, F.J. (2018). SCANPY: large-scale single-cell gene expression data analysis. Genome Biol. *19*, 15. https://doi.org/10.1186/s13059-017-1382-0.
180. Huang, W., Bhaduri, A., Velmeshev, D., Wang, S., Wang, L., Rottkamp, C.A., Alvarez-Buylla, A., Rowitch, D.H., and Kriegstein, A.R. (2020). Origins and Proliferative States of Human Oligodendrocyte Precursor Cells. Cell *182*, 594–608.e11. https://doi.org/10.1016/j.cell.2020.06.027.

## STAR★METHODS

### KEY RESOURCES TABLE

| REAGENT or RESOURCE | SOURCE | IDENTIFIER |
|---|---|---|
| Antibodies | | |
| Rabbit anti-Bdnf | Abcam | Cat#: ab108319; RRID: AB_10862052 |
| Rat anti-Bcl11b | Abcam | Cat# ab18465; RRID: AB_2064130 |
| Rabbit anti-Cox6A2 | Novus Biologicals | Cat#: NBP1-31112; RRID: AB_2085447 |
| Mouse anti-ErbB4 | Thermo Fisher Scientific | Cat#: MA5-12888; RRID: AB_10986112 |
| Rabbit anti-Gbx2 | Proteintech | Cat#: 21639-1-AP; RRID: AB_2878896 |
| Goat anti-GFP (Green Fluorescent Protein) | Abcam | Cat#: ab6658; RRID: AB_305631 |
| Mouse anti-HNA (Human Nuclei Antigen) | Millipore Sigma | Cat#: MAB1281; RRID: AB_94090 |
| Rabbit anti-Map2 | Proteintech | Cat#:17490-1-AP; RRID: AB_2137880 |
| Rabbit anti-MAPK (ERK1/2) phosphorylated (T202/Y204) | Cell Signaling | Cat#: 9101; RRID: AB_331646 |
| Rabbit anti-Mef2c | Abcam | Cat#: ab227085; RRID: AB_3080861 |
| Mouse anti-Mki67 | BD Biosciences | Cat#: 550609; RRID: AB_393778 |
| Mouse anti-Nestin | Thermo Fisher Scientific | MA1-110; RRID: AB_2536821 |
| Rabbit anti-Nkx2.1 | Abcam | Cat#: ab76013; RRID: AB_1310784 |
| Mouse anti-Nr2f2 | R&D Systems | Cat#: PP-H7147-00; RRID: AB_2155627 |
| Rabbit anti-Pvalb | Swant | Cat#: PV27; RRID: AB_2631173 |
| Rabbit anti-Psd95 | Thermo Fisher Scientific | Cat#: 51-6900; RRID: AB_2533914 |
| Chicken anti-Rbfox3 (NeuN) | Millipore Sigma | Cat#: ABN91; RRID: AB_11205760 |
| Chicken anti-RFP (Red Fluorescent Protein) | Rockland Immunochemicals | Cat# 600-901-379; RRID: AB_10704808 |
| Rabbit anti-S6 phosphorylated (pS6) (S235/236) | Cell Signaling | Cat#: 2211; RRID: AB_331679 |
| Mouse anti-Satb2 | Abcam | Cat#: ab51502; RRID: AB_882455 |
| Mouse anti-Sox2 | Santa Cruz Biotechnology | Cat# sc-365823; RRID: AB_10842165 |
| Mouse anti-Sst | Santa Cruz Biotechnology | Cat# sc55565; RRID: AB_831726 |
| Mouse anti-Tcf7l2 | Millipore Sigma | Cat#: 05-511; RRID: AB_309772 |
| Bacterial and virus strains | | |
| eGFP Adenovirus (CMV promoter) | Vector Biolabs | Cat#: 1060 |
| Biological samples | | |
| GW18-19 Human medial ganglionic eminences | Primary tissue | N/A |
| GW21-22 Human cortex | Primary tissue | N/A |
| GW39-56 years Human postmortem brain tissue | Primary tissue | N/A |
| Chemicals, peptides, and recombinant proteins | | |
| 488-conjugated Streptavidin | Thermo Fisher Scientific | Cat#: S11223 |
| Allopregnanolone | Cayman Chemicals | Cat#: 16930 |
| B-27 Supplement | Thermo Fisher Scientific | Cat#: 17504044 |
| B-27 supplement minus Vitamin A | Thermo Fisher Scientific | Cat#: 12587010 |
| Biotin-conjugated WFA (Wisteria floribunda agglutinin) | Vector Laboratories | Cat#: B-1355-2; RRID: AB_2336874 |
| Chemically Defined Lipid Concentrate | Thermo Fisher Scientific | Cat#: 11905031 |
| DAPI (4′,6-Diamidino-2-Phenylindole, dihydrochloride) | Thermo Fisher Scientific | Cat#: D1306 |
| Dextrose | Millipore Sigma | Cat#: PHR1000 |
| DNase I | Millipore Sigma | Cat#: 69182 |
| Dorsomorphin | Millipore Sigma | Cat#: P5499 |
| Fibronectin | Millipore Sigma | Cat#: DLW354008 |
| Fluo8-AM | Millipore Sigma | Cat#: DLW354008 |

(*Continued on next page*)

*Continued*

| REAGENT or RESOURCE | SOURCE | IDENTIFIER |
|---|---|---|
| GlutaMAX Supplement | Thermo Fisher Scientific | Cat#: 35050061 |
| Heparin sodium salt | Millipore Sigma | Cat#: H3149 |
| Hoechst 33342 | Thermo Fisher Scientific | Cat#: 62249 |
| IWR1-ε | Cayman Chemical | Cat#: 13659 |
| Laminin | Millipore Sigma | Cat#: L2020 |
| LDN193189 dihydrochloride | Tocris | Cat#: 6053 |
| Matrigel Growth Factor Reduced (GFR) Basement Membrane Matrix | Corning | Cat#: 354230 |
| MEM Non-Essential Amino Acids | Thermo Fisher Scientific | Cat#: 11140050 |
| N-2 Supplement | Thermo Fisher Scientific | Cat#: 17502048 |
| N,N,N′,N′-Tetrakis(2-hydroxypropyl) ethylenediamine | Tokyo Chemical Industry | Cat# T0781 |
| PD325901 | Millipore Sigma | Cat#: PZ0162 |
| Poly-L-ornithine solution | Millipore Sigma | Cat#: P4957 |
| Rapamycin | Millipore Sigma | Cat#: R8781 |
| Recombinant Human BDNF | Millipore Sigma | Cat#: SRP3014 |
| Recombinant Human BMP7 | R&D Systems | Cat#: 354-BP |
| Recombinant Human EGF | R&D Systems | Cat#: 236-EG |
| Recombinant Human FGF-basic | Thermo Fisher Scientific | Cat#: PHG0261 |
| Recombinant Human Insulin solution | Santa Cruz Biotechnology | Cat#: sc-360248 |
| Retinoic acid | Millipore Sigma | Cat#: R2625 |
| Rho Kinase Inhibitor (Y-27632) | Tocris | Cat#: 1254 |
| SB431542 | Tocris | Cat#: 1614 |
| Smoothened Agonist (SAG) HCl | Selleckchem | Cat#: S7779 |
| Sodium Pyruvate | Millipore Sigma | Cat#: S8636 |
| SYTO 16 | Thermo Fisher Scientific | Cat#: S7578 |
| Urea | Millipore Sigma | Cat#: U5378 |
| **Critical commercial assays** | | |
| 10X Chromium Single Cell 3′ reagent kit V3 | 10X Genomics | Cat#: PN-1000092 |
| Click-iT Plus EdU Cell Proliferation Kit for Imaging® | Thermo Fisher Scientific | Cat#: C10640 |
| Papain Dissociation System | Worthington | Cat#: LK003150 |
| **Deposited data** | | |
| Raw and analyzed single cell RNA sequencing data | This paper | NCBI GEO: GSE278531 |
| Human reference genome NCBI build 38, GRCh38 | Genome Reference Consortium | https://www.ncbi.nlm.nih.gov/grc/human |
| Mouse reference genome NCBI build 39, GRCm39/mm39 | Genome Reference Consortium | https://www.ncbi.nlm.nih.gov/grc/mouse |
| 10x Genomics E18 mouse cortex example dataset | 10X Genomics | NCBI GEO: GSE93421 |
| Embryonic and perinatal mouse interneurons | Loo et al. 2019[52] | NCBI GEO: GSE123335 |
| Embryonic mouse interneurons | La Manno et al. 2021[53] | NCBI SRA: PRJNA637987 |
| Embryonic mouse interneurons | Mayer et al. 2018[31] | NCBI GEO: GSE104158 |
| Postnatal mouse interneurons | Zeisel et al. 2018[54] | NCBI SRA: SRP135960 |
| **Experimental models: Cell lines** | | |
| H2B.-1323.4 | Matsumoto et al. 2013[171] | RRID: CVCL_0G84 |
| H28126 | Romero et al. 2015[172] | N/A |
| WTC-11 | Miyaoka et al. 2014[173] | RRID: CVCL_Y803 |

(*Continued on next page*)

*Continued*

| REAGENT or RESOURCE | SOURCE | IDENTIFIER |
|---|---|---|
| HES-3 NKX2.1GFP/w | Goulburn et al. 2011[174] | RRID: CVCL_A5HB |
| **Experimental models: Organisms/strains** | | |
| Mouse: Ai14 B6;129S6-Gt(ROSA) 26Sortm14(CAG-tdTomato)Hze/J | The Jackson Laboratory | Cat#: 007908 |
| Mouse: Ai34 B6;129S-Gt(ROSA) 26Sortm34.1(CAG-Syp/tdTomato)Hze/J | The Jackson Laboratory | Cat#: 012570 |
| Mouse: Ai96 B6J.Cg-Gt(ROSA) 26Sortm96(CAG-GCaMP6s)Hze/MwarJ | The Jackson Laboratory | Cat#: 028866 |
| Mouse: C57BL/6 | Charles River | Cat#: 027 |
| Mouse: *Nkx2.1*-Cre (C57BL/6J-Tg (Nkx2-1-cre)2Sand/J | The Jackson Laboratory | Cat#: 008661 |
| Mouse: *Pvalb*-Cre B6.129P2-Pvalbtm1(cre)Arbr/J | The Jackson Laboratory | Cat#: 017320 |
| Mouse: *Sst*-Cre Ssttm2.1(cre)Zjh/J | The Jackson Laboratory | Cat#: 13044 |
| **Software and algorithms** | | |
| Prism 9.3.1 | GraphPad Software | RRID:SCR_002798 |
| Kallisto 0.46.2 | https://pachterlab.github.io/kallisto/about | RRID:SCR_016582 |
| CellBender 0.2.0 | https://github.com/broadinstitute/CellBender | RRID: SCR_025990 |
| Scrublet 0.2.2 | https://github.com/swolock/scrublet | RRID: SCR_018098 |
| Scanpy 1.8 | https://github.com/theislab/scanpy | RRID: SCR_018139 |
| Cell Ranger 5 | 10X Genomics | RRID: SCR_017344 |
| SIMS | https://sc-sims-app.streamlit.app/ | RRID: SCR_025787 |
| ImageJ 2.3.0 | National Institutes of Health | RRID:SCR_003070 |
| VirtualDub | https://www.virtualdub.org | RRID: SCR_026123 |
| Imaris 9.2 | Leica Microsystems | RRID: SCR_007370 |
| Leica Application Suite X | Leica Microsystems | RRID:SCR_013673 |
| **Other** | | |
| Air-liquid interface on hydrophilic polytetrafluoroethylene cell culture inserts | Millipore Sigma | Cat#: PICM0RG50 |
| Basal Medium Eagle | Millipore Sigma | Cat#: B9638 |
| BrainPhys Neuronal Medium | Stem Cell Technologies | Cat#: 05790 |
| Dulbecco's Modified Eagle Medium: Nutrient Mixture F-12 with GlutaMAX | Thermo Fisher Scientific | Cat#: 10565018 |
| Fetal Bovine Serum | Millipore Sigma | Cat#: F2442 |
| Glasgow Minimum Essential Medium | Thermo Fisher Scientific | Cat#: 11710035 |
| Hanks' Balanced Salt Solution | Millipore Sigma | Cat#: H8264 |
| Hyclone characterized fetal bovine serum | Cytova | Cat#: SH30071.03 |
| Knockout Serum Replacement | Thermo Fisher Scientific | Cat#: 10828028 |
| Leibovitz's L-15 Medium | Thermo Fisher Scientific | Cat#: 11415064 |
| mFreSR Medium | Stem Cell Technologies | Cat#: 05855 |
| Neurobasal A Medium | Thermo Fisher Scientific | Cat#: 10888022 |
| Neurobasal Medium | Thermo Fisher Scientific | Cat#: 21103049 |
| ReLeSR Passaging Reagent | Stem Cell Technologies | Cat#: 05872 |
| StemFlex Medium | Thermo Fisher Scientific | Cat#: A3349401 |

## EXPERIMENTAL MODEL AND STUDY PARTICIPANT DETAILS

### Live primary human cortical tissue collection

All primary fetal tissues were collected and processed under UCSF Gamete, Embryo, and Stem Cell Research Committee (GESCR) approval (Protocol #10–05113). Informed patient consent was obtained for all samples, with collection strictly adhering to legal and institutional ethical guidelines. All tissue samples were de-identified, and no sex or ancestry information was recorded. Second-trimester samples were obtained from surgical procedures. In compliance with legal and ethical regulations, investigators did not interfere with the surgery.

A total of nine samples were used in this study:

- Three GW22 samples were used to obtain cortical sections for grafting td-Tomato-positive mouse INs.
- Three GW21.6–23 samples were used for grafting unlabeled mouse INs onto cortical sections.
- Three GW18–19 samples were used for human MGE progenitor grafting.

For cortical sections, only samples with an intact cerebral cortex were selected. For human MGE grafting, samples were chosen when at least one entire brain hemisphere was intact, allowing for clear anatomical identification of the MGEs.

Brain tissue was immediately transported in ice-cold artificial cerebrospinal fluid (ACSF) composed of 125 mM sodium chloride (Millipore Sigma #S9888), 2.5 mM potassium chloride (Millipore Sigma #P3911), 1 mM magnesium chloride (Millipore Sigma #M8266), 2 mM calcium chloride (Millipore Sigma #C4901), 1.25 mM sodium phosphate monobasic (Millipore Sigma #71505), 25 mM sodium bicarbonate (Millipore Sigma #S5761), and 25 mM D-(+)-glucose (Millipore Sigma #G8270). Before use, this solution was bubbled with 95% $O_2$ and 5% $CO_2$. All tissue was used within 5 hours of collection.

Upon arrival at the lab, meninges were removed, and the tissue was either processed for organotypic culture or dissociated into cells, as detailed below. Occasionally, tissue with distinguishable MGEs was dissected, sectioned, and cryopreserved for future experiments. Freezing media included Dulbecco's Modified Eagle Medium: Nutrient Mixture F-12 with GlutaMAX (Thermo Fisher Scientific # 10565018), N-2 Supplement (Thermo Fisher Scientific # 17502048), B-27 Supplement (Thermo Fisher Scientific # 17504044), 20 ng/mL Human FGF-basic (Thermo Fisher Scientific # PHG0261), 20 ng/mL Recombinant Human EGF (R&D Systems # 236-EG), 20 μg/mL Human Insulin (Santa Cruz Biotechnology # sc-360248), 5 ng/mL human BDNF (Millipore Sigma # SRP3014), 10 μM Rho Kinase Inhibitor (Y-27632) (Tocris # 1254), 1.6 g/L D-(+)-glucose (Millipore Sigma # G8270), and 10% Dimethyl Sulfoxide (Cell Signaling Technology #1 2611).

### Postmortem primary human cortical tissue collection

Deidentified human specimens were collected postmortem with prior patient consent, following the ethical guidelines of the UCSF Committee on Human Research (Protocol # 10-02693). The postmortem interval (PMI) was less than 24 hours. All tissue samples were de-identified, and no sex or ancestry information was recorded. Specimens were evaluated by a neuropathologist and categorized as control samples. A total of four samples were used in this study, based on tissue availability:

- One GW39 sample.
- One 6 weeks post-birth sample.
- One 6 years old sample.
- One 57 years old sample.

The tissue was coronally sectioned, and when possible, one hemisphere was cut axially. One-millimeter blocks were fixed in 4% paraformaldehyde (PFA) (Thermo Fisher Scientific #28908) for two days, then cryoprotected in a 30% sucrose gradient (Millipore Sigma # S8501). The tissue was embedded in Tissue-Tek O.C.T. Compound (Sakura # 4583), cryosectioned at 30 μm using a cryostat (Leica Biosystems # CM3050), and mounted on glass slides.

### Mouse lines and husbandry

All mouse experiments were conducted in compliance with UCSF Institutional Animals Care and Use Committee guidelines (Protocol # AN178775-02). The mouse lines used were previously described: *Nkx2.1*-Cre (C57BL/6J-Tg(Nkx2-1-cre)2Sand/J[59] The Jackson Laboratory #008661), *Sst*-Cre (Ssttm2.1(cre)Zjh/J[120]; The Jackson Laboratory #13044), *Pvalb*-Cre (B6.129P2-Pvalbtm1(cre)Arbr/J[80]; The Jackson Laboratory \# 017320), Ai14 (B6;129S6-Gt(ROSA)26Sortm14(CAG-tdTomato)Hze/J[60]; The Jackson Laboratory #007908), Ai34 (B6;129S-Gt(ROSA)26Sortm34.1(CAG-Syp/tdTomato)Hze/J[73]; The Jackson Laboratory #012570), and Ai96 (B6J.Cg-Gt(ROSA)26Sortm96(CAG-GCaMP6s)Hze/MwarJ[75]; The Jackson Laboratory #028866). Mice were of the C57BL/6J background, and developmental staging was calculated with the plug date as E0.5. The experiments were done in mouse embryos, and therefore no sex information was recorded.

### Cell lines

We used three previously described iPSC lines: H2B.-1323.4 (female; RRID: CVCL_0G84),[171] H28126 (male),[172] and WTC-11 (male, Asian; RRID: CVCL_Y803).[173] Additionally, we employed the human embryonic stem cell (hESC) line HES-3 NKX2.1GFP/w (female;

RRID: CVCL_A5HB).[174] The cell lines were not authenticated. Mycoplasma testing by MycoAlert (Lonza # LT07-318) confirmed lack of contamination.

## METHOD DETAILS

### Pluripotent stem cells maintenance

Pluripotent stem cells were cultured in StemFlex Medium (Thermo Fisher Scientific #A3349401) with Penicillin/Streptomycin (Thermo Fisher Scientific #15140122). Cell passaging was done using ReLeSR (Stem Cell Technologies #05872), following the manufacturer's instructions. Cells were cryopreserved in mFreSR medium (Stem Cell Technologies #05855).

### Culture of human and mouse organotypic cortical sections

#### *Preparation of ACSF and tissue collection*

Fresh ACSF was prepared prior to tissue collection. The composition of ACSF included 125 mM sodium chloride (Millipore Sigma # S9888), 2.5 mM potassium chloride (Millipore Sigma # P3911), 1 mM magnesium chloride (Millipore Sigma # M8266), 2 mM calcium chloride (Millipore Sigma # C4901), 1.25 mM sodium phosphate monobasic (Millipore Sigma # 71505), 25 mM sodium bicarbonate (Millipore Sigma # S5761), and 25 mM D-(+)-glucose (Millipore Sigma # G8270). The solution was continuously bubbled with a gas mixture of 95% $O_2$ and 5% $CO_2$ to maintain optimal oxygenation and pH balance.

#### *Tissue embedding and sectioning*

After collection, tissue was stored in ACSF before embedding in 3% low-gelling agarose (Millipore Sigma # A9414). The embedded tissue was sectioned at 300 μM using a vibratome (Leica).

#### *Slice culture at the air-liquid interface*

Slices were cultured at the air-liquid interface on hydrophilic polytetrafluoroethylene cell culture inserts (Millipore Sigma # PICM0RG50) in a medium containing 32% Hanks' Balanced Salt Solution (Millipore Sigma # H8264), 60% Basal Medium Eagle (Millipore Sigma # B9638), 5% Fetal Bovine Serum (Millipore Sigma # F2442), 1% D-(+)-glucose (Millipore Sigma # G8270), 1X N2 Supplement, and 100 U/mL Penicillin/Streptomycin. The medium was replenished every 2-3 days to maintain slice viability.

### Human cortical organoids generation

#### *iPSC aggregation and early differentiation*

To generate human cortical organoids, we followed a modified version of our previously established protocol.[68] iPSCs were dissociated into single cells and reaggregated at a density of 10,000 cells per aggregate in lipidure-coated 96-well V-bottom plates, using 100 μL of StemFlex Medium supplemented with 10 μM Rho Kinase Inhibitor (Y-27632, Tocris # 1254) on Day -1.

#### *Cortical induction*

On Day 0, the medium was replaced with cortical differentiation medium containing Glasgow Minimum Essential Medium (Thermo Fisher Scientific # 11710035), 20% Knockout Serum Replacement (Thermo Fisher Scientific # 10828028), 0.1 mM MEM Non-Essential Amino Acids (Thermo Fisher Scientific # 11140050), 1 mM Sodium Pyruvate (Millipore Sigma # S8636), 0.1 mM 2-Mercaptoethanol (Millipore Sigma # M3148), and 100 U/mL Penicillin/Streptomycin. The medium was further supplemented with 20 μM Rho Kinase Inhibitor (Y-27632, Days 0-6), 3 μM WNT Inhibitor (IWR1-ε, Cayman Chemical # 13659, Days 0-18), and 5 μM TGF-Beta Inhibitor (SB431542, Tocris # 1614, Days 0-18). Media changes occurred on Days 3, 6, and subsequently every 2-3 days until Day 18.

#### *Neuronal differentiation and maintenance*

On Day 18, organoids were transferred to ultra-low adhesion plates (Millipore Sigma # CLS3471) and placed on an orbital shaker at 90 revolutions per minute in neuronal differentiation medium. This medium contained Dulbecco's Modified Eagle Medium: Nutrient Mixture F-12 with GlutaMAX (Thermo Fisher Scientific # 10565018), 10% (v/v) Hyclone characterized fetal bovine serum (Cytova # SH30071.03), 1X N-2 Supplement (Thermo Fisher Scientific # 17502048), 1X Chemically Defined Lipid Concentrate (Thermo Fisher Scientific # 11905031), and 100 U/mL Penicillin/Streptomycin. Media was changed every 2-3 days.

From Day 35 onward, neuronal differentiation medium was supplemented with 5 μg/mL Heparin sodium salt (Millipore Sigma # H3149) and 0.5% v/v Matrigel Growth Factor Reduced (GFR) Basement Membrane Matrix (Corning # 354230).

For scRNA-seq experiments, we removed fetal bovine serum from this media.

#### *Neuronal maturation*

From Day 70, organoids were cultured in neuronal maturation media containing BrainPhys Neuronal Medium (Stem Cell Technologies # 05790), 10% (v/v) Hyclone characterized fetal bovine serum, 1X N-2 Supplement, 1X Chemically Defined Lipid Concentrate (Thermo Fisher Scientific # 11905031), 1X B-27 Supplement (Thermo Fisher Scientific # 17504044), 100 U/mL Penicillin/Streptomycin, and 1% v/v Matrigel GFR.

### Human MGE organoids generation

#### *ESC aggregation and early differentiation*

MGE organoids were generated following a modified version of a previously published protocol.[93] The ESC line HES-3 NKX2.1GFP/w was dissociated and reaggregated at a density of 10,000 cells per well in lipidure-coated 96-well V-bottom plates. The cells were

cultured in StemFlex medium supplemented with Rho Kinase Inhibitor Y-27632 on Day -1. On Day 0, the medium was replaced with Dulbecco's Modified Eagle Medium: Nutrient Mixture F-12 with GlutaMAX, containing 20% (v/v) Knockout Serum Replacement, 1 mM MEM Non-Essential Amino Acids, 0.1 mM 2-Mercaptoethanol, and 100 U/mL Penicillin/Streptomycin. The medium was further supplemented with 5 μM dorsomorphin (Millipore Sigma # P5499), 10 μM TGF-beta inhibitor SB431542, and 10 μM Rho Kinase Inhibitor Y-27632. Medium changes occurred on Days 2 and 4, with the Rho Kinase Inhibitor omitted from the subsequent changes.

#### *Neuronal differentiation and maintenance*

On Day 6, the organoids were transferred to neuronal differentiation medium, which comprised Neurobasal A medium (Thermo Fisher Scientific # 10888022), 1X B-27 supplement minus Vitamin A (Thermo Fisher Scientific # 12587010), 1X GlutaMAX supplement (Thermo Fisher Scientific # 35050061), and 100 U/mL Penicillin/Streptomycin. The medium was replaced every 2-3 days. On Day 18, organoids were moved to ultra-low adhesion plates and cultured on an orbital shaker at 90 revolutions per minute.

Neuronal differentiation medium was supplemented with small molecules as follows: From Days 6 to 11, 20 ng/mL Human Recombinant EGF (R&D Systems # 236-EG), 20 ng/mL Human FGF-basic (FGF-2/bFGF) Recombinant Protein (Thermo Fisher Scientific # PHG0261), and 3 μM WNT inhibitor IWR1-ε were included. On Days 12-15, the medium also contained 100 nM SHH pathway agonist Smoothened Agonist (SAG) HCl (Selleckchem # S7779) and 100 nM retinoic acid (Millipore Sigma # R2625). From Days 16 to 24, retinoic acid was removed, and 100 nM allopregnanolone (Cayman Chemicals # 16930) was added. After Day 25, no small molecules were included in the medium.

### Human thalamic organoids generation

#### *iPSC aggregation and early differentiation*

Thalamic organoids were generated following a previously described protocol.[175] Briefly, iPSCs were clump dissociated into ultra-low attachment 6-well plates and cultured for 8 days in Dulbecco's Modified Eagle Medium: Nutrient Mixture F-12 with GlutaMAX, supplemented with 15% (v/v) Knockout Serum Replacement, 1 mM MEM Non-Essential Amino Acids, 0.1 mM 2-Mercaptoethanol, 100 U/mL Penicillin/Streptomycin, 10 μM SB431542, 100 nM LDN193189 dihydrochloride (Tocris # 6053), and 4 μg/mL human insulin (Santa Cruz Biotechnology # sc-360248). The medium was replaced every other day.

#### *Neuronal induction*

On day 9, the plates were placed on a shaker operating at 90 rpm, and the organoids were cultured for an additional 8 days in patterning medium, which consisted of Dulbecco's Modified Eagle Medium: Nutrient Mixture F-12 with GlutaMAX, supplemented with 15% Dextrose (Millipore Sigma # PHR1000), 0.1 mM 2-Mercaptoethanol, 1X N2 Supplement, 2X B-27 Supplement minus Vitamin A, 30 ng/mL recombinant human BMP7 (R&D Systems # 354-BP), 1 μM PD325901 (Millipore Sigma # PZ0162), and 100 U/mL Penicillin/Streptomycin. The medium was replaced every other day.

#### *Neuronal differentiation and maintenance*

From Day 17 onward, the organoids were cultured in differentiation medium composed of a 1:1 mix of Neurobasal Medium (Thermo Fisher Scientific # 21103049) and Dulbecco's Modified Eagle Medium: Nutrient Mixture F-12 with GlutaMAX, supplemented with 2X B-27 Supplement, 1X N2 Supplement, 0.1 mM MEM Non-Essential Amino Acids, 100 U/mL Penicillin/Streptomycin, and 50 μM 2-Mercaptoethanol. The medium was replaced every other day.

### Mouse cortical organoids generation

Mouse E14.5 cortices were carefully dissected and chopped into small pieces. The tissue was then dissociated using the Worthington Papain Dissociation System (Worthington # LK003150) according to the manufacturer's instructions. An enzyme solution was prepared by resuspending 20 units of papain per mL, along with 1 mM L-cysteine and 0.5 mM EDTA in Earle's Balanced Salt Solution (EBSS). This enzyme solution was activated by incubating at 37°C for 30 minutes.

Following activation, 200 units of DNase I per mL were added. The chopped tissue was then transferred into the papain and DNase I solution and incubated at 37°C while shaking at 90 rpm for an additional 30 minutes. The tissue was mechanically dissociated using flamed glass Pasteur pipets (Fisher Scientific # 13-678-6B) and washed in 1X PBS containing 0.1% Bovine Serum Albumin (Millipore Sigma # A3311), followed by centrifugation at 300 rcf for 3 minutes.

The resulting cell suspension was resuspended and aggregated at a density of 10,000 cells per well in lipidure-coated 96-well V-bottom plates. The cortical organoid differentiation medium consisted of Dulbecco's Modified Eagle Medium: 10% (v/v) Hyclone characterized fetal bovine serum, Nutrient Mixture F-12 with GlutaMAX supplement, 1X N-2 Supplement, 1X Chemically Defined Lipid Concentrate, 5 μg/mL Heparin sodium salt, and 1% v/v Matrigel Growth Factor Reduced (GFR) Basement Membrane Matrix, LDEV-free, along with 100 U/mL Penicillin/Streptomycin. The medium was changed every 2-3 days.

After 10 days in culture, the organoids were transferred to neuronal maturation media, which contained BrainPhys Neuronal Medium, 10% (v/v) Hyclone characterized fetal bovine serum, 1X N-2 Supplement, 1X Chemically Defined Lipid Concentrate, 1X B-27 Supplement, 100 U/mL Penicillin/Streptomycin, and 1% v/v Matrigel Growth Factor Reduced (GFR) Basement Membrane Matrix, LDEV-free. At this stage, the organoids were cultured in ultra-low adhesion plates (Millipore Sigma # CLS3471) on an orbital shaker at 90 revolutions per minute.

### Dissociation and 2D culture of primary human and mouse cortical neurons

Prior to tissue dissociation, glass-bottom cell culture plates (NEST # 801006) were coated overnight at 37°C with a 0.1% Poly-L-ornithine solution (Millipore Sigma # P4957). The plates were then washed three times with sterile water. Following this, they were coated overnight at 37°C with a mixture of 5 μg/mL Laminin (Millipore Sigma # L2020) and 1 μg/mL Fibronectin (Millipore Sigma # DLW354008) resuspended in PBS.

Mouse E14.5 cortices and human GW22 cortices were dissected and chopped into small pieces. The cortices were then dissociated using the Worthington Papain Dissociation System (for details, see the section on mouse cortical organoids generation). The resuspended cells were plated at a concentration of 100,000 cells per well. Cells were cultured in cortical organoid differentiation medium, which consisted of Dulbecco's Modified Eagle Medium: Nutrient Mixture F-12 with GlutaMAX, 10% (v/v) Hyclone characterized fetal bovine serum, 1X N-2 Supplement, 1X Chemically Defined Lipid Concentrate, 5 μg/mL Heparin sodium salt from porcine intestinal mucosa, and 1% v/v Matrigel Growth Factor Reduced (GFR) Basement Membrane Matrix, LDEV-free, along with 100 U/mL Penicillin/Streptomycin. The medium was changed every 2-3 days.

### Dissociation and infection of human MGEs

Cryopreserved GW18-19 human MGE tissue stocks were thawed in warm Leibovitz's L-15 Medium (Thermo Fisher Scientific # 11415064). Following thawing, the cells were dissociated using the Worthington Papain Dissociation System (for details, see the section on mouse cortical organoids generation). The cells were then concentrated by centrifugation at 300 g for 2 minutes and resuspended in warm cortical differentiation media. The cells were infected for 1 hour with an eGFP adenovirus (Vector Biolabs # 1060), which ubiquitously expresses eGFP under the CMV promoter, at a titer of 1 x 10^7 PFU/ml. After infection, the cells were washed once in warm cortical differentiation media and resuspended in the same media at a concentration of 1,000 cells/μl for immediate grafting onto organoids (for details, see the section on grafting of MGE-cIN progenitors and Sst-positive INs). eGFP expression was detectable as early as 12 hours post-infection, with strong expression observed 48 hours post-infection.

### Grafting of MGE-cIN progenitors and Sst-positive INs

E13.5 MGE tissue was microdissected and transferred to ice-cold Leibovitz's L-15 Medium (Thermo Fisher Scientific # 11415064) supplemented with 180 μg/mL DNase I (Millipore Sigma # 69182). The tissue was mechanically dissociated on ice by pipetting using a P1000 micropipette. Dissociated cells were concentrated by centrifugation for 4 minutes at 300 rcf.

For organoid grafting, the organoids were transferred to individual wells of lipidure-coated 96-well V-bottom plates. A total of 200 μL of fresh cortical organoid neuronal differentiation medium was added, consisting of Dulbecco's Modified Eagle Medium: Nutrient Mixture F-12 with GlutaMAX, 10% (v/v) Hyclone characterized fetal bovine serum, 1X N-2 Supplement, 1X Chemically Defined Lipid Concentrate (Thermo Fisher Scientific # 11905031), 5 μg/mL Heparin sodium salt from porcine intestinal mucosa, and 1% v/v Matrigel Growth Factor Reduced (GFR) Basement Membrane Matrix, LDEV-free, along with 100 U/mL Penicillin/Streptomycin. Human organoids were 6-8 weeks old at the time of grafting, while mouse organoids had been cultured for 2 weeks prior. We then added 50,000 MGE cells to each well and incubated the organoids for 24 hours at 37°C. Following this incubation, the organoids were carefully transferred to ultra-low-attachment tissue culture plates and incubated on an orbital shaker at 90 rpm at 37°C. The medium was changed every 2-3 days.

For grafting onto human and mouse organotypic cultures, cells were resuspended at a concentration of 1,000 cells/μL. The cell concentrate was then pipetted directly onto the organotypic cultures to facilitate integration.

For co-culture with 2D cortical neurons, 1,000 cells were added to each well of the cortical cultures.

For grafting postmitotic neurons, all ganglionic eminences of *Sst*-Cre::Ai14 mice at E14.5 were microdissected and dissociated. During microdissection, efforts were made to remove the ventricular zone as thoroughly as possible.

### mTOR inhibition

All experiments utilized 250 nM rapamycin (Millipore Sigma # R8781). experimental organoids, rapamycin was incorporated into the media. Control experiments received media without rapamycin. The medium was changed every 2-3 days.

### Immunohistochemistry and confocal imaging

Organoids were collected and fixed in 4% paraformaldehyde PFA (Thermo Fisher Scientific # 28908) and cryopreserved in 30% sucrose (Millipore Sigma # S8501). They were embedded in a solution containing 50% Tissue-Tek O.C.T. Compound (Sakura # 4583) and 50% 30% sucrose dissolved in 1X phosphate-buffered saline (PBS) at pH 7.4 (Thermo Fisher Scientific # 70011044). Sections were cut to 12 μm using a cryostat (Leica Biosystems # CM3050) and mounted directly onto glass slides. Following three washes of 10 minutes in 1X PBS, the sections were incubated in a blocking solution consisting of 5% v/v donkey serum (Millipore Sigma # D9663), 2% w/v gelatin (Millipore Sigma # G9391), and 0.1% Triton X-100 (Millipore Sigma # X100) for 1 hour. Primary antibodies were incubated overnight at 4°C, followed by three washes for 30 minutes and incubation with secondary antibodies for 90 minutes at room temperature. The sections were then washed three times for 30 minutes in PBS, followed by a final wash in sterile water for 10 minutes.

Whole human and mouse organotypic sections were fixed with 4% PFA for 2 hours at room temperature and subsequently washed in PBS at 4°C overnight. Blocking was conducted for one day at 4°C. Primary antibody incubation occurred for 3 days at 4°C,

followed by three washes in PBS, each lasting 2 hours. Secondary antibody incubation was also for 3 days at 4°C, followed by similar washing procedures.

For human postmortem tissue, mounted slides were defrosted at 4°C for 24 hours and then equilibrated to room temperature for 3 hours. Antigen retrieval was performed using a solution containing 10 mM trisodium citrate dihydrate (Millipore Sigma # S1804) and 0.05% Tween 20 (Millipore Sigma # P1379) at pH 6.0, heated to 95°C for 10 minutes. Samples were washed with TNT buffer (100 mM Tris-HCl [Thermo Fisher Scientific # 15567027], 150 mM sodium chloride [Millipore Sigma # S9888], and 0.1% Tween 20) for 10 minutes, repeated three times, then incubated with 1% hydrogen peroxide (Millipore Sigma # H1009) in PBS for 2 hours. Slides were blocked for 2 hours with TNB solution (100 mM Tris-HCl, 150 mM sodium chloride, and 0.36% w/v bovine serum albumin [BSA] [Millipore Sigma # A2153]). Primary antibodies were incubated overnight at 4°C. The following day, slides were washed three times in TNT buffer. Biotinylated secondary antibodies diluted in TNB were added for 2.5 hours at room temperature. Sections were then incubated with 1:200 streptavidin-horseradish peroxidase (Millipore Sigma # RABHRP3) in TNB for 30 minutes, followed by a 4-minute incubation with tyramide-conjugated fluorophores. The dilutions and order of the used fluorophores were as follows: Cy5 at 1:50. In cases where tyramide was not used, Alexa-conjugated secondary antibodies were employed along with biotinylated secondaries.

#### *Primary antibodies used*

- Rabbit anti-Bdnf (Abcam # ab108319; RRID: AB_10862052; 1:100)
- Rat anti-Bcl11b (Abcam # ab18465; RRID: AB_2064130; 1:100)
- Rabbit anti-Cox6A2 (Novus Biologicals # NBP1-31112; RRID: AB_2085447; 1:100)
- Mouse anti-ErbB4 (Thermo Fisher Scientific # MA5-12888; RRID: AB_10986112; 1:100)
- Rabbit anti-Gbx2 (Proteintech # 21639-1-AP; RRID: AB_2878896; 1:250)
- Goat anti-eGFP (Abcam # ab6658; RRID: AB_305631; 1:100)
- Mouse anti-HNA (Millipore Sigma # MAB1281; RRID: AB_94090; 1:100)
- Rabbit anti-Map2 (Proteintech # 17490-1-AP; RRID: AB_2137880; 1:100)
- Rabbit anti-MAPK (ERK1/2) phosphorylated (T202/Y204) (Cell Signaling # 9101; RRID: AB_331646; 1:100)
- Rabbit anti-Mef2c (Abcam # ab227085; RRID: AB_3080861; 1:250)
- Mouse anti-Mki67 (BD Biosciences # 550609; RRID: AB_393778; 1:600)
- Mouse anti-Nestin (Thermo Fisher Scientific # MA1-110; RRDI: AB_2536821; 1:1000)
- Rabbit anti-Nkx2.1 (Abcam # ab76013; RRID: AB_1310784; 1:100)
- Mouse anti-Nr2f2 (R&D Systems # PP-H7147-00; RRID: AB_2155627; 1:100)
- Rabbit anti-Pvalb (Swant # PV27; RRID: AB_2631173; 1:250)
- Rabbit anti-Psd95 (Thermo Fisher Scientific # 51-6900; RRID: AB_2533914; 1:100)
- Chicken anti-Rbfox3 (NeuN) (Millipore Sigma # ABN91; RRID: AB_11205760; 1:200)
- Chicken anti-RFP (Rockland Immunochemicals # 600-901-379; RRID: AB_10704808; 1:100)
- Rabbit anti-S6 phosphorylated (pS6) (S235/236) (Cell Signaling # 2211; RRID: AB_331679; 1:100)
- Mouse anti-Satb2 (Abcam # ab51502; RRID: AB_882455; 1:100)
- Mouse anti-Sox2 (Santa Cruz Biotechnology # sc-365823; RRID: AB_10842165; 1:500)
- Mouse anti-Sst (Santa Cruz Biotechnology # sc55565; RRID: AB_831726; 1:100)
- Mouse anti-Tcf7l2 (Millipore Sigma # 05-511; RRID: AB_309772; 1:250)

#### *Secondary antibodies*

Secondary antibodies were from the Alexa series (Thermo Fisher Scientific), used at a dilution of 1:250. Additionally, biotin-conjugated WFA (Vector Laboratories # B-1355-2; RRID: AB_2336874; 1:200) was visualized using Alexa 488-conjugated streptavidin (Thermo Fisher Scientific # S11223; 1:500). Nuclear counterstaining was performed using 300 nM DAPI (4',6-Diamidino-2-Phenylindole, dihydrochloride) (Thermo Fisher # D1306).

#### *Antigen retrieval*

Only the Bdnf antibody required antigen retrieval, achieved by incubating the slides at 95°C for 20 minutes in the antigen retrieval solution (10 mM trisodium citrate dihydrate and 0.05% Tween 20 at pH 6.0) prior to blocking.

#### *Confocal imaging*

Imaging was conducted using an inverted confocal microscope (Leica CTR 6500) with Leica Application Suite X software (Leica; RRID: SCR_013673). Images were processed using ImageJ 2.3.0 software (NIH; RRID: SCR_003070), while overlays and quantifications were performed using Adobe Photoshop version 2020 (Adobe; RRID: SCR_014199).

### Whole organoid immunostaining, clearing, and lightsheet imaging

Organoids were fixed at room temperature for 45 minutes in 4% paraformaldehyde. After fixation, they were washed three times in PBS and stored at 4°C. For whole-organoid immunostaining and tissue clearing, the organoids were blocked for 24 hours at room temperature in PBS supplemented with 0.2% gelatin and 0.5% Triton X-100 (Millipore Sigma # X100) (PBSGT). Samples were then incubated with primary antibodies for 7 days at 37°C with agitation at 70 rpm in PBSGT supplemented with 1 mg/ml saponin (Quillaja sp; Millipore Sigma # S4521) (PBSGTS).

Following primary antibody incubation, samples were washed six times in PBSGT over the course of one day at room temperature. For nuclear staining, we utilized SYTO 16 green fluorescent dye (Thermo Fisher Scientific # S7578). Secondary and nuclear staining was performed for 1 day at 37°C with agitation at 70 rpm in PBSGTS. Samples were then washed six times in PBSGT over the course of one day at room temperature.

Whole organoid clearing was performed using ScaleCUBIC-1 solution as described by Susaki et al. (2015).[176] Briefly, the solution contained 25% wt urea (Millipore Sigma # U5378), 25% wt N,N,N',N'-Tetrakis(2-hydroxypropyl)ethylenediamine (Tokyo Chemical Industry # T0781), and 15% Triton X-100 dissolved in distilled water. Organoids were incubated in ScaleCUBIC-1 solution overnight at room temperature with agitation at 90 rpm. Whole organoid imaging was performed using a custom-made lattice light sheet microscope (UCSF Biological Imaging Development Center), and images were deconvoluted using the Richardson-Lucy algorithm. Image processing was carried out using Imaris 9.2 software (Bitplane).

### EdU (5-Ethynyl-2′-deoxyuridine) labeling

EdU labeling was performed using the Click-iT Plus EdU Cell Proliferation Kit for Imaging® (Thermo Fisher Scientific # C10640), adapting the manufacturer's instructions for tissue slides. Briefly, grafted organoids were treated with 10 μM EdU from the moment of grafting for 48 hours. Organoids were then transferred to media without EdU, and the media was replaced every other day throughout the experiments. After fixation and sectioning (as described in the immunohistochemistry and confocal imaging section), organoid sections were washed twice for 3 minutes each with 3% bovine serum albumin (BSA) (Millipore Sigma # A2153) dissolved in PBS. The tissue was then permeabilized for 20 minutes using 0.5% Triton X-100 (Millipore Sigma # X100) diluted in PBS, followed by two 3-minute washes in 3% BSA diluted in PBS. Following permeabilization, the tissue was incubated for 30 minutes in a solution containing 88% Click-iT® Reaction Buffer, 2% copper protectant, 0.0024% Alexa Fluor® picolyl azide, and 10% reaction buffer additive. The tissue was then washed twice in 3% BSA. Nuclear counterstaining was performed using 300 nM DAPI.

### Single cell transcriptomics analysis of existing datasets

Public datasets from mouse models were analyzed, including E13.5 and E14.5 ganglionic eminences and P10 subcortex,[31] as well as three samples from the 10X Genomics E18 mouse cortex dataset comprising 1.3 million cells, and E14 and neonatal cortex and subcortex data.[52] These datasets were downloaded as raw FASTQ or BAM files, which were subsequently converted to FASTQ format. Gene quantification was performed using Kallisto (version 0.46.2; RRID: SCR_016582; https://pachterlab.github.io/kallisto/)[177] with Mus musculus ENSEMBL release 100 transcript annotations.

The Kallisto-Bus output matrix files, encompassing both introns and exons, were processed using CellBender (version 0.2.0; RRID: SCR_025990; https://github.com/broadinstitute/CellBender) to filter out likely ambient RNA. Only droplets with a probability greater than 0.99 of being cells were retained for analysis. Droplets that detected fewer than 600 genes, or had more than 40% ribosomal or 15% mitochondrial reads, were excluded from the dataset. Doublets were identified and removed using Scrublet (version 0.2.2; https://github.com/swolock/scrublet; RRID: SCR_018098) with a threshold parameter set to 0.5.

Using Scanpy (version 1.8; https://github.com/theislab/scanpy; RRID: SCR_018139), counts in droplets were read-depth normalized, log-transformed, and expression values for each gene were scaled across all cells. Principal component analysis (PCA) was performed on the 6000 most variable genes, followed by balanced K-nearest neighbors mapping, UMAP projection, and Leiden clustering.[178] Clusters exhibiting high expression levels of Gad1, Gad2, and Dlx genes, along with Lhx6 and Nkx2.1, were included in the analysis. The term "VMF" refers to ventromedial forebrain regions, including the septum, preoptic area, and preoptic hypothalamus.

### Fluorescent-activated cell sorting experiments

Grafted organoids were dissociated into single-cell suspensions using the Worthington Papain Dissociation System (Worthington # LK003150) following the manufacturer's instructions. To minimize RNA degradation, 3,500 units/ml of RNase Inhibitor was added. We processed 10 grafted organoids individually.

After dissociation, the cells were washed twice with PBS and resuspended in PBS supplemented with 1% ultrapure bovine serum albumin (Thermo Fisher Scientific # AM2618) and 4,900 units/ml of RNase Inhibitor. The samples were kept on ice until sorting. FACS was performed using a BD FACSAria Fusion Flow Cytometer with a 130 μm nozzle. Prior to sorting, the samples were incubated with Hoechst 33342 (Thermo Fisher Scientific # 62249). Gating was as follows: Forward and side scatter were used to identify individual cells, while Hoechst 33342 stained nuclei to confirm cell identity. Subsequently, td-Tomato-positive cells were selected for sorting. Each dissociated organoid was sorted separately, and the sorted cells were pooled for single-cell RNA sequencing.

### Single-cell RNA library preparation and sequencing

A total of 75,000 FACS-purified td-Tomato-positive events (putative cells) were used for this experiment. Immediately after sorting, libraries were prepared using the 10X Chromium Single Cell 3′ reagent kit V3 (10X Genomics # PN-1000092). Following library preparation, the libraries were sequenced on Illumina HiSeq and NovaSeq platforms.

### Single-cell RNA sequencing data processing

Transcriptomes were aligned to both the human (GRCh38) and mouse (GRCm39/mm39) reference genomes, integrating the td-Tomato sequence into the mouse genome. Alignments were performed using Cell Ranger version 5 (10X Genomics;

RRID:SCR_017344). Cells aligning to the human genome and td-Tomato-negative mouse cells were excluded, resulting in a final dataset of 225 td-Tomato-positive mouse cells. Subsequent analysis was carried out in Scanpy 1.10.2.[179] The raw counts expression matrix was loaded as an AnnData object, normalized by read depth, log-transformed, and scaled per gene across the dataset. Cells with fewer than 200 detected genes and genes expressed in fewer than three cells were filtered out. The raw and processed data have been deposited in GEO, under accession number GSE278531.

### Deep learning-based cell classification

Td-Tomato-positive cells were classified using SIMS (RRID: SCR_025787), a transformer-based label transfer deep learning architecture previously validated on neuronal single-cell data.[162] The SIMS model was trained on a subset of single-cell RNA expression data with pre-annotated labels from a published dataset compilation,[6] specifically focusing on MGE and cortical interneurons. This subset included 51,402 cells and 15 cell labels. The datasets include: Publicly available E18 mouse brain from 10X Genomics (NCBI GEO # 20GSE93421), and the datasets reported in La Manno et al., 2021[53] (NCBI SRA # PRJNA637987); Loo et al., 2019[52] (NCBI GEO # GSE123335), Mayer et al., 2018[31] (NCBI GEO # GSE104158); and Zeisel et al., 2018[54] (NCBI SRA # SRP135960). The trained model is accessible via the SIMS web app: https://sc-sims-app.streamlit.app/.

### Soma size measurements

To minimize potential bias in image acquisition, we reused images obtained during marker quantifications, selecting random sections for analysis. Files were processed using ImageJ 2.3.0 (NIH; RRID: SCR_003070). We utilized the Z Project function to create a single-plane image from the z-stacks, selecting Maximal Intensity as the projection type. The freehand selection tool was then employed to delineate the area of the maximal soma size. Finally, the Measure tool was used to calculate the area of the largest soma.

### Live imaging of organoids

Live imaging was conducted as previously described.[180] Initially, grafted organoids were transferred to hydrophilic polytetrafluoroethylene cell culture inserts (Millipore Sigma # PICM0RG50) and placed on a six-well glass-bottom tissue culture plate to facilitate culture in an air-liquid interface. The medium for culture was cortical organoid neuronal differentiation medium, excluding Matrigel. Organoids were incubated for 6 h at 37°C prior to imaging to allow for tissue flattening.

Imaging was performed on an inverted Leica TCS SP5 confocal microscope equipped with an on-stage incubator that maintained a chamber atmosphere of 5% $CO_2$, 8% $O_2$, and balanced $N_2$. The chamber temperature was set to 37°C. Slices were imaged continuously for 24 hours using a 10X air objective (with 2X zoom) at 20-minute intervals.

### Calcium imaging

Calcium imaging of mouse INs was performed using the genetically encoded calcium indicator GCaMP6s, specifically expressed in the INs through the use of the *Nkx2.1*-Cre::Ai96 mouse line. Imaging was conducted on an inverted confocal microscope (Leica CTR 6500) with the Leica Application Suite X software (Leica Microsystems; RRID: SCR_013673). Images were captured at 1.2-second intervals and processed using ImageJ 2.3.0 software (NIH; RRID: SCR_003070).

For human PNs, we utilized organoids grafted with *Nkx2.1*-Cre::Ai14-labeled mouse INs. Control organoids, derived from the same batches, did not receive grafts. Before imaging, organoids were incubated at 37°C for 20 minutes in 4 μM Fluo-8 AM (Abcam, #ab142773). Imaging was performed immediately after staining, as described above.

After acquisition, video files were initially saved in the .avi format. To improve compatibility and editing flexibility, these files were converted to uncompressed .avi format using VirtualDub (https://www.virtualdub.org, RRID: SCR_026123). For further image processing and analysis, the files were additionally converted to .tiff format using ImageJ 2.3.0 (NIH; RRID: SCR_003070). Regions of interest (ROIs) were defined using the ROI Manager in ImageJ, enabling precise and comprehensive analysis across multiple regions of the organoids. To analyze calcium imaging data, we utilized the Time-Lapse Video plugin in ImageJ, which provided detailed insights into intensity-versus-time patterns, facilitating a thorough evaluation of the calcium transients.

## QUANTIFICATION AND STATISTICAL ANALYSIS

Immunohistochemistry quantifications spanned $\geq$2 independent batches (3–10 organoids per batch), with multiple sections analyzed per organoid. All cells of interest were quantified per section, and total counts per organoid were calculated by summing cells across all sections. Total cell counts are provided in Table S1.

All statistical analyses were conducted using Prism 9.3.1 (GraphPad Software; RRID: SCR_002798). Conditions were compared using an unpaired parametric Student's t-test without Welch's correction. For all conditions: * = $p < 0.05$; ** = $p < 0.01$; *** = $p < 0.001$; **** = $p < 0.0001$.